**REPUBLIC OF TURKEY**
**YILDIZ TECHNICAL UNIVERSITY**
**GRADUATE SCHOOL OF NATURAL AND APPLIED SCIENCES**

# DETERMINATION OF SANDS' DYNAMIC PROPERTIES BY USING BENDER-EXTENDER ELEMENTS

**BABAK ROUZEGARI**

**MSc. THESIS**
**DEPARTMENT OF CIVIL ENGINEERING**
**PROGRAM OF GEOTECHNICAL ENGINEERING**

**ADVISER**
**ASSOC. PROF. DR. HAVVANUR KILIÇ**

**İSTANBUL, 2013**

**REPUBLIC OF TURKEY**

**YILDIZ TECHNICAL UNIVERSITY**

**GRADUATE SCHOOL OF NATURAL AND APPLIED SCIENCES**

# DETERMINATION OF SANDS' DYNAMIC PROPERTIES BY USING BENDER-EXTENDER ELEMENTS

A thesis submitted by Babak ROUZEGARI in partial fulfillment of the requirements for the degree of **MASTER OF SCIENCE** is approved by the committee on 19.08.2013 in Department of Civil Engineering, Geotechnical Engineering Program.

**Thesis Adviser**

Assoc. Prof. Dr. Havvanur KILIÇ

Yıldız Technical University

**Approved By the Examining Committee**

Assoc. Prof. Dr. Havvanur KILIÇ

Yıldız Technical University _____

Assoc. Prof. Dr. Mehmet BERİLGEN

Yıldız Technical University _____

Assoc. Prof. Dr. Özer ÇİNİCİOĞLU

Boğaziçi University _____

This study was supported by the Scientific Research Projects Coordination Unit of Yıldız Technical University Grant No: 2011-05-01-KAP03.

# ACKNOWLEDGEMENTS

I would sincerely like to thank all those who made this effort possible. Firstly, I would like to express my heartiest respect and deepest gratitude to my supervisor Assoc. Prof. Dr. Havvanur KILIÇ for the constant support, useful comments and kind engagement through the process of this master thesis.

I would also like to thank Prof. Dr. Kutay ÖZAYDIN, Prof. Dr. Mustafa YILDIRIM, Assoc. Prof. Dr. Mehmet BERİLGEN, Assoc. Prof. Dr. Pelin TOHUMCU ÖZENER, Assoc. Prof. Dr. Şükrü ÖZÇOBAN, Assist. Prof. Dr. Saadet Arzu BERİLGEN, Dr. Cem AKGÜNER, Dr. Murat Ergenekon SELÇUK and Çiğdem ÖZÇELİK for providing me with their valuable knowledge and precious experience during my master studies.

To avoid being ungrateful, Many thanks to all my friends Emre AKINAY, Mustafa KİRKİT, Selçuk DEMİR, Balbora MERT, Emrah TÜRER, Selvinaz DADALOĞLU and Lale ÖNER for their unconditional friendship and limitless help during my studies and the present thesis.

This thesis is dedicated to my father, Mansour ROUZEGARI, my mother, Rina ZEHTABIYAN and my brother Atabak ROUZEGARI who were strongly supportive of my endeavor, without their kind encouragements, reminders and patience my studies and this thesis would have no chance for development.

August, 2013

Babak ROUZEGARI

# TABLE OF CONTENTS

Page

LIST OF SYMBOLS ..... viii
LIST OF ABBREVIATIONS ..... ix
LIST OF FIGURES ..... x
LIST OF TABLES ..... xiii
ABSTRACT ..... xiv
ÖZET ..... xvi
CHAPTER 1
INTRODUCTION ..... 1
1.1 Literature Review ..... 2
1.2 Objective of the Thesis ..... 11
1.3 Hypothesis ..... 11
CHAPTER 2
THEORETICAL BACKGROUND ..... 12
2.1 Introduction ..... 12
2.2 Piezoelectric Transducers ..... 13
2.3 Wave propagation in soils ..... 16
2.3.1 Compression Wave Velocity ..... 17
2.3.2 Shear Wave Velocity ..... 18
2.3.3 Poisson's Ratio ..... 19
2.4 Wave Travel Distance ..... 20
2.5 Wave Travel Time ..... 21
2.5.1 First Time of Arrival ..... 21
2.5.2 First Peak to Peak Time ..... 21
2.6 Noise ..... 22
2.6.1 Background Noise ..... 22
2.6.2 Residual Vibration ..... 22
2.6.3 Cross-Talk ..... 23
2.7 Near Field Effect ..... 23
2.8 Strain Level ..... 24

2.9 The Behavior of Sands in Triaxial Test ..... 25

CHAPTER 3

PIEZOELECTRIC ELEMENTS ..... 28

3.1 Introduction ..... 28
3.2 Single Layer Piezo Motors ..... 28
3.3 Single Layer Piezo Generators ..... 29
3.4 2-Layer Elements ..... 30
3.5 Bender Element ..... 31
3.5.1 Bending Motor (Transmitter) ..... 31
3.5.2 Bending Generator (Receiver) ..... 31
3.6 Extender Element ..... 31
3.6.1 Extension Motor (Transmitter) ..... 31
3.6.2 Extension Generator (Receiver) ..... 32
3.7 Elements Polarization ..... 32
3.8 Series and Parallel Wiring Configuration ..... 32
3.9 Application of Piezoelectric Elements ..... 33

CHAPTER 4

TEST EQUIPMENT AND SAND SPECIMEN ..... 35

4.1 Bender-Extender Elements ..... 35
4.1.1 Element Type and Specification ..... 36
4.1.2 Wiring ..... 36
4.1.3 Grounding ..... 38
4.1.4 Waterproofing ..... 39
4.1.5 Housing ..... 39
4.2 Data Acquisition System ..... 40
4.2.1 Function Generator ..... 41
4.2.2 Digital Oscilloscope ..... 42
4.3 Power Amplifier ..... 43
4.4 Triaxial Test Apparatus ..... 44
4.4.1 LoadTrac II/FlowTrac II ..... 44
4.4.2 Cell ..... 45
4.4.3 Caps ..... 46
4.5 Test Sand and Specimen Preparation ..... 48

CHAPTER 5

$V_S$ and $V_P$ MEASUREMENT TEST RESULTS ..... 51

5.1 $V_S$ and $V_P$ Measurement Tests' Properties ..... 51
5.1.1 Tests under Isotropic Confining Stress ..... 52
5.1.2 Tests under Anisotropic Confining Stress ..... 53
5.1.3 Transmitted Signal Properties and Wave Travel Time Measurements ..... 54
5.1.4 Monotonic Triaxial Shearing Test Properties ..... 54
5.2 Test Result for Dry Specimens under Isotropic Stress ..... 55
5.2.1 Test Results for Different frequencies ..... 55
5.2.2 Test Results for Different Void Ratios ..... 56
5.2.3 Test Results for Different Relative Densities ..... 57

5.2.4 Test Results for Different Confining Pressures ..... 59
5.2.5 Effect of Relative Density and Isotropic Confining Pressure on Sand Specimen's Poisson's Ratio ..... 61
5.3 Test Result for Dry Specimens under Anisotropic Stress ..... 63
5.3.1 Test Results for Different Mean Effective Stresses ..... 63
5.3.2 Variation of Sand Specimen's Poisson's Ratio with mean Effective Stress ..... 66
5.4 $V_S$ and $V_P$ Changes during Monotonic Shearing ..... 67
5.4.1 Drained Monotonic Shearing ..... 67
5.4.2 Undrained Monotonic Shearing ..... 69

CHAPTER 6

SUMMARY AND CONCLUSION ..... 73

REFERENCES ..... 77

CURRICULUM VITAE ..... 81

# LIST OF SYMBOLS

| | |
|---|---|
| $D_{10}$ | Effective grain size |
| $D_{50}$ | Average grain size |
| $D_r$ | Relative density |
| e | Void ratio |
| $e_{max}$ | Maximum void ratio |
| $e_{min}$ | Minimum void ratio |
| $e_0$ | Initial void ratio |
| f | Frequency |
| $G_s$ | Specific gravity |
| G | Shear modulus |
| $G_0$ | Initial shear modulus |
| $G_{max}$ | Maximum shear modulus |
| $M_{max}$ | Maximum constrained modulus |
| $V_S$ | Shear wave velocity |
| $V_P$ | Compression wave velocity |
| $\lambda$ | Wave length |
| L | Wave path length |
| $t_0$ | First time of arrival |
| $t_{pp}$ | Time between first peak to peak |
| $V_{pp}$ | Peak to peak voltage |
| $\gamma$ | Shear strain |
| $\sigma$ | Normal stress |
| $\varepsilon$ | Normal strain |
| $p'$ | Mean effective stress |
| $\sigma'_1$ | Effective deviatoric stress |
| $\sigma'_3$ | Effective confining stress |
| $\nu$ | Poisson's Ratio |

## LIST OF ABBREVIATIONS

| | |
|---|---|
| BE | Bender-Extender |
| BT | Bender Transducer |
| CNC | Computer Numerical Control |
| CP | Confining Pressure |
| DAQ | Data Acquisition |
| NA | Not Available |
| PCI | Peripheral Component Interconnect |
| RC | Resonant Column |

# LIST OF FIGURES

Page


Figure 1.1 Piezoelectric Transducers Used in the Profilometer [10] ..... 3
Figure 1.2 Piezoelectric Transducers Installed in a Corer Head [9] ..... 4
Figure 1.3 Bender Elements or Bimorph Transducers Developed Originally by Shirley and Anderson [11] ..... 4
Figure 1.4 Shear Wave Signal on Lucite Rod Using Bimorph Transducers, [11] ..... 5
Figure 1.5 Comparison of the $G_{max}$ Measured Using Bender Elements and Resonant Column, [14] ..... 6
Figure 1.6 Oedemeter Adapted with Bender Elements, [15] ..... 6
Figure 1.7 (a) Base Pedestal with Compression and Bender Transducers, (b) Base Pedestal with Compression and Shear Plate Transducers, [5] ..... 7
Figure 1.8 Typical Examples of Shear Wave Arrivals at Receiver for Bender Elements and Shear Plates, [5] ..... 8
Figure 1.9 Comparison of Variations of the Vs with Confining Pressure Measured Using bender element, shear plate and resonant column, [5] ..... 9
Figure 1.10 The Variation of the Poisson Ratio with Relative Density at Different Effective Confining Pressures for Medium-grained Sand, [18] ..... 10
Figure 1.11 The Variation of the Poisson Ratio with Effective Confining Pressure at Different Relative Densities for Medium-grained Sand, [18] ..... 10
Figure 2.1 Characteristic strain-stiffness curve of soil's non-linear behavior [1] ..... 12
Figure 2.2 Pair of Bender-Extender Elements Mounted in Triaxial Test Apparatus . 14
Figure 2.3 Body Wave Propagating within a Uniform Infinite Medium: (a) Compression Waves, (b) Shear Waves [36] ..... 16
Figure 2.4 Type of Vibration in Rods: (a) Longitudinal, (b) Torsional, (c) Flexural [37]. ..... 17
Figure 2.5 first time of arrival ($t_0$) and the time between first peak to peak ($t_{PP}$), [44] ..... 21
Figure 2.6 (a) Proper Grounding, without Cross-talk, (b) Poor Grounding, With Cross-talk, (Red line is transmitted signal and blue line is received signal) ..... 23
Figure 2.7 The Results of Drained Triaxial tests on (a) A Dense and (b) A Loose Sample of Brasted Sand, [55] ..... 26
Figure 2.8 Data from Undrained Triaxial Tests on (a) Medium Dense and (b) Loose Samples of Brasted Sand, [55] ..... 27
Figure 3.1 (a) Longitudinal Motor, (b) Transverse Motor, Contracting [56] ..... 29
Figure 3.2 (a) Longitudinal Generator, (b) Transverse Generator, Compressed on sides [56] ..... 30

Figure 3.3 Two-Layer Element Structure [56] ..... 31
Figure 3.4 Types of Piezoelectric Elements: (*a*) x-poled; (*b*) y-poled [35] ..... 32
Figure 3.5 Bender element wiring configuration using (*a*) x-poled series and (*b*) y-poled parallel configurations, [56] ..... 33
Figure 3.6 Extender element wiring configuration using (*a*) x-poled parallel and (*b*) y-poled series configurations, [56] ..... 33
Figure 4.1 (a) Triaxial Test Apparatus, (b) New Triaxial Cell, (c) Linear Power Amplifier, (d) Data Acquisition System ..... 35
Figure 4.2 Transducer Part Number, [56] ..... 36
Figure 4.3 (a) Piezoelectric Element, (b) Modified Element, (c) Bender-Extender Element ..... 37
Figure 4.4 Cables ..... 38
Figure 4.5 Bender-Extender Element Grounding and Waterproofing ..... 39
Figure 4.6 (a) Bender-Extender Element, (b) Housing ..... 40
Figure 4.7 Elements Before and After Fixing by Epoxy in Housing ..... 40
Figure 4.8 (a) PCI-6115 DAQ board, (b) BNC-2110 connector block ..... 41
Figure 4.9 Computer Program Interface ..... 42
Figure 4.10 Piezo EPA-104 Linear Power Amplifier ..... 43
Figure 4.11 Peak Voltage Delivered to Capacitive Load at Peak Current Rating as a Function of Operating Frequency [56] ..... 44
Figure 4.12 (a) LoadTrac II, (b) FlowTrac II ..... 45
Figure 4.13 New Triaxial Cell ..... 46
Figure 4.14 New Triaxial caps ..... 47
Figure 4.15 (a) Porous Stones, (b) Porous Stone's molds ..... 48
Figure 4.16 Grain Size Distribution Curve ..... 49
Figure 4.17 Prepared Sand Specimen ..... 50
Figure 5.1 Finding Wave Travel Time by First Peak to Peak Time Method ..... 54
Figure 5.2 Variations of $V_S$ with Initial Void Ratio ..... 56
Figure 5.3 Variations of $G_{max}$ with Initial Void Ratio ..... 56
Figure 5.4 Variations of $V_P$ with Initial Void Ratio ..... 57
Figure 5.5 Variations of $M_{max}$ with Initial Void Ratio ..... 57
Figure 5.6 Variations of $V_S$ with Initial Relative Density ..... 58
Figure 5.7 Variations of $G_{max}$ with Initial Relative Density ..... 58
Figure 5.8 Variations of $V_P$ with Initial Relative Density ..... 59
Figure 5.9 Variations of $M_{max}$ with Initial Relative Density ..... 59
Figure 5.10 Variations of $V_S$ with Confining Pressure ..... 60
Figure 5.11 Variations of $G_{max}$ with Confining Pressure ..... 60
Figure 5.12 Variations of $V_P$ with Confining Pressure ..... 61
Figure 5.13 Variations of $M_{max}$ with Confining Pressure ..... 61
Figure 5.14 Variations of Poisson's Ratio with Initial Relative Density ..... 62
Figure 5.15 Variations of Poisson's Ratio with Confining Stress ..... 62
Figure 5.16 Variations of $V_S$ with Mean effective Stress ..... 64
Figure 5.17 Variations of $G_{max}$ with Mean effective Stress ..... 64
Figure 5.18 Variations of $V_P$ with Mean effective Stress ..... 65
Figure 5.19 Variations of $M_{max}$ with Mean effective Stress ..... 65
Figure 5.20 Variations of Poisson's Ratio with Mean effective Stress ..... 66
Figure 5.21 Drained Monotonic Shearing Test Stress-Strains Behavior ..... 67

Figure 5.22 Variations of $V_S$ during Drained Monotonic Shearing..... 68
Figure 5.23 Variations of $V_P$ during Drained Monotonic Shearing..... 68
Figure 5.24 Undrained Monotonic Shearing Tests' Total Deviatoric Stress Behavior 70
Figure 5.25 Undrained Monotonic Shearing Tests' Pore Pressure Behavior..... 70
Figure 5.26 Undrained Monotonic Shearing Tests' Effective Deviatoric Stress Behavior ..... 71
Figure 5.27 Variations of $V_S$ during Undrained Monotonic Shearing..... 71
Figure 6.1 Grain Size Distribution Curves in Different Researches..... 75
Figure 6.2 Variations of $V_S$ with Isotropic Confining Pressure in Different Researches ..... 76
Figure 6.3 Variations of Poisson's Ratio with Isotropic Confining Pressure..... 76

# LIST OF TABLES

Page


Table 4.1 the Index Properties of the Sand, Used in This Study ..... 49
Table 5.1 ID and Properties of Isotropic Tests ..... 52
Table 5.2 ID and Properties of Anisotropic Tests ..... 53
Table 5.3 Value of $V_S$ for different input frequency under Constant Relative density and Confining Pressure ..... 55
Table 5.4 Value of $V_P$ for different input frequency under Constant Relative density and Confining Pressure ..... 55
Table 5.5 Test Result for Dry Specimens under Isotropic Stress ..... 63
Table 5.6 Test Result for Dry Specimens under Anisotropic Stress ..... 67
Table 5.7 $V_S$ and $V_P$ Measurement During Drained Monotonic Shearing ..... 69
Table 5.8 $V_S$ Measurement During Undrained Monotonic Shearing ..... 72
Table 6.1 The Index Properties of the Sands in Different Researches ..... 75

# ABSTRACT

## DETERMINATION OF SANDS' DYNAMIC PROPERTIES BY USING BENDER-EXTENDER ELEMENTS

Babak ROUZEGARI

Department of Civil Engineering

MSc. Thesis

Adviser: Assoc. Prof. Dr. Havvanur KILIÇ

Geotechnical engineering required knowledge of the dynamic properties of the soil to analyze dynamic loadings such as machinery vibrations, earthquakes and ocean waves. Bender-extender elements can provide small strain dynamic soil properties by measuring body wave velocities (i.e. shear wave and compression wave velocities) and as a non-destructive method prevent detrimental effects of sample disturbance.

In Soil Mechanics Laboratory of Yıldız Technical University, a bender-extender test apparatus was set up for this purpose. In this study, a series of bender-extender test were performed on uniformly graded (SP) coarse sand samples with varying initial void ratios. Test results show that (i) shear and compression wave velocities decrease as the initial void ratio increases (ii) shear and compression wave velocities increase as the confining effective stress (for both isotropic and anisotropic stress conditions) increases (iii) Poisson's Ratio decreases as the confining effective stress (for both isotropic and anisotropic stress conditions) increases (iv) input frequency does not have a considerable effect on body wave velocity measurement (v) during drained shearing, body wave velocities increase until a threshold axial strain is reached and decrease thereafter (vi) during undrained shearing body wave velocities increase as axial strain increases, as expected.

**Keywords:** Bender elements, Extender elements, small strains, dynamic behavior of sands, wave velocity, Poisson's Ratio, maximum shear modulus, maximum constrained modulus, laboratory tests.

# ÖZET

## KUMLARIN DİNAMİK ÖZELLİKLERİNİ BENDER-EXTENDER ELEMANLAR KULLANILARAK BELİRLENMESİ

Babak ROUZEGARI

İnşaat Mühendisliği Anabilim Dalı

Yüksek Lisans Tezi

Tez Danışmanı: Doç. Dr. Havvanur KILIÇ

Zeminlerin küçük deformasyon düzeyinde rijitliklerinin belirlenmesinde piezoelektrik elemanların (bender eleman, extender eleman, bender-extender eleman) kullanımı oldukça yararlıdır. Bu elemanlar, yaygın olarak silindirik formda hazırlanan bir zemin numunesinin üst ve alt yüzeylerine -verici ve alıcı olarak- yerleştirilir. Bir uçtaki eleman, verilen elektrik voltajını mekanik harekete dönüştürerek zemin içerisinde ilerleyen bir dalga oluşturur. Diğer uçtaki eleman ise, gelen dalga tarafından şekil değiştirmeye maruz kalır ve bunun sonucu olarak bir elektrik voltajı oluşturur. Oluşturulan dalganın bir uçtan diğer uca yolculuğu için geçen süre ve elemanlar arasındaki uzaklık dikkate alınarak mevcut yerleşim koşullarındaki zemin için dalga hızı belirlenir. Dalga hızının belirlenmesi ile zeminin küçük deformasyon düzeyindeki rijitlik modülü elastik teori dikkate alınarak hesaplanır. Piezoseramik elemanlar gönderdikleri dalga türüne göre (daha doğrusu gönderdikleri dalga nedeni ile maruz kaldıkları şekil değiştirmeye göre) adlandırılırlar. Sıkışma dalgası gönderen elemana "Extender Eleman", kayma dalgası gönderen elemana "Bender Eleman" ve her iki dalgayı da gönderebilen elemana "Bender-Extender Eleman" denmektedir. Piezoelektrik elemanların kullanımı tahribatsız bir yöntemdir ve bunun yanı sıra deneyin gerçekleştirilmesi oldukça pratiktir.

Yıldız Teknik Üniversitesi Zemin Mekaniği Laboratuvarı'nda zeminlerin küçük deformasyon düzeyinde rijitliklerinin belirlenmesi amacı ile bir bender/extender deney sistemi kurulmuştur. Bu çalışmada farklı başlangıç boşluk oranlarında hazırlanan uniform dane dağılımlı (SP) kaba kum numuneleri üzerinde bir dizi deney yapılmıştır. Bu deneylerden elde edilen sonuçlara göre (i) başlangıç boşluk oranı arttıkça, kayma dalgası ve sıkışma dalgası hızlarının azaldığı (ii) efektif çevre gerilmesi arttıkça , kayma

dalgası ve sıkışma dalgası hızlarının arttığı (iii) efektif çevre gerilmesi (hem izotropik ve hem de anizotropik gerilme durumlarında) arttıkça Poisson Oranı'nın azaldığı (iv) giriş frekansının bünye dalgası hızları üzerindeki etkisinin göz ardı edilebilir olduğu (v) drenajlı kesme sırasında bünye dalga hızlarının belirli bir eksenel şekil değiştirme düzeyine kadar arttığı ve sonrasında azalan bir eğilim izlediği (vi) drenajsız kesme sırasında -beklenildiği gibi- eksenel şekil değiştirme arttıkça bünye dalga hızlarının arttığı görülmüştür.

**Anahtar Kelimeler:** Bender elemanlar, Extender elemanlar, küçük şekil değiştirmeler, zemin dinamiği, Poisson Oranı, kumların dinamik davranışı, dalga hızı, maksimum kayma modülü, maksimum sıkışma modülü.

# CHAPTER 1

## INTRODUCTION

During seismic loading, soil layers are subjected to cyclic shear stresses with different amplitudes and frequencies that will induce transient and permanent deformations. The structures located on and the infrastructures located in these layers are going to be affected from these deformations and may be damaged. In addition, the change in the stress–strain-strength properties namely ‘‘dynamic properties’’ of soil layers during cyclic loading may have a significant influence on the stability of earth dams, embankments, retaining structures and natural slopes. Therefore, it is necessary to take into account the changes in dynamic characteristics of natural soil layers to decrease the vulnerability [1].

Dynamic material properties are needed in order to evaluate response and the stability of the surface layers. The basic dynamic soil characteristics needed for dynamic analyses are the small strain shear modulus, shear modulus reduction and the damping ratio increase with shear strain amplitude. The small strain shear modulus, $G_{max}$ (the value of shear modulus at very small strains ($\gamma \leq 5x10^{-4}\%$) is one of the important characteristic of soil deformability and plays a significant role in dynamic response analysis. $G_{max}$ is generally estimated by using laboratory or field tests related to seismic wave propagation and reduction curves are obtained based cyclic tests conducted in the laboratory [1].

Geotechnical engineering analyses, considering dynamic loading, require knowledge of the dynamic properties of the soil. Typical dynamic loading are earthquakes, ocean waves or machinery vibrations. The tremendous influence of soil conditions upon the dynamic response of the ground have leaded to improved and expanded techniques for the dynamic characterization of geotechnical materials.

Evaluation of the stiffness of geotechnical materials is usually crucial for modeling and solving any dynamic problem. Today, dynamic characterization of soil in terms of stiffness can be carried out using measurements of body wave velocities in-situ and in the laboratory.

Nowadays piezoelectric transducers are commonly used in geotechnical engineering to measure body wave velocities. When excited by an input voltage, the piezoelectric transducer changes its shape (i.e. bends or extends) and generates a mechanical excitation, hence acting as a signal transmitter. When subjected to mechanical excitation, it emits an electrical output, thus acting as a signal receiver. The time difference between the initiation of the transmitted wave and the first arrival of the received wave yields the travel time of the wave propagated through the soil specimen. The benefits of using piezoelectric transducers for measurement of body wave velocities are their small size and versatility that allows them to be embedded into the soil specimens used in different laboratory apparatus and a relatively simple way to measure body wave velocities based on direct-arrival-times. Additionally using piezoelectric elements in order to determine the small strain stiffness of soils is a non-destructive alternative to using other experimental devices. Also piezoelectric transducers have some shortcomings like their fragility and intolerance to water as a member of the circuit that have to be waterproofed.

### 1.1 Literature Review

Burland [2] and Atkinson [3] emphasized the notion of non-linear soil stiffness and the importance of its small-strain behavior. The testing of soils at small-strains can mainly be achieved by dynamic testing. The dynamic testing of soils in field is made using the cross-hole method, [4]. In this method sensors are placed in boreholes at same depth as transmitter (wave source) and receiver. The aim is to determine the shear velocity and by the way the maximum shear modulus of the soil medium.

Laboratory testing of soils at small strains, before the use bender and extender elements included the use of piezoceramic crystal transducers and resonant column test. Piezocrystals are used for direct measurement of either shear of compression wave velocities [5], while resonant column testing is a more complex way to determine the maximum shear modulus of soil. In resonant column testing, the soil samples are

excited, usually in torsion, and the resonance frequency of the first vibration mode is obtained to determine the maximum shear modulus of the soil [6].

Early works on the use of piezoelectric transducers in soil dynamics dates back to the 1963 (Hamilton [7] and Lawrence [8]). The transducers Lawrence [8] used were piezoelectric crystals. The initial measurements by using these transducers were focused on the compression wave velocities ($V_p$) and had the goal of characterizing the sea bottom. Thus, Hamilton [7] measured $V_p$ in underwater sediments by placing piezoelectric transducer probes on the sea bottom using a submarine. Shirley et al. [9] also used piezoelectric crystals for designing a sound speed profilometer by installing the transducers in corer barrel. The type of transducers used by Shirley et al. [9] was piezoelectric discs as shown in Figure 1.1. The piezoelectric transducers were set up in the corer head (see Figure 1.2) and this corer head was intruded into sea bottom and the soil profile was defined by measurements of $V_p$.

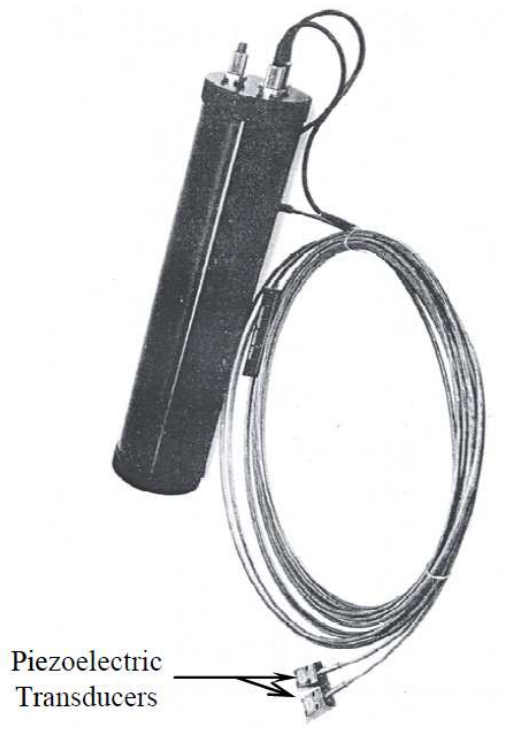



Figure 1.1 Piezoelectric Transducers Used in the Profilometer [10]

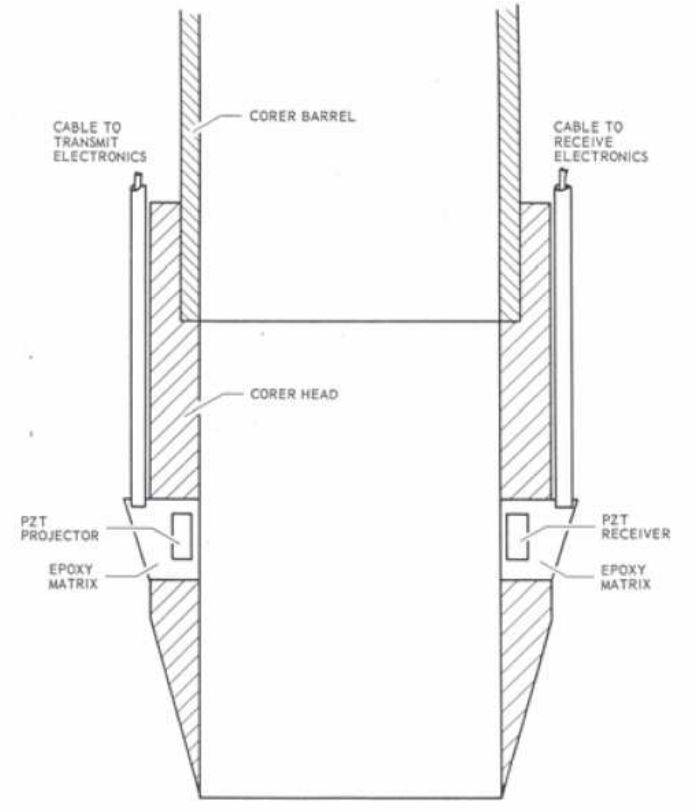



Figure 1.2 Piezoelectric Transducers Installed in a Corer Head [9]

Shirley and Anderson [11] and Shirley and Hampton [12] designed and used piezoelectric bender elements for $V_S$ measurements. Shirley and Anderson [11] specifically developed the bender elements, also called bimorphs, to measure $V_S$ and shear attenuation in sediments (see Figure 1.3). A shear-wave signal, that was obtained using these bender elements, is illustrated in Figure 1.4.

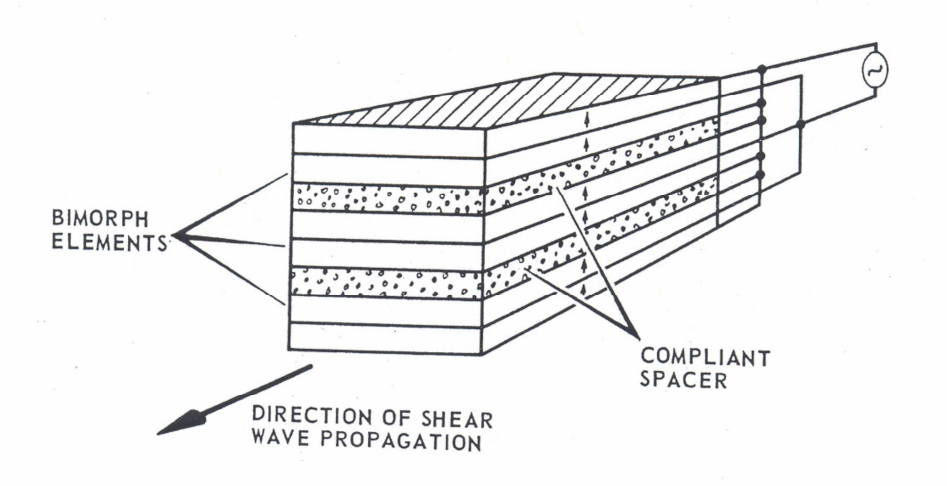



Figure 1.3 Bender Elements or Bimorph Transducers Developed Originally by Shirley and Anderson [11]

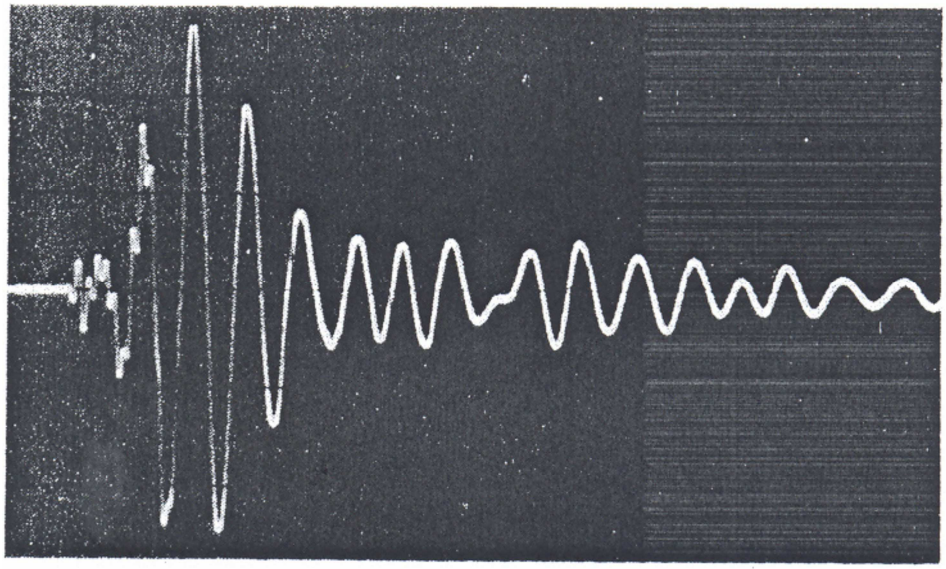


Figure 1.4 Shear Wave Signal on Lucite Rod Using Bimorph Transducers, [11]

Usage of piezoelectric transducers in different laboratory geotechnical testing devices such as the oedometer, the resonant column device and the triaxial cell were presented in several researches as follows. Schultheiss [13] developed the design of bender elements so that they could be fitted into laboratory test devices (i.e. oedometer, triaxial and simple shear test devices). Dyvik and Madshus [14] presented a study on bender element performance related with their wiring, concluding that parallel wiring suited the transmitting transducer and series wiring suited the receiver transducer. In order to validate their results Dyvik and Madshus [14] installed bender elements in a Drnevich Resonant Column and presented a comparative study between bender element transducers and better established resonant columns. Comparison of $G_{max}$ for five clay specimens, measured with both bender element and resonant column systems, is presented in Figure 1.5, [14].

Dyvik and Olsen [15] and Fam and Santamarina [16] instrumented oedometers with bender elements to monitor the stiffness of the soil specimens by $V_S$ measurements, at different stages of consolidation and loading. Figure 1.6 shows the oedometer apparatus adapted with bender elements.

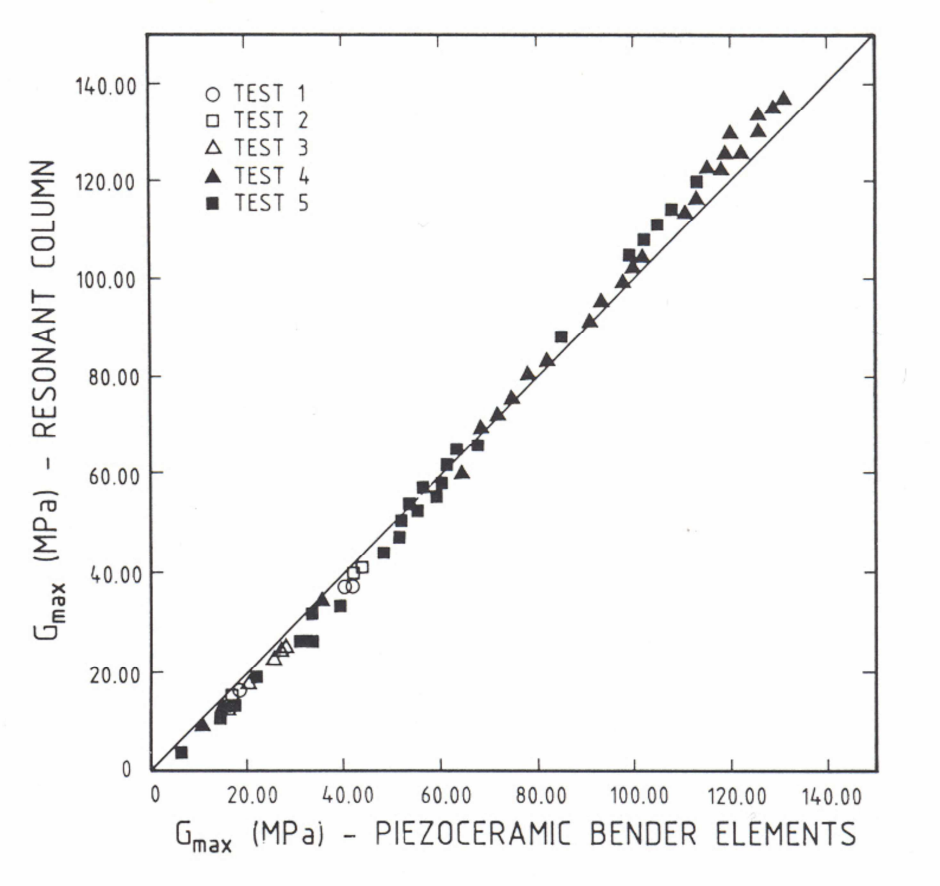



Figure 1.5 Comparison of the $G_{max}$ Measured Using Bender Elements and Resonant Column, [14]

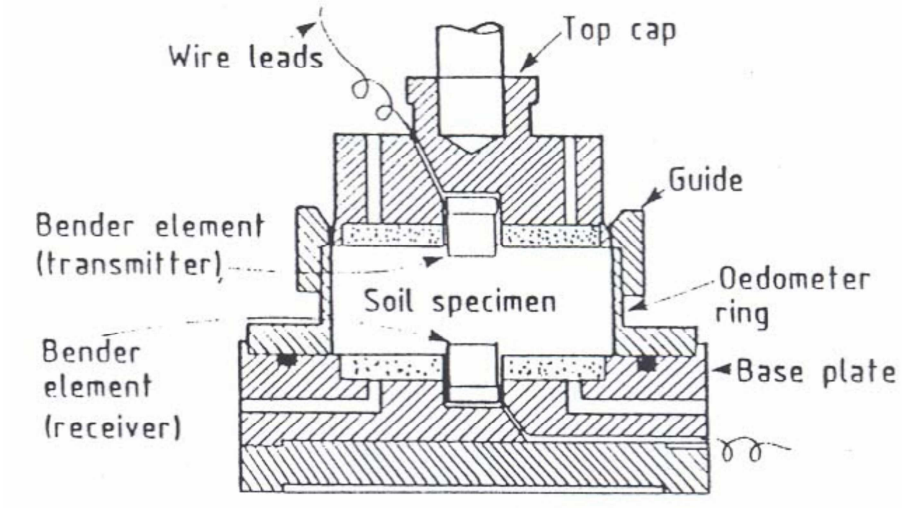



Figure 1.6 Oedemeter Adapted with Bender Elements, [15]

Brignoli et al. [5] developed an instrumented cyclic triaxial chamber with piezoelectric discs as compression wave transducers and two types of shear wave transducers (bender element and shear plate), as shown in Figure 1.7

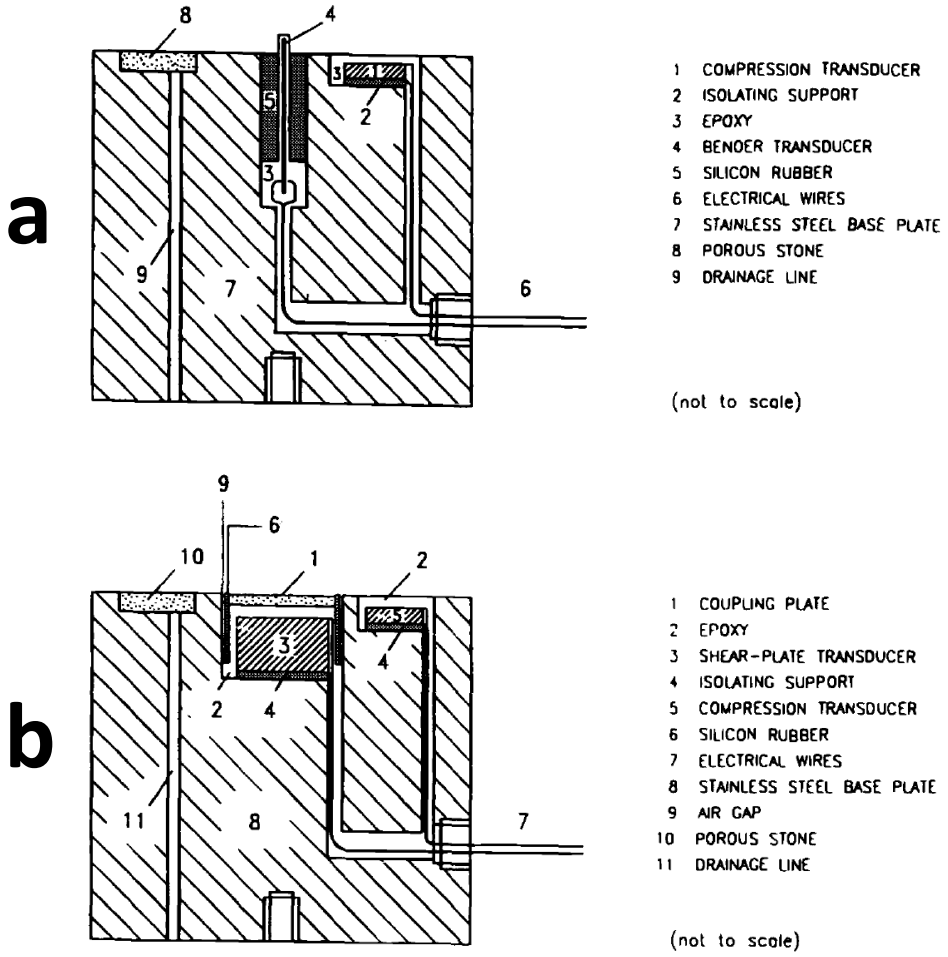



Figure 1.7 (a) Base Pedestal with Compression and Bender Transducers, (b) Base Pedestal with Compression and Shear Plate Transducers, [5]

Jovicic et al. [17] and Brignoli et al. [5] both focused on the phenomena relating bender element testing. Both explored the best way to interpret time domain results and both gave relevant consideration to near-field effect as a result of wave velocity dispersion. Figure 1.8 shows the six different received waveforms obtained by bender element and shear plate transducers, as well as the suggested selection of the arrival time for every case by Brignoli et al. [5].

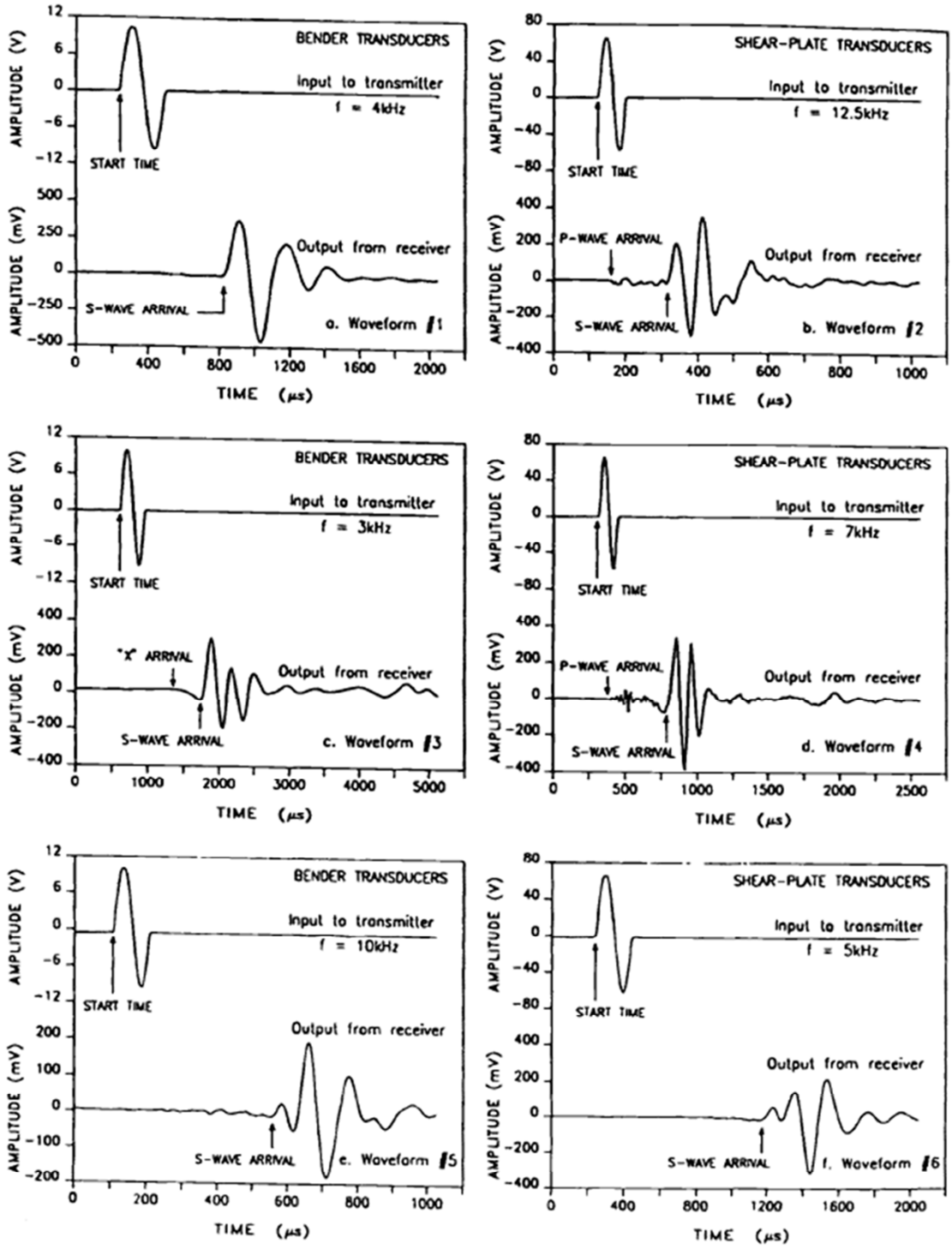



Figure 1.8 Typical Examples of Shear Wave Arrivals at Receiver for Bender Elements and Shear Plates, [5]

Jovicic et al. [17] also studied on the shape of the input signal and justified the use of an optimized sinusoidal pulse signal. Brignoli et al. [5] verified the results from bender element tests with those from tests by means of shear-wave transducers. Figure 1.9

presents comparison between $V_S$ values obtained from bender element, shear plate and resonant column by Brignoli et al. [5]. The soil specimen for this comparison was Ticino sand.

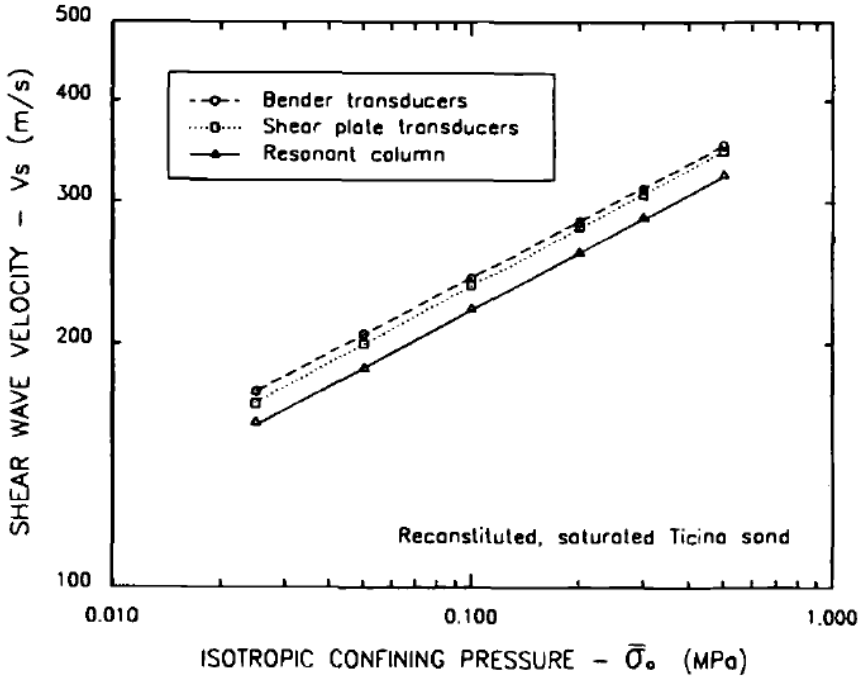



Figure 1.9 Comparison of Variations of the Vs with Confining Pressure Measured Using bender element, shear plate and resonant column, [5]

Kumar and Madhusudhan [18] presented a study on effect of relative density and confining pressure on Poisson ratio from bender and extender elements tests. It was noted that the magnitude of the Poisson ratio invariably decrease with an increase in the magnitude of effective relative density and confining pressure as illustrated in Figure 1.10 and Figure 1.11, [18].

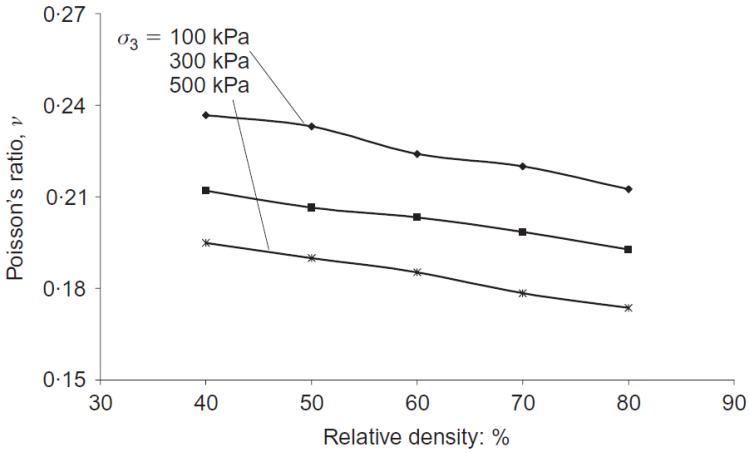



Figure 1.10 The Variation of the Poisson Ratio with Relative Density at Different Effective Confining Pressures for Medium-grained Sand, [18]

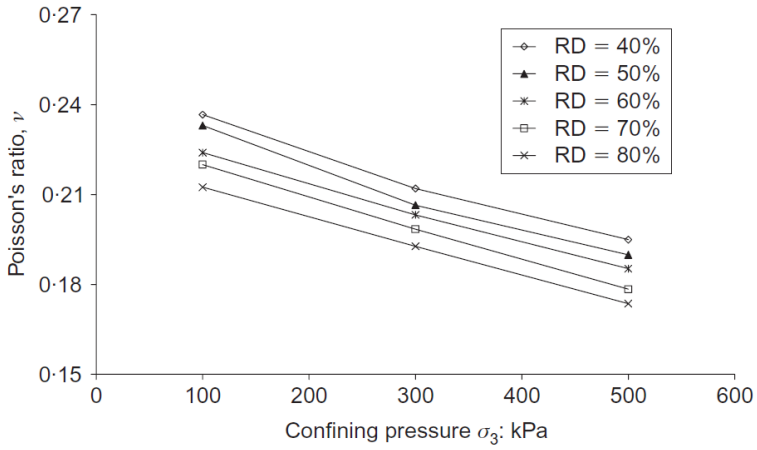



Figure 1.11 The Variation of the Poisson Ratio with Effective Confining Pressure at Different Relative Densities for Medium-grained Sand, [18]

## 1.2 Objective of the Thesis

Objectives in this research study are:

1. Development of piezoelectric transducers for use in the geotechnical laboratory's testing equipment for measuring the shear and compressional wave velocities in soil specimen by nondestructive method.
2. Sending and receiving signal and evaluating data on one platform. Using computer based card instead of function generator and digital oscilloscope for sending and receiving signal.
3. Incorporate the piezoelectric transducers in triaxial chamber.
4. Perform shear and compression waves velocity measurement at same specimen by using bender-extender transducer elements.
5. Monitoring changes of body wave velocities of sand during monotonic compression triaxial test.

## 1.3 Hypothesis

In the present note, an attempt has been made to determine both the P and S waves' velocities in dry and saturated sand samples with different relative densities and effective Stresses by using piezoelectric bender-extender elements in triaxial test apparatus.

# CHAPTER 2

# THEORETICAL BACKGROUND

## 2.1 Introduction

In normal working conditions, most part of the soil mass around a structure is subjected to small strains, less than 0.1%, with higher strains being achieved only locally, [2]. Besides, the relationship between strain and stiffness of soils is generally non-linear, [3]. Only at very small strains does the correlation between strain and stiffness behaves in a linear fashion. It is at these smaller strains that the shear stiffness reaches its maximum value, usually referred to as $G_0$ or $G_{max}$ (small-strain shear modulus). For this reason it is also known as small-strain shear stiffness. A characteristic soil strain-stiffness curve is presented in figure 2.1.

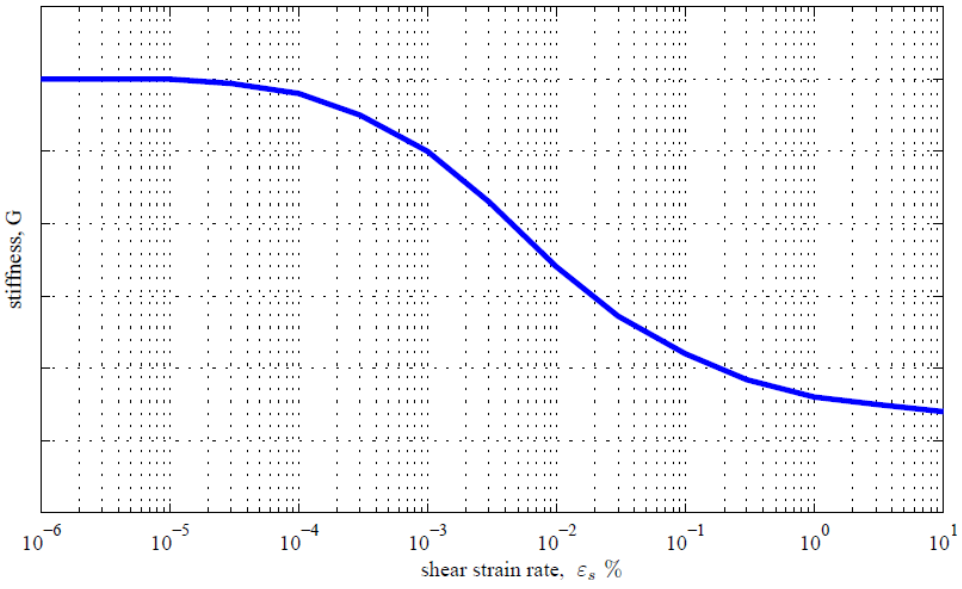



Figure 2.1 Characteristic strain-stiffness curve of soil's non-linear behavior [1]

When preparing a static or dynamic physical model of a geotechical structure it is relevant to take into account the non-linear behaviour of the soil. It is therefore necessary to obtain, among other properties of the medium, its small-strain shear stiffness, [19], [5]. Dyvik and Madshus [14] mentioned the relevance of using $G_{max}$ in the prediction of soil and soil-structures behavior during earthquakes, explosions, traffic vibration, machine vibration, wind loading and wave loading. In analysis where large strains are considered, the knowledge of $G_{max}$ is still relevant since it is one of the defining parameters when considering the soil's non-linear behaviour.

Stating the obvious, in order to obtain the small-strain stiffness, soils must be tested at small strains. Despite increasing precision from static test equipment such as local gauges, namely the use of LVDT (Linear Variable Differential Transformer), [20], [21], [22], dynamic methods remain the natural option to test at small and very small strain ranges, [3].

## 2.2 Piezoelectric Transducers

Bender-Extender elements are piezoelectric ceramic instruments used in laboratory geotechnical dynamic testing. A piezoelectric material changes its shape when a voltage differential of an electric signal is applied to it and generates electrical output when subjected to mechanical deformation, i.e., they generate a voltage differential when forced to bend. These transducers are generally used in pairs where one bender-extender element operates as a transmitter and the other as a receiver. The transmitting bender-extender element tip is generally embedded at one end of a soil sample and the receiving bender-extender element tip is, aligned with the transmitter, embedded at the other end. The transmitting bender-extender element transforms the input electric signal into a mechanical motion which disturbs the medium in which it is embedded. This disturbance propagates through the medium in the form of mechanical waves. Some components of these waves reach the other end of the sample where the receiving bender-extender element is at. Wave components with motion transversal to the receiving transducer's tip are capable of forcing it to bend, and consequently of generating an output electric signal. An example of a pair of bender-extender elements mounted on a triaxial-cell apparatus is presented in figure 2.2.

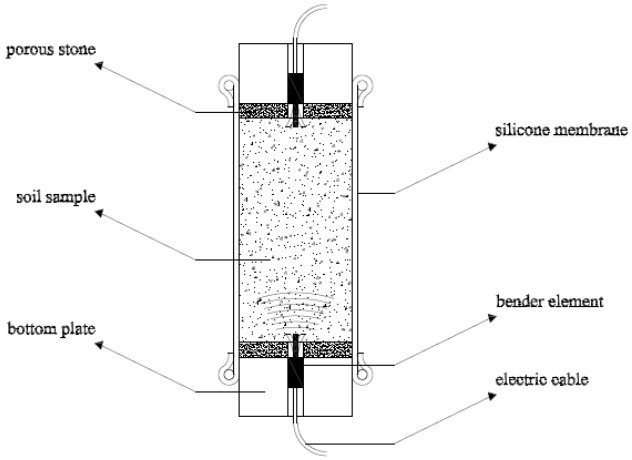



Figure 2.2 Pair of Bender-Extender Elements Mounted in Triaxial Test Apparatus, [45]

By comparing the input and output signals, it is possible to obtain the shear and compression wave velocity, which are characteristic of the medium. The characteristic shear and compression wave velocity can then be used to obtain the small-strain shear and constrained modulus of the medium, [23], as given by:

$$G_{max} = \boldsymbol{\rho} V_S^{\,2} \tag{1.1}$$

and

$$M_{max} = \boldsymbol{\rho} V_P^{\,2} \tag{1.2}$$

where $G_{max}$ is the small-strain shear modulus, $M_{max}$ is the small-strain constrained modulus, $\boldsymbol{\rho}$ is the medium's density, $V_S$ the characteristic shear wave velocity and $V_P$ the characteristic compression wave velocity.

Other dynamic methods such as the cross-hole method used in situ, and different piezoceramic transducers such as shear-plate transducers and compression-plate transducers used in laboratory can also be used to determine wave travel times, [5], [4]. Resonant columns are another laboratory dynamic device used to determine the shear-stiffness and the damping coefficient of the soil. Unlike the previous example, resonant columns use the torsional or flexural resonance frequency, rather than a wave velocity, to estimate the medium's properties, [24].

Arulnathan et al. [19] used a mini-hammer in a centrifuge model together with a number of accelerometers to determine the propagation velocity of shear waves in sand. The obtained results were in good agreement with equivalent bender element results

obtained for the same medium. AnhDan et al. [25] have also used accelerometers together with LVDT apparatus to obtain the small-strain stiffness of coarse soils.

In Audisio et al. [26] and Hope et al. [27], another example can be found of in situ dynamic testing, known as spectral analysis of surface waves, SASW. Using surface waves, more particularly Rayleigh waves, to test soil as done with the cross-hole method but with no need for bore-holes, makes the SASW testing method less expensive than the cross-hole method, [28].

The advantages of using bender elements are that they are relatively cheap and simple to manufacture. They can be used on their own or can easily be integrated into existing and common geotechnical equipment such as triaxial cells, oedometers or direct shear apparatus, [29], [30]. In this way it is possible to dynamically test soil samples under controlled load conditions, [31]. They can be used together with other dynamic test apparatus such as the resonant column, as done by Connolly and Kuwano [32].

Piezoelectric elements versatility allows them to be wired so as to operate both as a bender and an extender, enabling the detection of compression waves as well as of shear waves, as done by Lings and Greening [33] and later followed by Dano et al. [34] and Leong et al. [35]. A modification can make to the piezoelectric element to produce a bender-extender element capable of transmitting and receiving both S-waves and P-waves. The necessary modification is a three-wire configuration and then matching it with the corresponding type of polarization. Lings and Greening [33] further suggested that using a single pair of bender–extender elements enables both S-wave and P-wave velocity measurements to be made over exactly the same soil path, which facilitates the determination of the arrival of the S-wave, especially when it is obscured by the near-field effect. Lings and Greening [33] have also performed some preliminary testing on dry sand specimens to validate the use of bender–extender elements. The results showed that a single pair of bender–extender elements can successfully detect both shear and compression waves under various confining pressures. When testing saturated soils, compression wave are able to propagate at a faster velocity through the relatively incompressible fluid, which might interfere with the detection of the media characteristic compression wave velocity, [33].

## 2.3 Wave propagation in soils

Any disturbance in a soil deposit creates elastic stress waves that propagate through the deposit in all directions away from the disturbance. Stress waves are considered in the elastic range due to the small straining (recoverable) imposed to the media by the propagation of the wave.

Basically, stress waves can be classified as body waves and surface waves, depending on the requirement of an exposed surface (or interface) for the wave to exist. Waves propagating through the interior of the medium are called body waves and waves propagating along the surface of the medium are known as surface waves. In the case of an unbounded medium, waves can propagate as compression or shear waves. Compressional waves are in fact, the variation with time from compression to dilatational motions as illustrated in Figure 2.3a. In contrast, propagation of shear wave generates distortion of the medium as presented in Figure 2.3b.

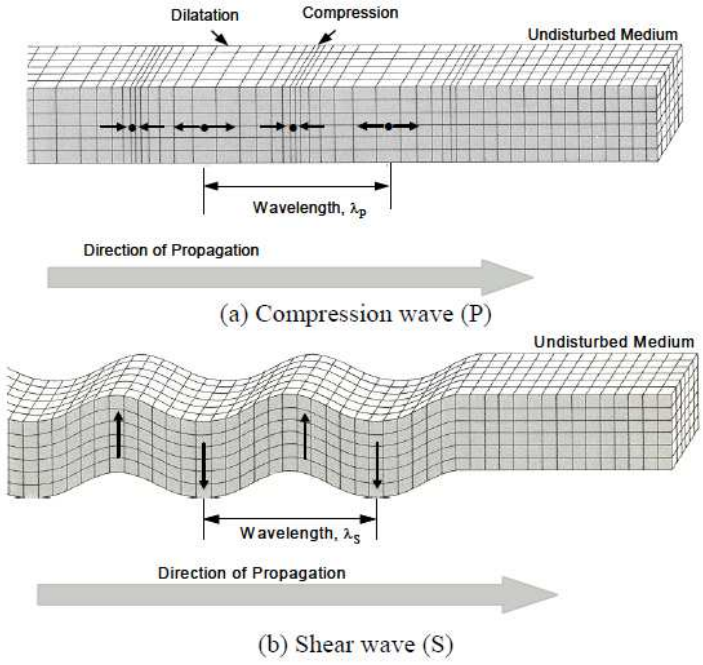



Figure 2.3 Body Wave Propagating within a Uniform Infinite Medium: (a) Compression Waves, (b) Shear Waves [36]

On the other hand, wave propagation in rods or bars represents an example of propagation in bounded medium. This situation is especially convenient for addressing geometrically the study of wave propagation in soil specimens. Furthermore, wave

propagation in rods can occur in three different manners: longitudinal (compression), torsional (shear) and lateral (flexural). These three types of waves generated in rods are shown in Figure 2.4.

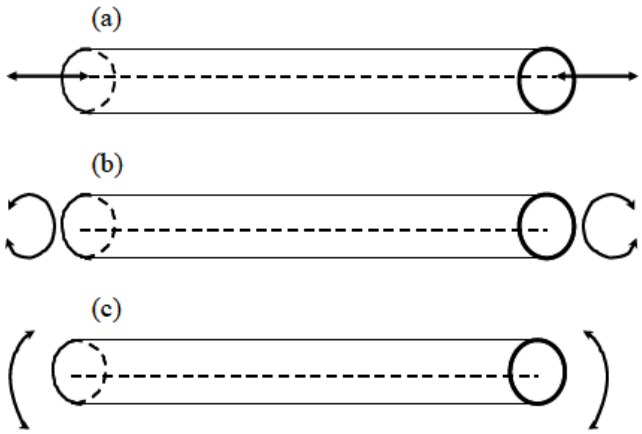



Figure 2.4 Type of Vibration in Rods: (a) Longitudinal, (b) Torsional, (c) Flexural [37].

### 2.3.1 Compression Wave Velocity

The particle motion of a compression wave, also called a primary or "P" wave, occurs along the direction of wave propagation as shown in Figure 2.3a.

$$\frac{\partial^2 u_x}{\partial t^2} = \frac{M}{\rho}\frac{\partial^2 u_x}{\partial x^2} \tag{2.1}$$

Where: $u_x$ is the particle motion in x direction, t is the time, M is the constrained modulus (which is valid only if no straining exists in y and z directions), and ρ is the mass density of the medium.

The solution of Equation 2.1 is presented in Equation 2.2 as follows:

$$u_x = Ae^{i(\omega t \pm \kappa x)} \tag{2.2}$$

Where: A is the maximum amplitude of the compression motion, ω is the angular frequency (ω = 2π/T), T is the period, κ is the wave number (κ = 2π/ λ), λ is the wavelength, and i is equal to$\sqrt{-1}$.

By substituting Equation 2.2 into Equation 2.1, the expression defined by Equation 2.3 is:

$$\frac{\omega}{\kappa} = \sqrt{\frac{M}{\rho}} \tag{2.3}$$

The ω/κ ratio is also defined as the ratio between the wavelength and the period (λ/T). Additionally, λ/T is equal to the distance of one cycle in space divided by the period or time of every cycle. In other words, the ratio λ/T represents the velocity that the wave travels through the medium. The frequency of a wave (f) is simply the inverse of its period (T), therefore, it is obtained that the constrained compression wave (Vp) is:

$$V_P = f\lambda = \sqrt{\frac{M}{\rho}} \tag{2.4}$$

It is important to point out the statements previously mentioned about the validity of relating the constrained modulus (M) and Vp depends entirely on the absence of lateral straining of the medium.

### 2.3.2 Shear Wave Velocity

The particle motion of a shear wave, also called secondary or "S" wave, is perpendicular to the direction of wave propagation, as illustrated in Figure 2.3b. Just as in the compression-wave case, the wave equation defines the particle's motion in distortional vibrations for an unbounded elastic medium, as expressed by Kolsky [38]:

$$\frac{\partial^2 u_y}{\partial t^2} = \frac{G}{\rho}\frac{\partial^2 u_y}{\partial x^2} \tag{2.5}$$

Where: $u_y$ is the particle motion in y direction while the wave is traveling in the x direction, t is the time, G is the shear modulus, and ρ is the mass density of the medium.

Equation 2.5 is solved in the same fashion as the wave equation for compression waves and likewise, its solution is expressed as:

$$u_y = Ae^{i(\omega t \pm \kappa x)} \tag{2.6}$$

By substituting Equation 2.6 into Equation 2.5, the relationship for ω/κ is:

$$\frac{\omega}{\kappa} = \sqrt{\frac{G}{\rho}} \tag{2.7}$$

and hence shear wave velocity (Vs) is:

$$V_S = f\lambda = \sqrt{\frac{G}{\rho}} \tag{2.8}$$

It is important to note that the shear wave velocity in an unbounded medium is exactly the same as the shear wave velocity in torsional waves in rods (Figure 2.4b). In other words, the shear wave velocity is independent of lateral boundary constraint because it does not create expansion or contraction perpendicular to the direction of the wave propagation.

### 2.3.3 Poisson's Ratio

Poisson's ratio (ν) is the ratio between the horizontal and vertical axial strains in uniaxial loading ($\varepsilon_x$ and $\varepsilon_y$, respectively) as:

$$\nu = \frac{\varepsilon_x}{\varepsilon_y} \tag{2.9}$$

$\varepsilon_x$ Is the axial horizontal strain and $\varepsilon_y$ is the axial vertical strain. Poisson's ratio (ν) can be calculated from the primary and secondary elastic wave velocities. The relationship between ν and $V_S$ and $V_P$ is established using one of the equivalences among ν with other elastic constants as:

$$\nu = \frac{3K-2G}{2(3K+G)} \tag{2.10}$$

G is the shear modulus and K is the bulk modulus. The bulk modulus (K) is defined as the ratio of the isotropic stress ($\sigma_0$) over the volumetric strain ($\varepsilon_v$) and is represented mathematically by:

$$K = \frac{\sigma_0}{\varepsilon_V} = \frac{\sigma_0}{\varepsilon_x+\varepsilon_y+\varepsilon_z} \tag{2.11}$$

This "$\varepsilon_v = \varepsilon_x + \varepsilon_y + \varepsilon_z$" simplification is only valid for small strains.

By using Equation 2.4, that defines the compression wave velocity in terms of the constrained Modulus (M), it is possible to substitute M by its equivalence based on the Bulk Modulus (K) and Shear Modulus (G) as:

$$V_P = \sqrt{\frac{M}{\rho}} = \sqrt{\frac{K+\frac{4}{3}G}{\rho}} \tag{2.12}$$

The relationship between $V_P$ and G was established in Equation 2.8. Thus, substituting Equations 2.8 and 2.12 into Equation 2.10 leads to:

$$\frac{V_P}{V_S} = \sqrt{\frac{2(1-\nu)}{(1-2\nu)}} \tag{2.13}$$

Equation 2.14 can be used to evaluate Poisson's ratio (ν) from primary and secondary wave velocities as:

$$\nu = \frac{2-\left(\frac{V_P}{V_S}\right)^2}{2-2\left(\frac{V_P}{V_S}\right)^2} \tag{2.14}$$

## 2.4 Wave Travel Distance

Determination of wave travel time and travel distance is necessary to calculate wave velocity in bender-extender element tests. Wave travel distance is easier one to determine. Shirley and Hampton [12] simply referring to it as the distance between the transducers. Dyvik and Madshus [14], followed by Brignoli et al. [5] and Viggiani and Atkinson [31] have proposed and justified the measurement of travel distance as the minimum distance between transducer tips, also known as tip-to-tip distance. The tip-to-tip travel distance is commonly assumed by a variety of authors, for instance Kuwano et al. [39], Dano and Hicher [40], Kawaguchi et al. [41] or Pennington et al. [42].

Dyvik and Madshus [14] compared the dynamic results from three different clay samples, using the resonant column and bender element tests. They observed that the results from the bender element test fitted best the resonant column results for travel distances measured tip-to-tip. Viggiani and Atkinson [31] used bender elements to test 3 samples with different heights, between 35mm and 85mm. For each sample, three travel time estimates were obtained for different stress states using square and sinusoidal pulse signals. The chosen linear relationship between the results from different samples, at similar stress states, indicates the correct travel distance to be the tip-to-tip distance. Brignoli et al. [5] also came to the conclusion that the correct travel distance must be

measured between two tips. Samples with different heights were tested with bender elements as well as with shear-plates which support his conclusion.

Alternatives to the tip-to-tip travel distance are not commonly proposed. Fam and Santamarina [43] used the distance between mid-embedded height but did not justify it.

## 2.5 Wave Travel Time

Three are different methods for determining wave's time of travel from transmitter to receiver. Two direct methods that used widely describe here:

### 2.5.1 First Time of Arrival

The first time of arrival refers to the time ($t_0$) between the start of the source signal and the start of the major cycle of the receiver signal by ignoring the initial portion of the weak signal (present if any), [44], (see Figure 2.5).

### 2.5.2 First Peak to Peak Time

In the first peak to peak method, the time of arrival refers to the time between ($t_{PP}$) the peak of the source signal and the first peak of the cycle of the receiver signal, ignoring the presence of initial weak portion of the curve), [44], (see Figure 2.5).

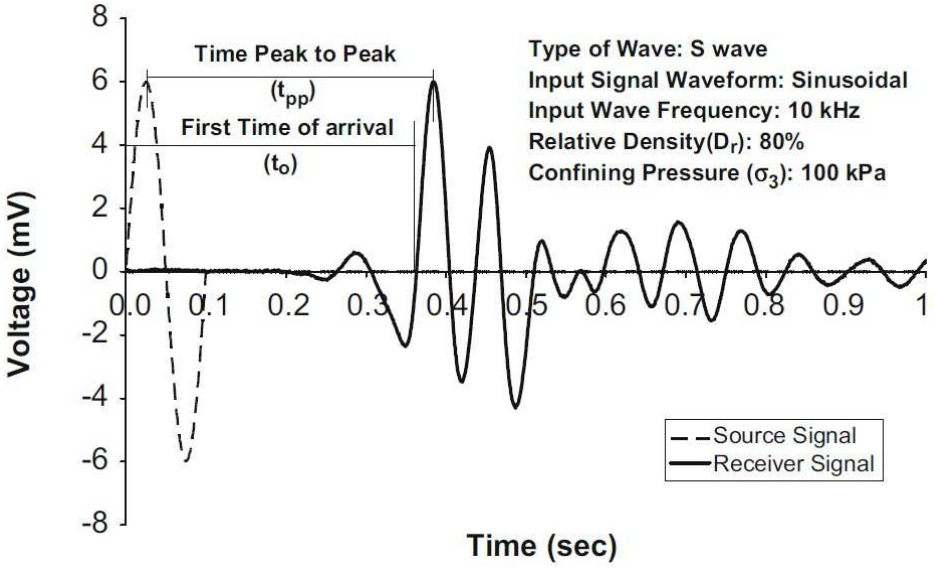



Figure 2.5 first time of arrival ($t_0$) and the time between first peak to peak ($t_{PP}$), [44]

## 2.6 Noise

Using bender-extender elements in dynamic testing required transmitting and receiving signals that involves electronic equipment to send, receive and proses electric signals. All of the electric circuit involved in the test set-up is potentially capable of picking up noise from the environment such as electro-magnetic signals. The bender-extender elements can serve as receivers of any residual vibration that might reach them, not only the vibration intended by the controlled excitation of the sample. As for example the vibrations from nearby roads traffic, people walking in or near the lab, other nearby test apparatus, any form of sound, etc. For these reasons, different forms of noise can be, and were indeed present in the laboratory work conducted. Three distinct sources of noise were distinguished during most of the experimental tests. These noises were classified as background electro-magnetic noise, residual vibrations and cross-talk.

### 2.6.1 Background Noise

Background noise from electro-magnetic signals is omnipresent in normal urban environments such as the one found at the civil engineering laboratories. Because the electric circuit is quite extensive, no reasonable amount of secondary grounding circuit was capable of preventing some amount of electro-magnetic noise from being picked up. It was picked up at amplitudes of 10 to 30mV which makes its presence quite significant in the received signal and insignificant in the transmitted signal. This type of background noise, when compared with the transmitted and received signals, is random in nature and can therefore be eliminated by consistently averaging the results, [45]. This procedure used to eliminate background noise.

### 2.6.2 Residual Vibration

Residual vibration is also noticeable in the received signal. Main reason of this kind of noise is other working test apparatus vibration in the lab. Noticeable vibration from the building structure due to students and staff walking by is also present. As with electro-magnetic background noise, this type of disturbance is random in nature, thus the same process of averaging the received signal results is valid to eliminate it, [45].

### 2.6.3 Cross-Talk

Cross-talk is a leakage from transmitted signal into the received signal (see Figure 2.6b). Santamarina [46] has frequently mentioned electromagnetic coupling phenomena related with bender element testing. These happened when the transmitting and receiving bender elements placed into a conductive medium, such as a water saturated soil. The transmitted electric signal is potentially capable of reaching the received bender element by being electrically conducted through the sample water almost instantaneously. An example of electromagnetic coupling is explored by Lee and Santamarina [47] and associated with the different wiring of the transducers. The solution for this type of cross-talk involves the proper grounding of the bender-extender element pair.

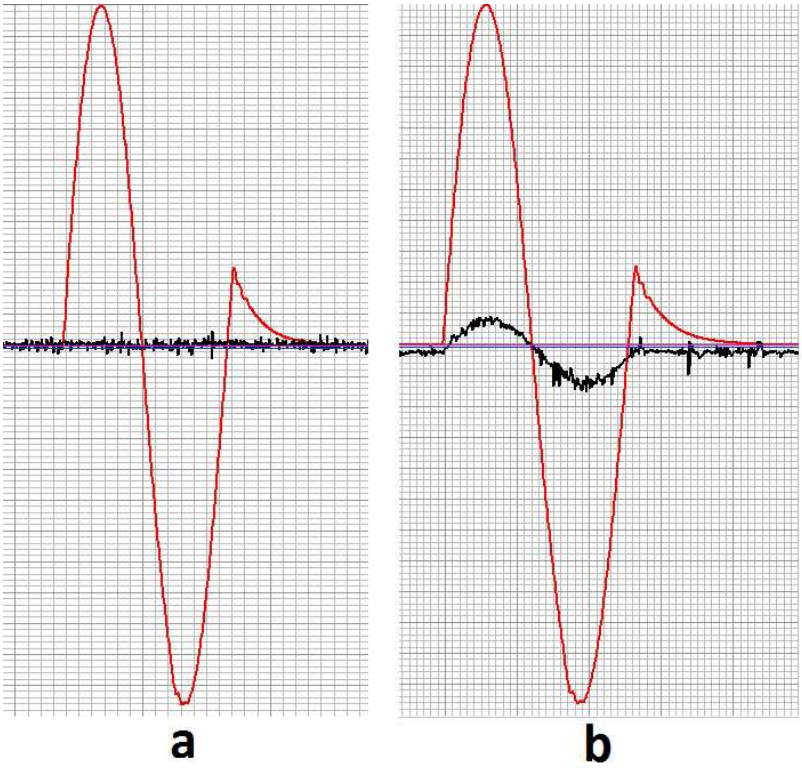



Figure 2.6 (a) Proper Grounding, without Cross-talk, (b) Poor Grounding, With Cross-talk, (Red line is transmitted signal and blue line is received signal)

## 2.7 Near Field Effect

The frequency dependent shear wave motion due to the P-wave interference (near field travelling at Vp) is termed as the near field effect, [44]. The presence of the near field effect affects the shape of the received signal and it creates a difficulty in finding

correctly the arrival of the shear wave in the bender elements tests, [5], [33], [13], [17], [42], [48], [47], [49], [50].

Jovicic et al. [17] indicated that the near field effect can be brought down by increasing the frequency of the input signal. In the existing literature, most of the bender elements tests have been done at a frequency lesser than 10 kHz, [48]. Near field effects are generally quantified in terms of the ratio of the wave path length (L) to the wave length ($\lambda$), [13]. For a given wave velocity, the wave length decreases continuously as the frequency increases. Theoretical analyses performed by Sanchez- Salinero et al. [49] showed that the near field effects remain significant when the value of $L/\lambda$ is less than unity and it was shown that the shape of the receiver signal will not be masked by the near field effects if this ratio is kept greater than 2. Arulnathan et al. [50], however, demonstrated that the receiver signal deteriorated as this ratio is increased and it was stated that this ratio should be greater than 1. Pennington et al. [42] found that this ratio needs to be between 2 and 10. Leong et al. [48] also used a 16 kHz signal and it was reported that this ratio should be greater than at least 3.33.

## 2.8 Strain Level

In normal working conditions most foundation structures causes strains lower than 0.1% to large volumes of the affected ground soil, only locally are higher strains achieved, [2]. Besides, soil has a non-linear elastic behavior where at small strains the stiffness is significantly higher than for larger strains, [3].

In situ soil testing, measuring strains above $10^{-1}$%, does not offer the capability of determining soil stiffness at lower strain levels. In terms of laboratory testing, static methods such as local gauges have a limited precision that does not allow them to measure strains lower than $10^{-3}$% for which a maximum stiffness can generally be obtained. Dynamic laboratory testing is then left as the single option to obtain measurements for the lowest strains, $\varepsilon < 10^{-2}$%, of which bender elements are a suitable example [51].

In terms of the shear strain levels involved in the use of bender elements, Dyvik and Madshus [14] estimated the transmitting transducer to be in the range of $\varepsilon \approx 10^{-3}$%. Leong et al. [48] estimated the strain level of the receiving bender element to be in the

range of $\varepsilon \approx 10^{-4}\%$, when touching the transmitting bender element. There is another estimate of strain level in the range of $\varepsilon \approx 10^{-4}\%$, given by Pennington [52].

## 2.9 The Behavior of Sands in Triaxial Test

Figure 2.7 and Figure 2.8 show typical triaxial test data obtained from standard drained and undrained compression tests performed by Eldin [53] on loose sand dense samples of Brasted sand. Information about behavior of sands of this section is after Atkinson and Bransby [54].

A cursory glance at Figures 2.7 and 2.8 will indicate the large differences in behavior between the four samples. The drained test on loose specimen (Figure 2.7b) gives a $q'$: $\varepsilon_a$ curve which reaches a flat maximum after about 20 per cent axial strain, while the sample compresses substantially as the test proceeds. At the end of the test, the sample appears to have reached an ultimate state, for there are negligible changes in stresses or in volume for continuing shear distortion.

In contrast, the dense sample (Figure 2.7a) exhibits a marked peak in its $q'$: $\varepsilon_a$ curve, and, thereafter, $q'$ decreases and is still decreasing at the end of the test. The sample contracts slightly initially, but then expands strongly until the end of the test. It is clear that no ultimate point has been reached at the end of the test, for this sample is still expanding and $q'$ is decreasing. It is worth noting, however, that the value of $q'$ at the end of test on the dense specimen seems to be decreasing toward the value (about 500 $kN/m^2$) observed at the ultimate point of the test on the loose specimen (Figure 2.7b).

The shape of the $q'$: $\varepsilon_a$ curves for the undrained tests (Figure 2.8), one on the medium dense specimen and one on a loos specimen that consolidated with similar stresses show very different values of $q'$ at failure. The pore water pressure changes at failure in the two tests are strikingly different; the loose specimen has a positive pore water pressure at failure, while the pore water pressure is large and negative for the medium dense specimen. The difference in pore water pressure at failure is the major cause of the large difference in the observed shear strength of two specimens, for the effective radial stress at failure in the dense specimen ($\sigma_r'$=550 $kN/m^2$) is substantially larger than that for the loose specimen ($\sigma_r'$=62 $kN/m^2$); the ratios of $\sigma_a'/\sigma_r'$ (3.3 and 3, respectively) are, however, almost the same for the two cases.

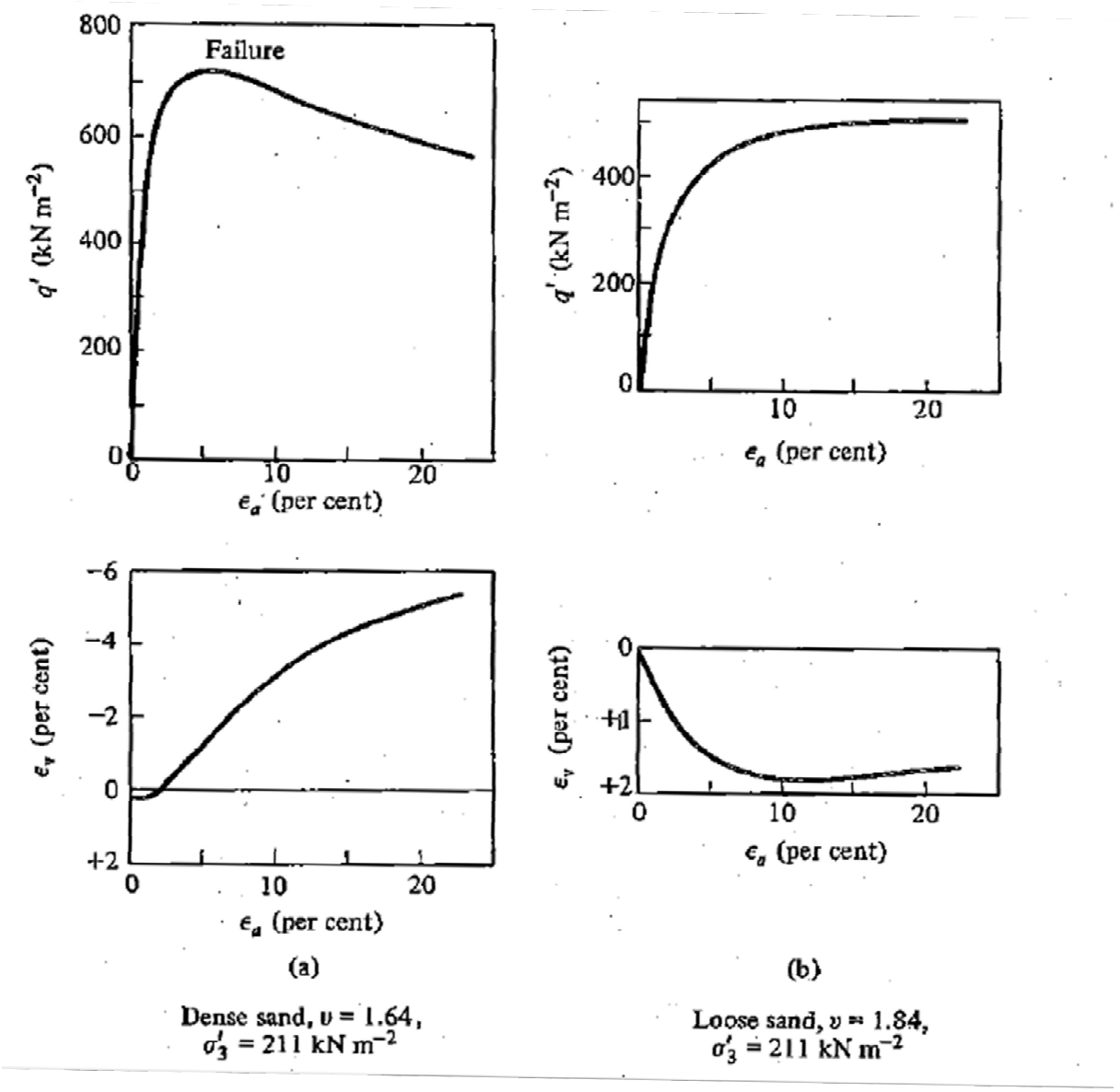



Figure 2.7 The Results of Drained Triaxial tests on (a) A Dense and (b) A Loose Sample of Brasted Sand, [55]

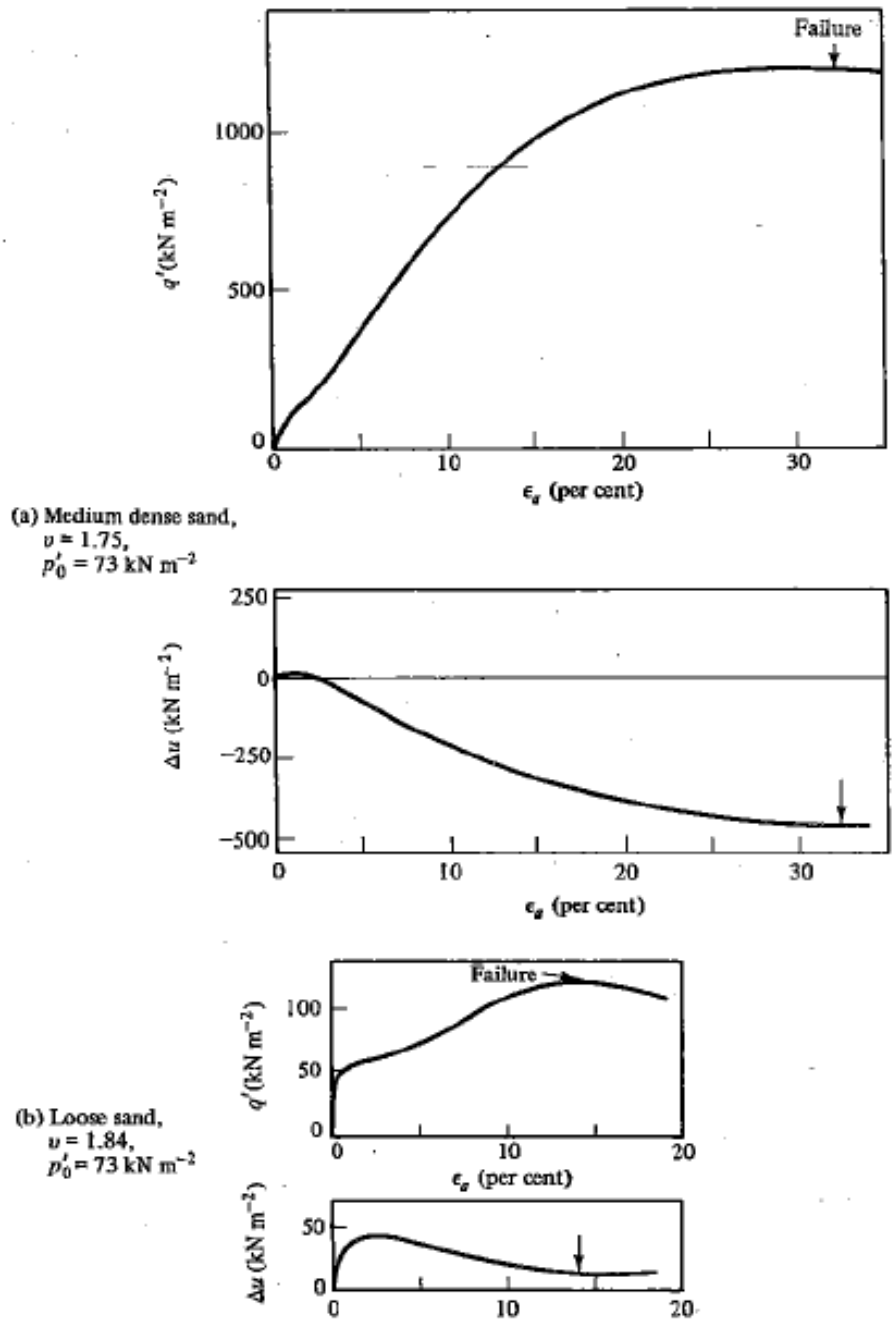



Figure 2.8 Data from Undrained Triaxial Tests on (a) Medium Dense and (b) Loose Samples of Brasted Sand, [55]

# CHAPTER 3

# PIEZOELECTRIC ELEMENTS

## 3.1 Introduction

Piezocelectric transducers are made of piezoceramic material. These transducers convert one form of energy to another. Piezo motors convert electrical energy to mechanical energy, and piezo generators convert mechanical energy to electrical energy. In most cases the same element can be used to perform either task. This means when a piezoelectric transducer is electrically stressed by a voltage, its dimensions change. When it is mechanically stressed by a force, it generates an electric charge. If the electrodes are not short-circuited, a voltage associated with the charge appears. A piezoelectric transducer is therefore capable of acting as either a sensing or transmitting element or both. These piezoelectric elements can be wired using two types of series and parallel configuration. By using a three-wire configuration on 2-layer elements, these elements can be used as both bender and extender element that called bender–extender elements. Most information about piezoelectric elements of this section is from the website of Piezo System, Inc. [56].

## 3.2 Single Layer Piezo Motors

Piezo motors convert voltage and charge to force and motion. When an electric field having the same polarity and orientation as the original polarization field is placed across the thickness of a single sheet of piezoceramic, the piece expands in the thickness or “longitudinal” direction (i.e. along the axis of polarization) and contracts in the transverse direction (perpendicular to the axis of polarization). This is represented in Figures 3.1. When the field is reversed, the motions are reversed. Sheets and plates

utilize this effect. However, the motion of a sheet in the thickness direction is extremely small (on the order of tens of nanometers). On the other hand, the transverse motion along the length is generally larger (on the order of microns to tens of microns) since the length dimension is often substantially greater than the thickness.

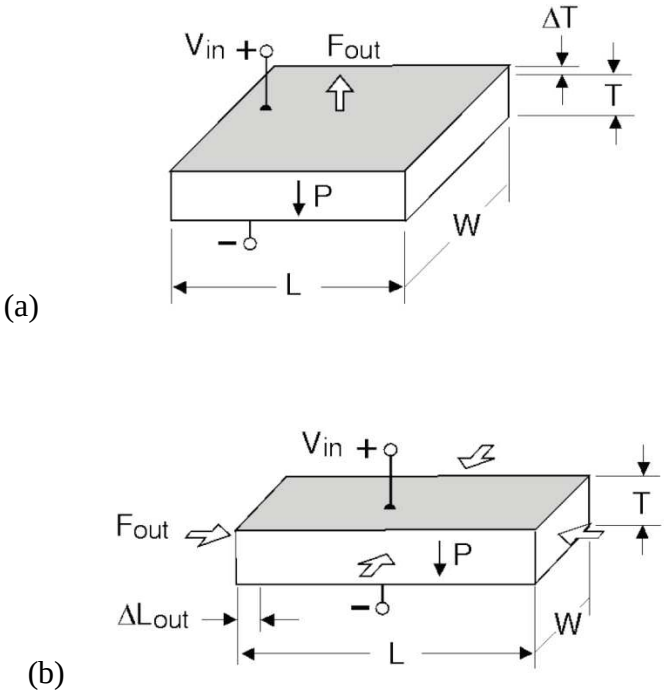



Figure 3.1 (a) Longitudinal Motor, (b) Transverse Motor, Contracting [56]

### 3.3 Single Layer Piezo Generators

Piezo generators convert force and motion to voltage and charge. When a mechanical stress is applied to a single sheet of piezoceramic in the longitudinal direction (parallel to polarization), a voltage is generated which tries to return the piece to its original thickness (Figure 3.2a). Similarly, when a stress is applied to a sheet in a transverse direction (perpendicular to polarization), a voltage is generated which tries to return the piece to its original length and width (Figure 3.2b). A piezo sheet bonded to a structural member which is stretched or flexed will induce electrical generation.

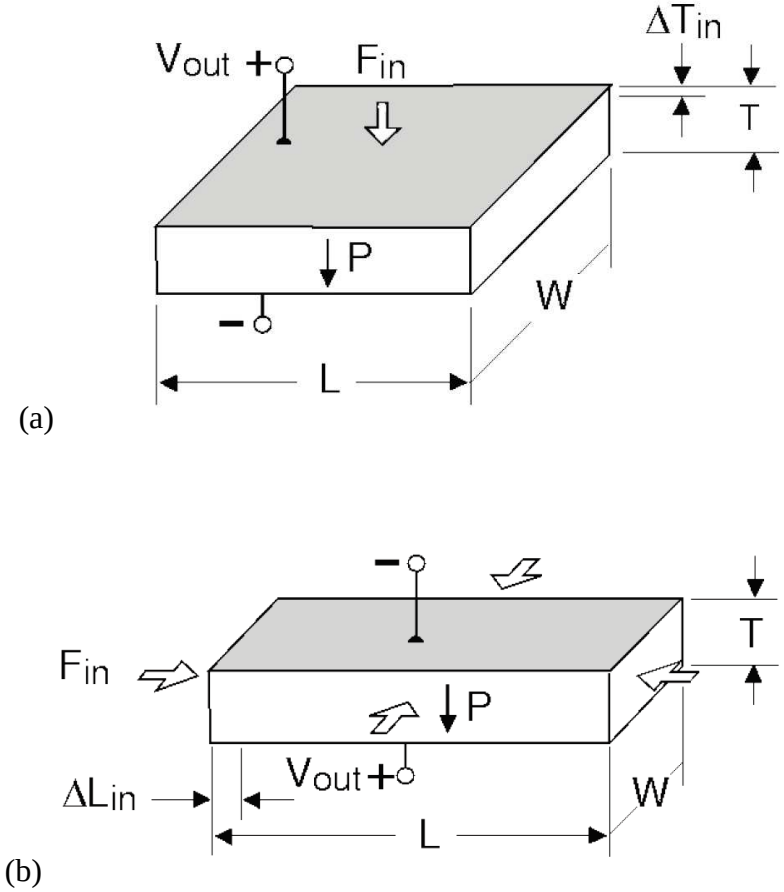



Figure 3.2 (a) Longitudinal Generator, (b) Transverse Generator, Compressed on sides [56]

### 3.4 2-Layer Elements

Two-layer elements can be made to elongate, bend, or twist depending on the polarization and wiring configuration of the layers.

A center shim laminated between the two piezo layers adds mechanical strength and stiffness, but reduces motion. “2-layer” refers to the number of piezo layers. The “2-layer” element actually has nine layers, consisting of: four electrode layers, two piezoceramic layers, two adhesive layers, and a center shim (see Figure 3.3). The two layers offer the opportunity to reduce drive voltage by half when configured for parallel operation.

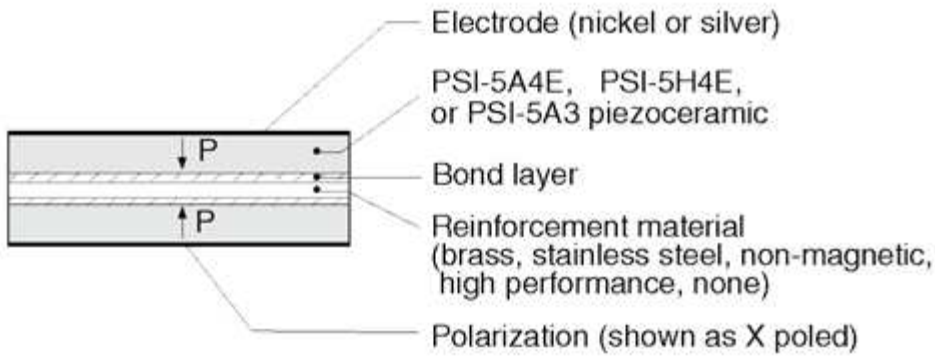



Figure 3.3 Two-Layer Element Structure [56]

## 3.5 Bender Element

### 3.5.1 Bending Motor (Transmitter)

A 2-layer element produces curvature when one layer expands while the other layer contracts. These transducers are often referred to as benders, bimorphs, or flexural elements. Bender motion on the order of hundreds to thousands of microns, and bender force from tens to hundreds of grams is typical. By changing the direction of the electric field continuously, the direction of the curvature of the element deformation will change continuously. Thus, the element will vibrate and work as a wave generator.

### 3.5.2 Bending Generator (Receiver)

When a mechanical force causes a suitably polarized 2-layer element to bend, one layer is compressed and the other is stretched. Charge develops across each layer in an effort to counteract the imposed strains. This charge may be collected as received signal.

## 3.6 Extender Element

### 3.6.1 Extension Motor (Transmitter)

A 2-layer element behaves like a single layer when both layers expand (or contract) together. If an electric field is applied which makes the element thinner, extension along the length and width results typically only motion along one axis is utilized. Extender motion on the order of microns to tens of microns, and force from tens to hundreds of Newton is typical.

### 3.6.2 Extension Generator (Receiver)

When a mechanical stress causes both layers of a suitably polarized 2-layer element to stretch (or compress), a voltage is generated which tries to return the piece to its original dimension. Essentially, the element acts like a single sheet of piezo. The metal shim sandwiched between the two piezo layers provides mechanical strength and stiffness while shunting a small portion of the force.

## 3.7 Elements Polarization

There are two types of piezoelectric elements, x-poled and y-poled (Figure 3.4), which differ with respect to their direction of polarization. The x-poled piezoelectric element refers to the condition where the directions of the polarization for each of the two layers are pointing in opposite directions, generally towards each other. The y-poled piezoelectric element refers to the condition where the directions of the polarization for each of the two layers are pointing in the same direction.

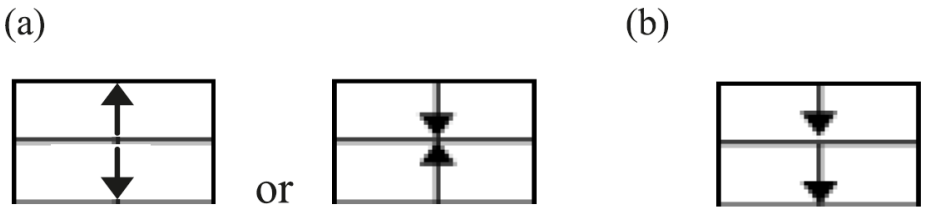



Figure 3.4 Types of Piezoelectric Elements: (*a*) x-poled; (*b*) y-poled [35]

## 3.8 Series and Parallel Wiring Configuration

Two-layer piezoelectric elements can be wired using two types of configuration, series and parallel. In the series configuration, the excitation voltage is applied across the two piezoceramic layers at once, as seen in Figures 3.5*a* and 3.6*b*. In the parallel configuration, the excitation voltage is applied to the piezoceramic layers and the center shim as seen in Figurs 3.5*b* and 3.6*a*. To transmit and (or) receive a S-wave and hence, act as a bender, the x-poled and y-poled piezoceramic elements have to be connected in series and parallel configuration, respectively, ( see Figure 3.5). To transmit and (or) receive a P-wave and hence, act as an extender element, the x-poled and y-poled piezoceramic elements have to be connected in parallel and series configuration, respectively, (see Figure 3.6).

As the excitation voltage is applied to each of the piezoceramic layers, the motion sensitivity of the parallel configuration in terms of deflection per unit of applied voltage is greater by a factor of two as compared with the series configuration. In other words, for the same motion, the parallel configuration requires only half of the voltage needed for the series operation. Therefore, the parallel configuration is better suited as a transmitter as it gives a stronger mechanical motion for a given excitation voltage. However, the series configuration is better suited as a receiver as it gives a higher output voltage for a given mechanical excitation.

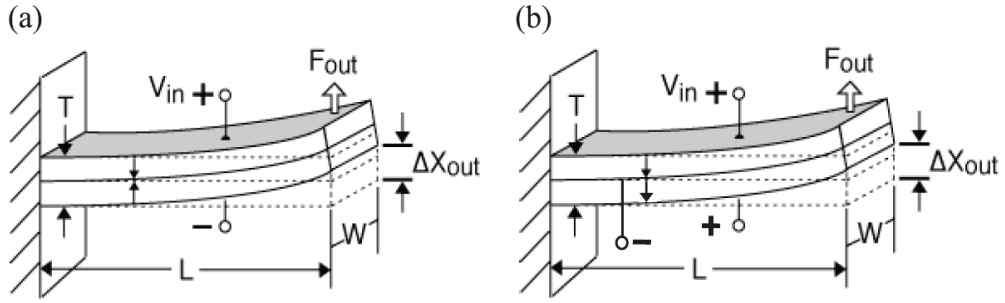



Figure 3.5 Bender element wiring configuration using (*a*) x-poled series and (*b*) y-poled parallel configurations, [56]

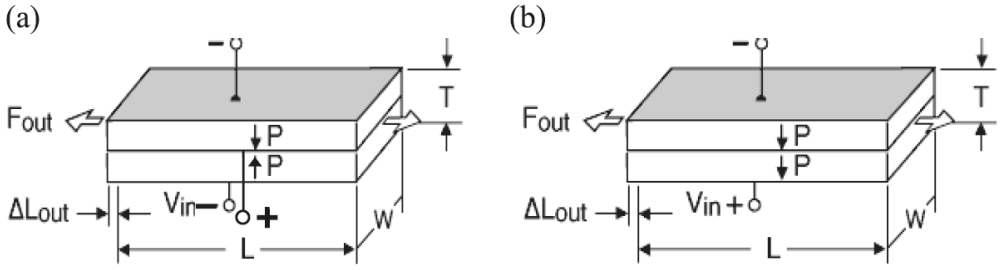



Figure 3.6 Extender element wiring configuration using (*a*) x-poled parallel and (*b*) y-poled series configurations, [56]

### 3.9 Application of Piezoelectric Elements

The piezoelectric elements have adaptive structure that has many engineering applications, such as control transducers for aerospace systems and health monitorings of structures.

The Piezoelectric elements enable geotechnical engineers to determine wave velocity through soil’s porous media and may be incorporated into other laboratory tests, such as resonant column, triaxial or odometer tests.

# CHAPTER 4

# TEST EQUIPMENT AND SAND SPECIMEN

Figure 4.1 shows all main test equipment used in this study.

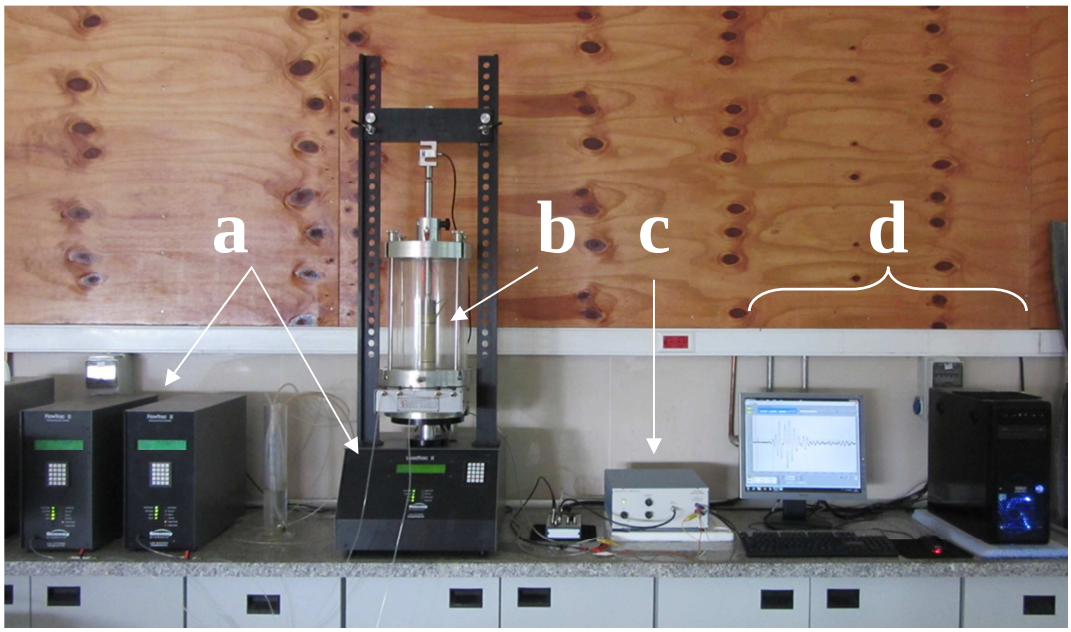



Figure 4.1 (a) Triaxial Test Apparatus, (b) New Triaxial Cell, (c) Linear Power Amplifier, (d) Data Acquisition System

## 4.1 Bender-Extender Elements

Bender-extender elements in this study are modified 2-layer piezoelectric elements with three-wire configuration wiring. This kind of element enables us to transmit and receive both p-waves and s-waves, as done by Lings and Greening [33] and later followed by Dano et al. [34] and Leong et al. [35].

The necessary modification is a three-wire configuration and then matching it with the corresponding type of polarization. Lings and Greening [33] further suggested that using a single pair of bender–extender elements enables both S-wave and P-wave

velocity measurements to be made over exactly the same soil path, which facilitates the determination of the arrival of the S-wave, especially when it is obscured by the near-field effect. Lings and Greening [33] have also performed some preliminary testing on dry sand specimens to validate the use of bender–extender elements. The results showed that a single pair of bender–extender elements can successfully detect both shear and compression waves under various confining pressures.

### 4.1.1 Element Type and Specification

The piezoelectric elements used in this study are types T220-A4-303X and T220-A4-303Y from Piezo System, Inc. (see Figure 4.2). The dimensions for the 303 series are 31.8mm, 12.7mm, 0.51 mm (See Figure 4.3a For Comparison).

**TRANSDUCER PART NUMBERS** — OPTIONS LISTED IN COLUMNS UNDER HEADINGS

| T | 2 | 20 | - | A4 | | - | 303 | X | |
|---|---|---|---|---|---|---|---|---|---|
| Mounting Styles | Number of Piezo Layers | Thickness Designation | | Piezoceramic Materials | Reinforcement Materials | | Size Designation | Polarization | Intended Use |
| T - Transducer Only<br><br>No Mount<br>No Wires | 2 | 15 (.015")<br>16 (.016")<br>19 (.019")<br>20 (.020")<br>23 (.023")<br>26 (.026")<br>34 (.034") | | -A4 PSI-5A4E<br>-H4 PSI-5H4E<br><br>-A3 PSI-5A3 | (blank) - Standard Brass Shim<br>SS - High Strength Stainless Steel<br>NM - Non-magnetic<br>CL - High Performance<br>NO - No shim | | -103<br>-203<br>-303<br>-503 | X-Poled<br><br>Y-Poled | Not used for Transducer Elements |

Figure 4.2 Transducer Part Number, [56]

In series operation our bender-extender elements have an input limit of ±180V and in parallel operation input limit is ±90V. As we use parallel connection for transmitter element ±90V amplitude is used for sending signals.

### 4.1.2 Wiring

Piezoelectric elements are sensitive pieces and need great care during modification. In order to modify piezoelectric element (see Figure 4.3a) to three-wire configuration (see Figure 4.3c) and use it as bender-extender element, First of three wires should connect to one of side's nickel electrode of element and second one to another side. As the bender-extender element functions symmetrically, there is no difference between two sides. Third wire should connect to center brass shim. By nickel sides being at outside of the element, soldering the first two was easy (using soldering grease in soldering for

better and stronger connection is necessary). But for connecting third wire to center shim, a part of brass layer should be accessible and this achieved by removing part of upper layers of one side in CNC machine and the element cut in half (The dimensions for modified elements are 15.9mm, 12.7mm, 0.51mm) as seen in Figure 4.3b. Then wires connected by soldering. It is better to have the solder near the edge to have a longer effective length, but if it touches the other side and connects them, there will be a short circuit. Soldering has to be performed very carefully. There should not be any conductive connection between the wires and enough portion of the shield has to be kept intact for grounding.

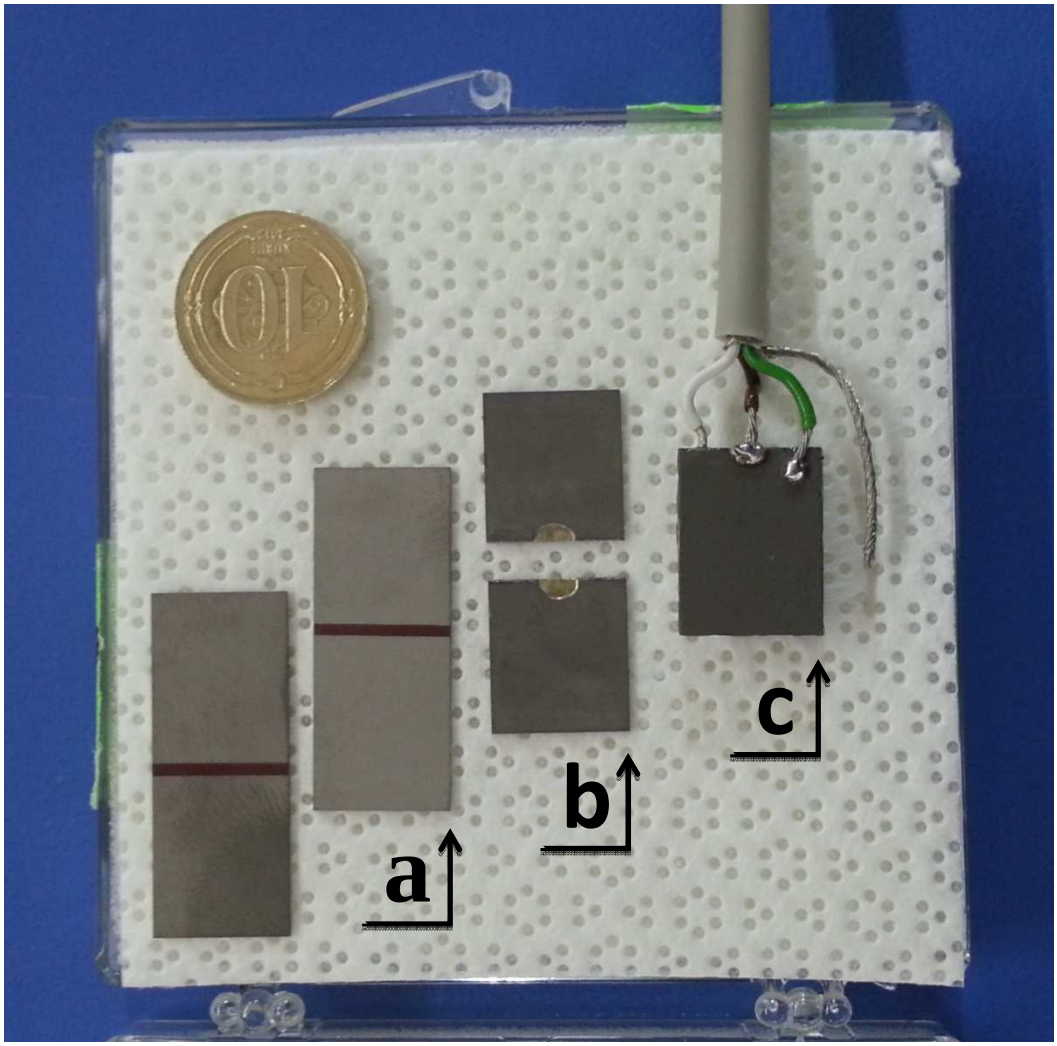



Figure 4.3 (a) Piezoelectric Element, (b) Modified Element, (c) Bender-Extender Element

As wave source, our parallel connecting bender-extender elements have an input limit of ±90V. However, when used as a receiver, the reading data is at mV range.

Considering the ambient charge in the medium and around the setup, it is absolutely necessary to prevent those exterior factors already creating noise within the same range. For accurate and clear test results, the cable has to be shielded to prevent ambient noise, [57]. The shield eliminates the magnetic effects of the equipment around. The advantage of using this kind of a cable is the effective shielding layer and ease of grounding (Figure 4.4).

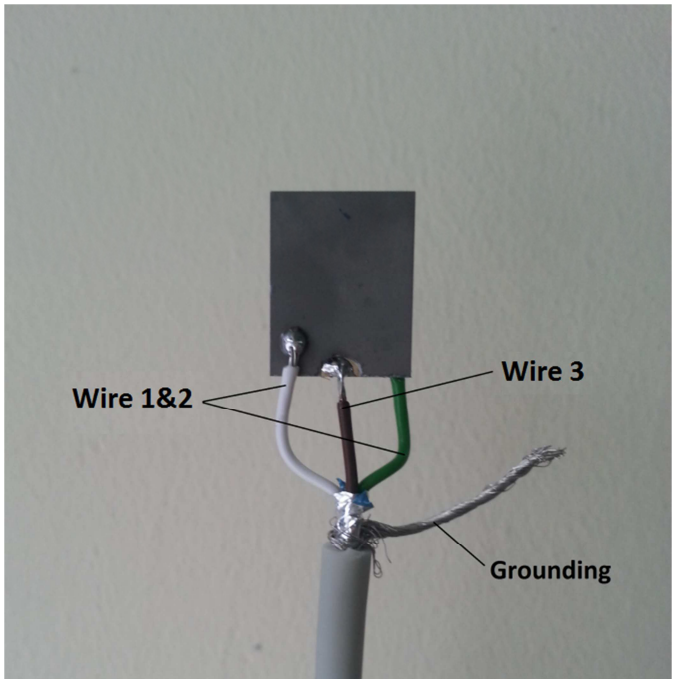



Figure 4.4 Cables

### 4.1.3 Grounding

When crosstalk occurs, the receiver bender-extender element picks a signal exactly at the same time source is excited. Since it has to take time for a physical wave to travel a distance, anything shown at zero time at the receiving end cannot be a wave. In order to better test results and eliminate these signals and other noises, the bender–extender elements have to fabricate with shielding and grounding. For electrical shielding we needed to benefit from Faraday's cage and this can be achieved by creating a circle made of conductive materials around the bender-extender element. Any excess charges deposited on the inner surface of the Faraday cage migrated to the outer surface of the cage, where they could produce no electric fields within the enclosure. By the help of grounding wire, all those free charges could be removed.

The electrical shielding was provided by insulating the bender–extender element with duct tape followed by aluminum tape (see Figure 4.5). The grounding wire (shield of the cable) touches the electrical shield (aluminum Tape) which goes all the way to the other end of the cable. At this end the shield of the cable attached to the grounding member of equipment (best result came from earth grounding of the amplifier).

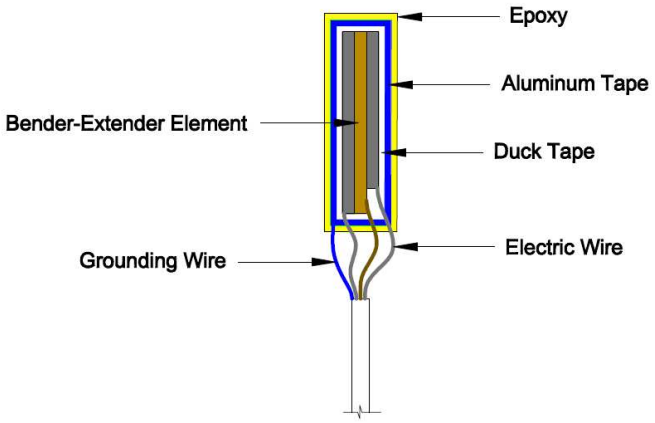



Figure 4.5 Bender-Extender Element Grounding and Waterproofing

### 4.1.4 Waterproofing

As the bender-extender elements are used in saturated specimen, they have to be waterproofed as a member of the circuit. After wiring and grounding the elements was waterproofed by coating it with a thin layer of epoxy (Devcon 2 Ton Epoxy) resin (see Figure 4.6). This layer also has other benefits for the system. Firstly, it protects the material against corrosion and increases the durability of the members. Secondly, it provides a shield for mechanical impacts and makes it stronger. The last but not the least, it isolates the element from undesired charges [57].

### 4.1.5 Housing

Housing is a plastic piece designed to place the bender-extender element into different triaxial test's special cap and pedestal as seen in figure 4.6b.

After the epoxy layer on the bender-extender element dried, the element and housing held fixed by Pliers and empty space of housing filled with epoxy and waited till it dried. About two thirds of the bender-extender element (about 5mm) placed into the epoxy that includes all soldered areas (see Figure 4.7).

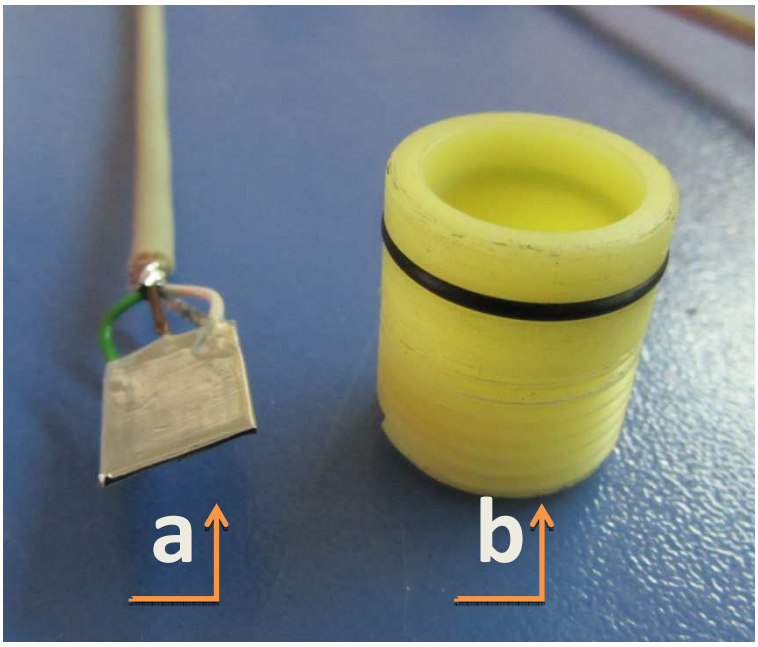



Figure 4.6 (a) Bender-Extender Element, (b) Housing



Figure 4.7 Elements Before and After Fixing by Epoxy in Housing

## 4.2 Data Acquisition System

Data acquisition system consists of PCI-6115 simultaneous sampling multifunction DAQ board (Figure 4.8a), BNC-2110 connector block (Figure 4.8b), their connection cable and LabVIEW software from National Instruments [58] and a computer as seen in Figure 4.1. Bout BNC-2110 connector block and connection cable are shielded for

preventing noise effect. This system can be used both as function generator and digital oscilloscope.

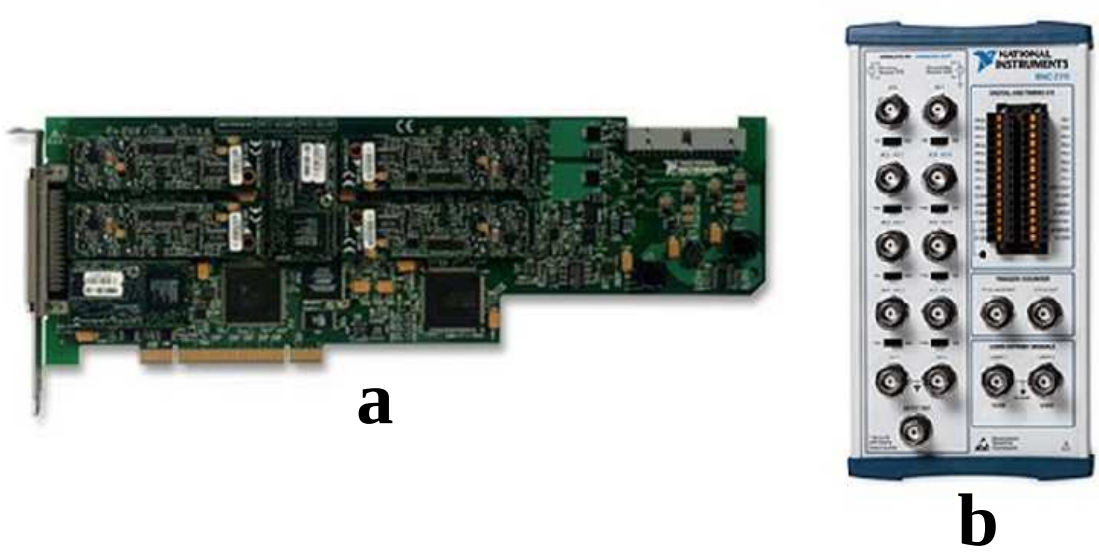



Figure 4.8 (a) PCI-6115 DAQ board, (b) BNC-2110 connector block

### 4.2.1 Function Generator

As function generator the system can send electrical signals to the circuit which is wired to the bender-extender element and creates shear or compression waves.

The properties of this signals controlled by a computer program that written in LabVIEW software by Marmatek Engineering Ltd. This program enables us to generate signal with different waveforms (sinusoidal, square, saw-tooth and triangle), amplitudes and frequencies (see Figure 4.9).

The system has two analog outputs with maximum signal output amplitude of ±10V which needs to be amplified to transmit higher energy to the transmitter bender-extender element (Higher energy for transmitter means higher amplitude for receiving signal).

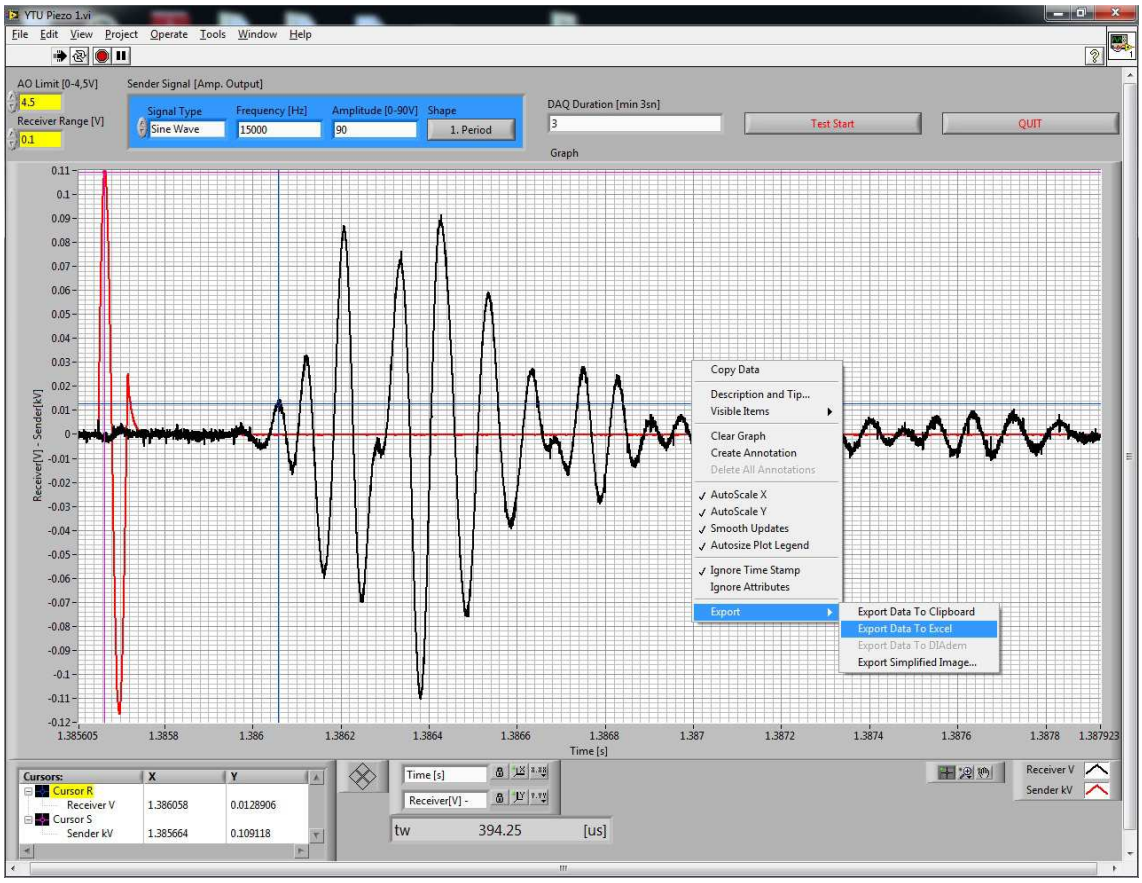



Figure 4.9 Computer Program Interface

### 4.2.2 Digital Oscilloscope

When receiver bender-extender element converts the motion of wave that transmitted by the transmitter through the soil specimen into electrical signals, as digital oscilloscope the system can exhibit those signals in waveforms by converting analog signals to digital data.

The system's analog inputs have a 10MS/s sampling rate per channel. Both the transmitter and receiver signals data can be collected by the system. Time difference between one point of transmitted signal and one point of received signal can be determined by using program's pointers. The computer program (see Figure 4.9) can present and store this data in different digital format (e.g., .xls). The program's lack of integrated filtering or data averaging function can cause problem in low amplitude measurements.

## 4.3 Power Amplifier

Power amplifier is needed for amplifying the voltage of the sending signal coming from the waveform generator to the transmitter bender-extender element. Higher voltage output means higher energy for wave transmitter and higher amplitude for received signal.

The computer card PCI-6115/ BNC-2110 waveform generator's maximum output voltage is ±10 V (20 Vpp). The power amplifier, Piezo EPA-104 (Figure 4.10), is capable of amplifying the waveform generator voltage from 20 Vpp up to 200 Vpp. However, the maximum voltage our piezoelectric transducers can take in parallel configuration for both the x-poled and y-poled piezoelectric elements is ±90 V. For this reason applied voltage was limited to ±90 V to avoid depolarization of the bender–extender elements.




Figure 4.10 Piezo EPA-104 Linear Power Amplifier

Piezo EPA-104 is a low noise generating linear power amplifier which does not cause any lag time during the amplifying process which is very important for velocity measurement type of tests. However it causes a distortion on the high frequency signals. The maximum voltage it can provide decreases as the frequency of the signal passes beyond limits as shown in Figure 4.11.

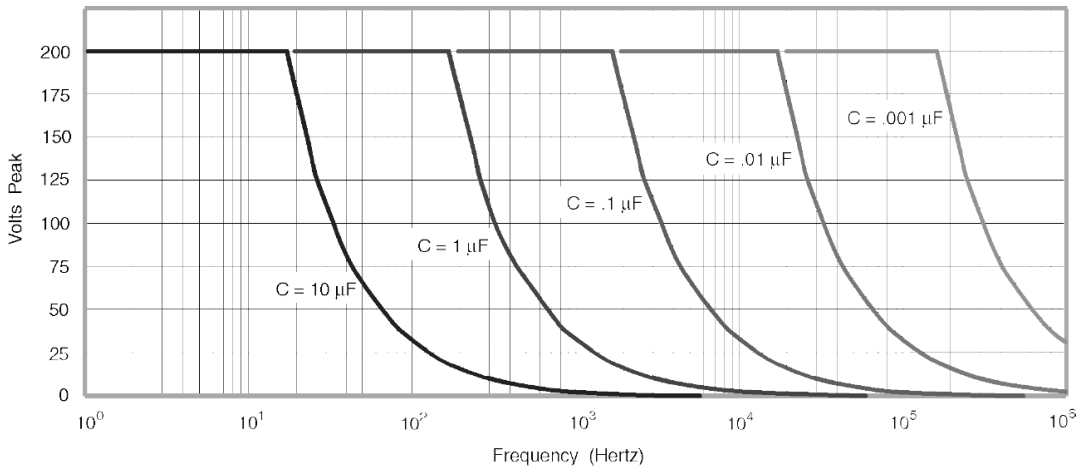



Figure 4.11 Peak Voltage Delivered to Capacitive Load at Peak Current Rating as a Function of Operating Frequency [56]

## 4.4 Triaxial Test Apparatus

The triaxial test apparatus that used in this study is LoadTrac II/FlowTrac II (from Geocomp Corporation [59] with new designed cell and caps for use with bender-extender elements. LoadTrac II/FlowTrac II is an automatically controlled triaxial soil testing system. This soil testing system could apply an axial loading and a lateral confining pressure in a computer-controlled way. The information about LoadTrac II and FlowTrac II of this section is from the Geocomp Corporation [59] LoadTrac II and FlowTrac II user's manuals.

### 4.4.1 LoadTrac II/FlowTrac II

LoadTrac-II (see figure 4.12a) is a versatile and intelligent system composed of a load frame and a computer with monitor. The load frame houses a high speed, precision micro stepper motor that moves the load platen and thereby applies a vertical load to the soil specimen. An embedded control board with a dedicated CPU uses readings from the force and displacement transducers to determine what signals should be sent to the stepper motor. The control board is capable of applying a new vertical load increment within one second and accurately maintaining that load while monitoring the displacement.

FlowTrac-II (see figure 4.12b) is an intelligent, versatile system composed of a flow pump and a computer with monitor. The flow pump, which regulates pressure and

volume in a test cell, houses a high speed, precision micro stepper motor that moves a piston in a water-filled cylinder. An embedded control board with a dedicated CPU uses readings from the pressure transducer mounted at the end of the cylinder to determine what signals should be sent to the stepper motor. The number of motor steps is used to compute volume change.

The computer and monitor are used for displaying test results in real time, and for editing test results and producing a report after the test has been completed.

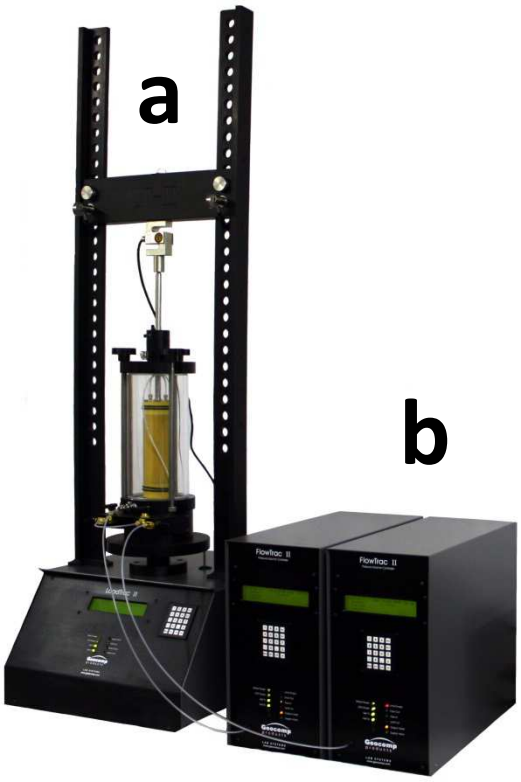



Figure 4.12 (a) LoadTrac II, (b) FlowTrac II

### 4.4.2 Cell

New triaxial cell is designed based on original Geocomp cell with some modification for use with new caps and passing bender-extender elements electric cables into the cell (see Figure 4.13).



Figure 4.13 New Triaxial Cell

After some preliminary tests and modification cell get ready to use by solving leakage problem at around plexiglass and pedestal cap. Cell's Piston settings were found as instructed in LoadTrac II user's manual.

### 4.4.3 Caps

New cap design allows easily installing and removing bender-extender element into or from caps as seen in Figure 4.14.



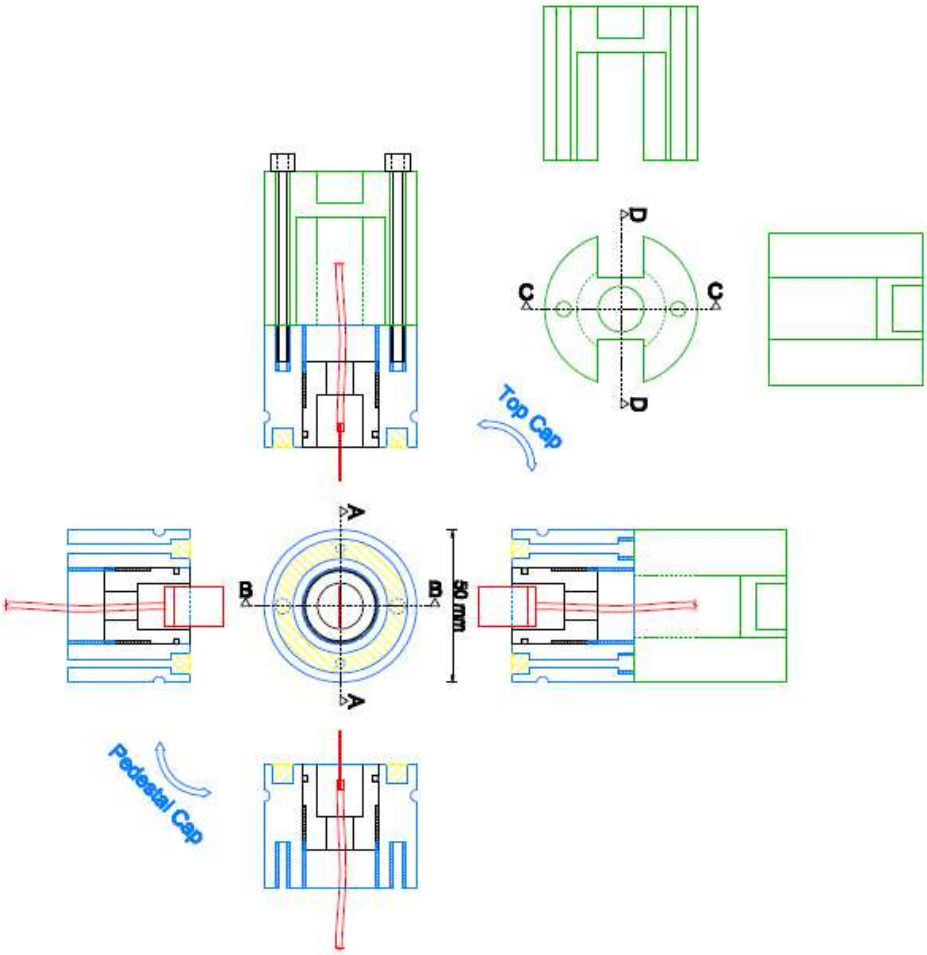



Figure 4.14 New Triaxial caps

The porous stones (see Figure 4.15a) of these caps prepared by passing the sand specimen of this study from sieve number 40 and mix the passing part with epoxy and placed in special mold (see Figure 4.15b) by tamping. It left for drying for a day before use. After some trial and error epoxy weight equal to 4% of mixture's seen appropriate for required strength and permeability. Coefficient of permeability for manufactured porous stones was found around $2x10^{-4}$ cm/s.

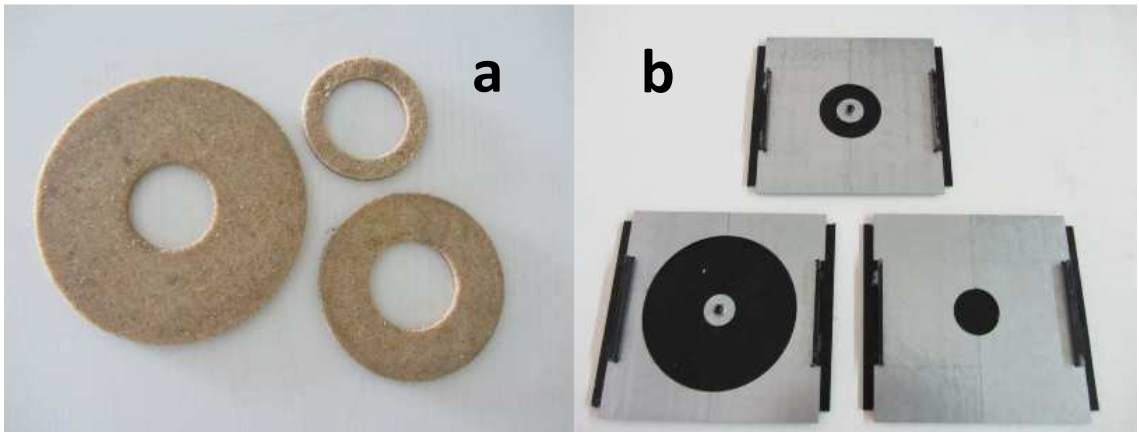



Figure 4.15 (a) Porous Stones, (b) Porous Stone's molds

## 4.5 Test Sand and Specimen Preparation

The grain size distribution curve of the sand, used in this study is shown in Figure 4.16. The index properties are given in Table 4.1.

The specimens were prepared by tapping the dry sand into a mold in five layers to the required density. Before separating the mold, the specimens (diameter 50 mm, height 105 mm) were enclosed in a membrane and vacuum equal to 15 kPa was applied. Then specimens were placed in a triaxial cell (see Figure 4.17). Uniformity Coefficient and Coefficient of Curvature calculated by Equation 4.1 and Equation 4.2 respectively.

$$C_u = (D_{60} / D_{10}) \quad (4.1)$$

$$C_c = (D_{30})^2 / (D_{60} x D_{10}) \quad (4.2)$$

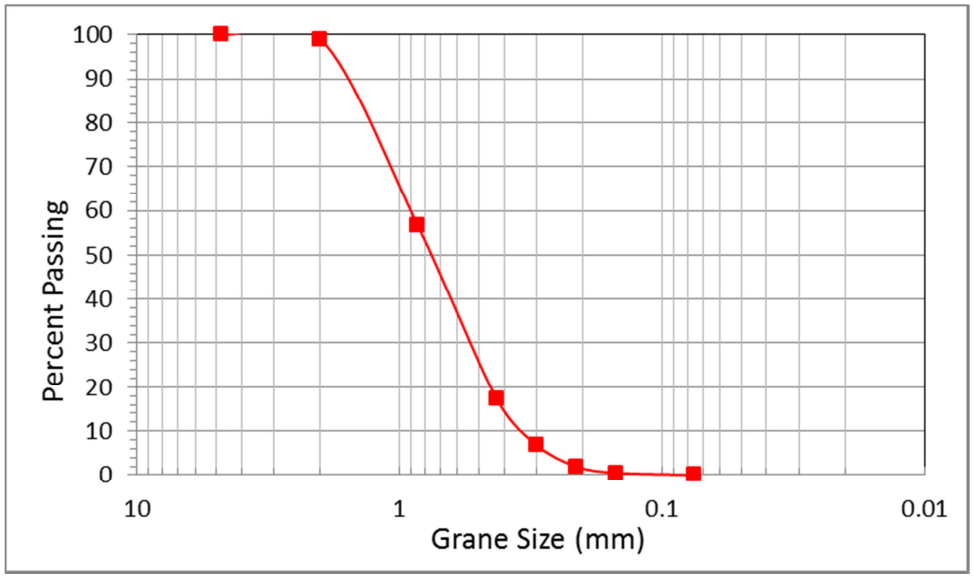



Figure 4.16 Grain Size Distribution Curve

Table 4.1 the Index Properties of the Sand, Used in This Study

| | |
|---|---|
| Unified Soil Classification | SP |
| Specific Gravity | 2.65 |
| Maximum Void Ratio, $e_{max}$ | 0.81 |
| Minimum Void Ratio, $e_{min}$ | 0.50 |
| Median Grain Size, $D_{50}$ (mm) | 0.76 |
| Effective Grain Size, $D_{10}$ (mm) | 0.35 |
| Uniformity Coefficient, $C_u$ | 2.57 |
| Coefficient of Curvature, $C_c$ | 0.92 |

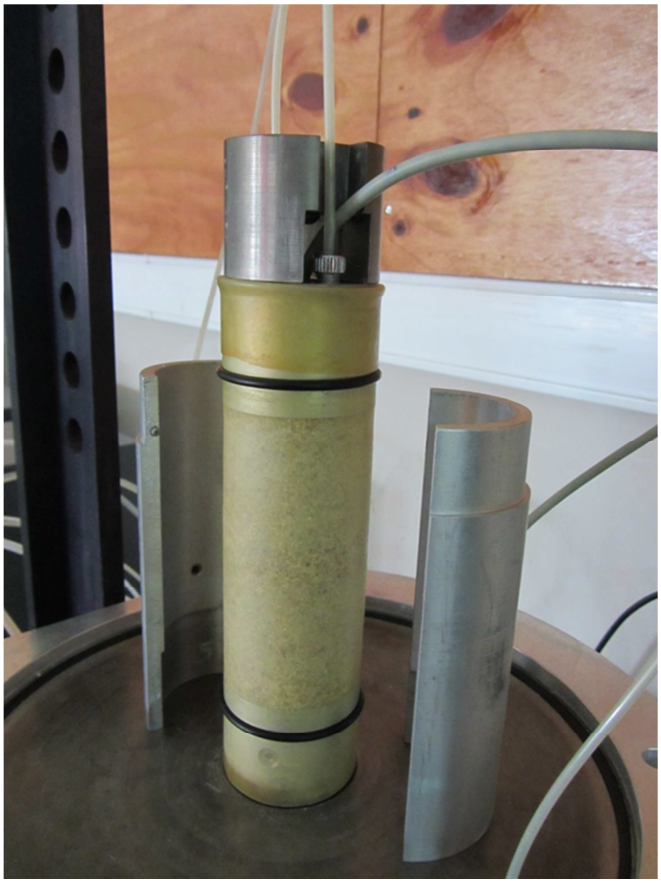


Figure 4.17 Prepared Sand Specimen

# CHAPTER 5

## $V_S$ and $V_P$ MEASUREMENT TEST RESULTS

The main goals of this study was to develop a working bender-extender element test setup and observing effects of initial void ratio of sand specimen and loading conditions at static and shearing states on shear and compression wave velocity measurement. Example tests were performed and results are presented to demonstrate the achievement of these goals.

This chapter is organized into four sections. The first part of the chapter (Section 5.1) contains all triaxial specimens' initial condition and test properties. The second part of the chapter (Sections 5.2 and 5.3) covers the results about effects of different transmitted signal frequency, Specimen initial void ratio and confining pressure on $V_S$ and $V_P$ and their corresponding $G_{max}$, $M_{max}$ and Poisson's Ratio. The third part of the chapter (Section 5.4) shows variation of $V_S$ and $V_P$ during sand specimens' drained and undrained monotonic shearing.

### 5.1 $V_S$ and $V_P$ Measurement Tests' Properties

Table 5.1 and 5.2 present the ID, the initial properties and BE element function of tests were run in this study. The wave velocity measurements of body waves in dry and saturated sand specimens were performed in the triaxial device. The dimensions of all sand specimens were 50 mm in diameter and 105 mm in height. The penetration of BE elements in sand specimens was 10 mm.

In test ID "Dr(a)(b)(c)k(d)(e)": (a) denotes relative density percent, (b) denotes the stress state in consolidation phase ("i" for isotropic stress state or "a" for anisotropic stress state), (c) denotes the amount of confining stress, (d) denotes if the sample is dry

or saturated (“D” for dry or “S” for saturated) and (e) denotes the piezoelectric element type (“B” for bender element or “E” for extender element).

### 5.1.1 Tests under Isotropic Confining Stress

In these tests sand specimens were subjected to isotropic confining stress ($\sigma'_3 = \sigma'_1$).

Table 5.1 ID and Properties of Isotropic Tests

| Test ID | Initial Void Ratio ($e_0$) | Relative Density ($D_r$, %) | Effective Vertical Stress ($\sigma'_1$, kPa) | Effective Horizontal Stress ($\sigma'_3$, kPa) | Saturation Ratio ($S_r$) | Element Function (Bender or Extender) | Transmitted Frequencies (kHz) |
|---|---|---|---|---|---|---|---|
| Dr50i50kDB | 0.655 | 50 | 50 | 50 | 0 | B | 5, 10, 15, 20 |
| Dr50i100kDB | 0.655 | 50 | 100 | 100 | 0 | B | 5, 10, 15, 20 |
| Dr50i200kDB | 0.655 | 50 | 200 | 200 | 0 | B | 5, 10, 15, 20 |
| Dr50i400kDB | 0.655 | 50 | 400 | 400 | 0 | B | 5, 10, 15, 20 |
| Dr50i50kDE | 0.655 | 50 | 50 | 50 | 0 | E | 5, 10, 15, 20, 25, 30 |
| Dr50i100kDE | 0.655 | 50 | 100 | 100 | 0 | E | 5, 10, 15, 20, 25, 30 |
| Dr50i200kDE | 0.655 | 50 | 200 | 200 | 0 | E | 5, 10, 15, 20, 25, 30 |
| Dr50i400kDE | 0.655 | 50 | 400 | 400 | 0 | E | 5, 10, 15, 20, 25, 30 |
| Dr70i50kDB | 0.593 | 70 | 50 | 50 | 0 | B | 5, 10, 15, 20 |
| Dr70i100kDB | 0.593 | 70 | 100 | 100 | 0 | B | 5, 10, 15, 20 |
| Dr70i200kDB | 0.593 | 70 | 200 | 200 | 0 | B | 5, 10, 15, 20 |
| Dr70i400kDB | 0.593 | 70 | 400 | 400 | 0 | B | 5, 10, 15, 20 |
| Dr70i50kDE | 0.593 | 70 | 50 | 50 | 0 | E | 5, 10, 15, 20, 25, 30 |
| Dr70i100kDE | 0.593 | 70 | 100 | 100 | 0 | E | 5, 10, 15, 20, 25, 30 |
| Dr70i200kDE | 0.593 | 70 | 200 | 200 | 0 | E | 5, 10, 15, 20, 25, 30 |
| Dr70i400kDE | 0.593 | 70 | 400 | 400 | 0 | E | 5, 10, 15, 20, 25, 30 |
| Dr90i50kDB | 0.531 | 90 | 50 | 50 | 0 | B | 5, 10, 15, 20 |
| Dr90i100kDB | 0.531 | 90 | 100 | 100 | 0 | B | 5, 10, 15, 20 |
| Dr90i200kDB | 0.531 | 90 | 200 | 200 | 0 | B | 5, 10, 15, 20 |
| Dr90i400kDB | 0.531 | 90 | 400 | 400 | 0 | B | 5, 10, 15, 20 |
| Dr90i50kDE | 0.531 | 90 | 50 | 50 | 0 | E | 5, 10, 15, 20, 25, 30 |
| Dr90i100kDE | 0.531 | 90 | 100 | 100 | 0 | E | 5, 10, 15, 20, 25, 30 |
| Dr90i200kDE | 0.531 | 90 | 200 | 200 | 0 | E | 5, 10, 15, 20, 25, 30 |
| Dr90i400kDE | 0.531 | 90 | 400 | 400 | 0 | E | 5, 10, 15, 20, 25, 30 |

### 5.1.2 Tests under Anisotropic Confining Stress

In these tests sand specimens were subjected to anisotropic confining stress with horizontal to vertical effective stress ratio of 0.3 ($\sigma'_3 = 0.3 * \sigma'_1$).

Table 5.2 ID and Properties of Anisotropic Tests

| Test ID | Initial Void Ratio ($e_0$) | Initial Relative Density ($D_r$, %) | Effective Vertical Stress ($\sigma'_1$, kPa) | Effective Horizontal Stress ($\sigma'_3$, kPa) | Saturation Ratio ($S_r$) | Element Function (Bender or Extender) | Transmitted Frequencies (kHz) |
|---|---|---|---|---|---|---|---|
| Dr50a50-15kDB | 0.655 | 50 | 50 | 15 | 0 | B | 10, 15, 20 |
| Dr50a100-30kDB | 0.655 | 50 | 100 | 30 | 0 | B | 10, 15, 20 |
| Dr50a200-60kDB | 0.655 | 50 | 200 | 60 | 0 | B | 10, 15, 20 |
| Dr50a400-120kDB | 0.655 | 50 | 400 | 120 | 0 | B | 10, 15, 20 |
| Dr50a50-15kDE | 0.655 | 50 | 50 | 15 | 0 | E | 15, 20. 25 |
| Dr50a100-30kDE | 0.655 | 50 | 100 | 30 | 0 | E | 15, 20. 25 |
| Dr50a200-60kDE | 0.655 | 50 | 200 | 60 | 0 | E | 15, 20. 25 |
| Dr50a400-120kDE | 0.655 | 50 | 400 | 120 | 0 | E | 15, 20. 25 |
| Dr70a50-15kDB | 0.593 | 70 | 50 | 15 | 0 | B | 10, 15, 20 |
| Dr70a100-30kDB | 0.593 | 70 | 100 | 30 | 0 | B | 10, 15, 20 |
| Dr70a200-60kDB | 0.593 | 70 | 200 | 60 | 0 | B | 10, 15, 20 |
| Dr70a400-120kDB | 0.593 | 70 | 400 | 120 | 0 | B | 10, 15, 20 |
| Dr70a50-15kDE | 0.593 | 70 | 50 | 15 | 0 | E | 15, 20. 25 |
| Dr70a100-30kDE | 0.593 | 70 | 100 | 30 | 0 | E | 15, 20. 25 |
| Dr70a200-60kDE | 0.593 | 70 | 200 | 60 | 0 | E | 15, 20. 25 |
| Dr70a400-120kDE | 0.593 | 70 | 400 | 120 | 0 | E | 15, 20. 25 |
| Dr50a50-15kSB | 0.655 | 50 | 50 | 15 | 0.92 | B | 10, 15, 20 |
| Dr50a100-30kSB | 0.655 | 50 | 100 | 30 | 0.87 | B | 10, 15, 20 |
| Dr50a200-60kSB | 0.655 | 50 | 200 | 60 | 0.92 | B | 10, 15, 20 |
| Dr50a400-120kSB | 0.655 | 50 | 400 | 120 | 0.93 | B | 10, 15, 20 |
| Dr70a50-15kSB | 0.593 | 70 | 50 | 15 | 0.86 | B | 10, 15, 20 |
| Dr70a100-30kSB | 0.593 | 70 | 100 | 30 | 0.87 | B | 10, 15, 20 |
| Dr70a200-60kSB | 0.593 | 70 | 200 | 60 | 0.93 | B | 10, 15, 20 |
| Dr70a400-120kSB | 0.593 | 70 | 400 | 120 | 0.94 | B | 10, 15, 20 |

### 5.1.3 Transmitted Signal Properties and Wave Travel Time Measurements

In this study the sinusoidal wave form was used as transmitting signal. The advantage of using sinusoidal waves among others (saw-tooth and square) is ease of interpreting the received data and preventing possible damages to the equipment [57].

All the bender–extender element tests were performed with 90 Vpp input voltage, which is the highest voltage that can be used.

To investigate the effect of input frequencies, input frequencies between 1 and 30 kHz was applied in the bender–extender element tests. Results are presented for input frequencies between 5 and 20 kHz for S-waves and input frequencies between 5 and 30 kHz for P-waves as these frequencies showed best assessable receiver signals.

There are different methods used by researchers for finding wave travel time. The first peak to peak time method was used in this study that takes the time between the peak of the source signal and the first peak of the cycle of the receiver signal, (see Figure 5.1).

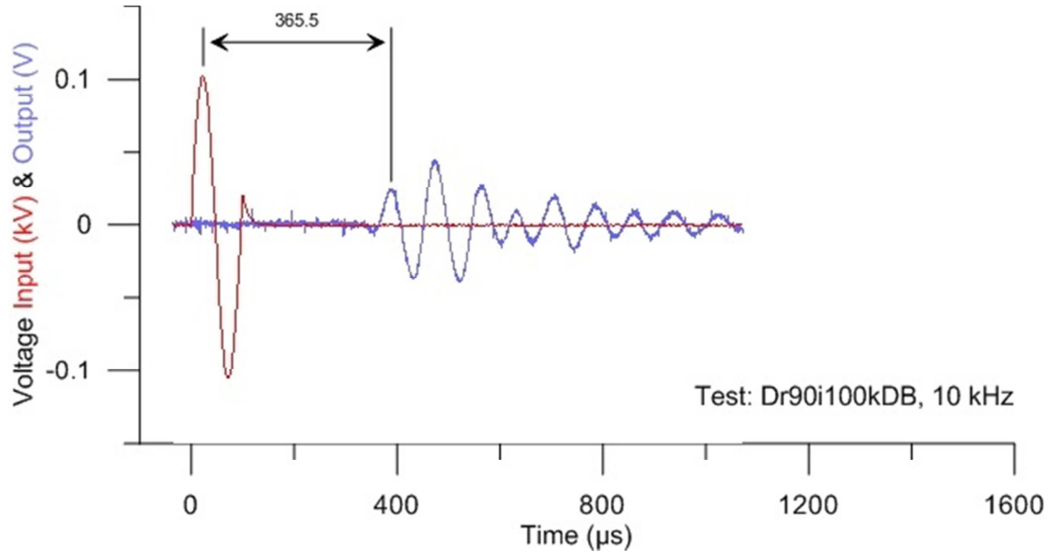



Figure 5.1 Finding Wave Travel Time by First Peak to Peak Time Method

### 5.1.4 Monotonic Triaxial Shearing Test Properties

All dry sand specimens under anisotropic confining stress subjected to drained monotonic shearing and all saturated sand specimens under anisotropic confining strees subjected to undrained monotonic shearing. Body wave velocities ($V_S$ and $V_P$) were measured at certain axial strains during shearing. Input frequency of 15 kHz was used for transmitted signal during shearing. In order to having enough time for collecting

data, shearing speed of 0.2 strain/min was used. Results for $V_S$ and $V_P$ changes during monotonic shearing in triaxial test apparatus are presented at section 5.4.

## 5.2 Test Result for Dry Specimens under Isotropic Stress

### 5.2.1 Test Results for Different frequencies

Table 5.3 and Table 5.4 show effect of input frequency on value of $V_S$ and $V_P$ under constant relative density and confining pressure. As seen in Table 5.3 and Table 5.4 as expected variation of input frequency does not have a considerable effect on $V_S$ and $V_P$ measurement, especially at frequencies greater than 10 kHz.

Table 5.3 Value of $V_S$ for different input frequency under Constant Relative density and Confining Pressure

| Shear Wave Velocity ($V_S$, m/s) | | | | | |
|---|---|---|---|---|---|
| Relative Density ($D_r$, %) | Confining Pressure (kPa) | Input Frequency (kHz) | | | |
| | | 5 | 10 | 15 | 20 |
| 50 | 50 | 176 | 174 | 177 | 178 |
| | 100 | 214 | 211 | 210 | 212 |
| | 200 | 272 | 279 | 288 | 293 |
| | 400 | 333 | 314 | 314 | 313 |
| 70 | 50 | 182 | 201 | 200 | 203 |
| | 100 | 221 | 218 | 221 | 224 |
| | 200 | 272 | 266 | 267 | 270 |
| | 400 | 332 | 320 | 318 | 321 |
| 90 | 50 | 188 | 185 | 187 | 189 |
| | 100 | 240 | 233 | 233 | 234 |
| | 200 | 306 | 292 | 289 | 289 |
| | 400 | 375 | 347 | 341 | 340 |

Table 5.4 Value of $V_P$ for different input frequency under Constant Relative density and Confining Pressure

| Compression Wave Velocity ($V_P$, m/s) | | | | | | | |
|---|---|---|---|---|---|---|---|
| Relative Density ($D_r$, %) | Confining Pressure (kPa) | Input Frequency (kHz) | | | | | |
| | | 5 | 10 | 15 | 20 | 25 | 30 |
| 50 | 50 | 326 | 354 | 353 | 355 | 355 | 356 |
| | 100 | 396 | 400 | 410 | 412 | 411 | 411 |
| | 200 | 494 | 472 | 478 | 478 | 480 | 482 |
| | 400 | 539 | 551 | 562 | 565 | 566 | 566 |
| 70 | 50 | 333 | 354 | 354 | 359 | 359 | 359 |
| | 100 | 412 | 414 | 422 | 415 | 433 | 433 |
| | 200 | 504 | 497 | 500 | 504 | 507 | 513 |
| | 400 | 607 | 573 | 581 | 580 | 592 | 594 |
| 90 | 50 | 373 | 375 | 414 | 417 | 417 | 418 |
| | 100 | 414 | 413 | 447 | 444 | 444 | 447 |
| | 200 | 535 | 531 | 548 | 539 | 539 | 541 |
| | 400 | 639 | 659 | 645 | 631 | 631 | 632 |

### 5.2.2 Test Results for Different Void Ratios

Figure 5.2 and Figure 5.3 show the variation of $V_S$ and its corresponding $G_{max}$ with initial void ratio for sand specimen. Figure 5.4 and Figure 5.5 present similar results for $V_P$ and $M_{max}$. The initial void ratio varied from 0.531 to 0.655%.

As observed in Figures 5.2 and 5.3, the $V_S$ and $G_{max}$ decrease as the initial void ratio increases.

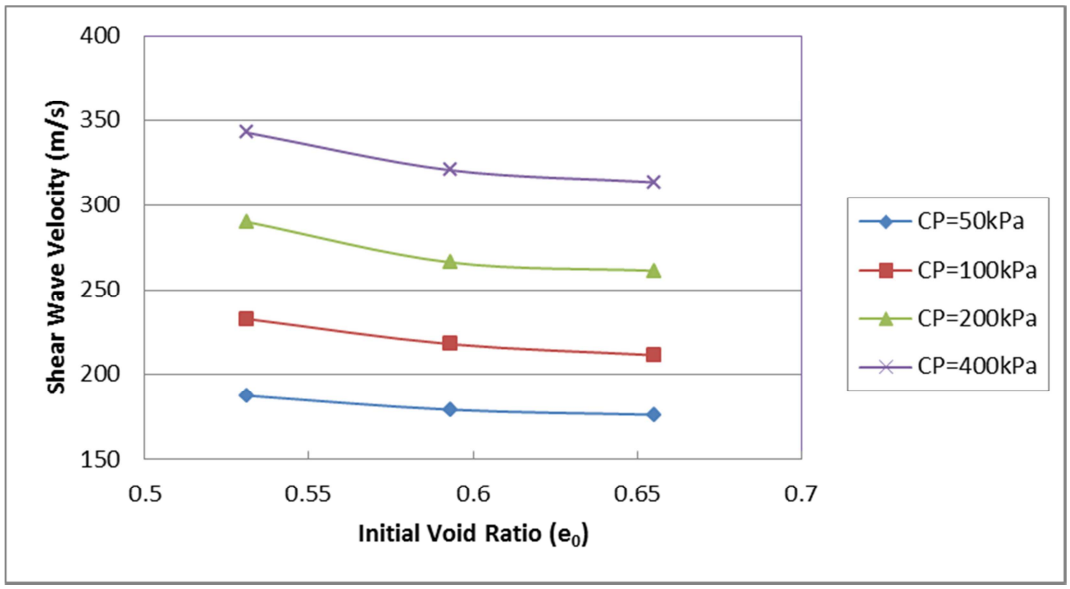



Figure 5.2 Variations of $V_S$ with Initial Void Ratio

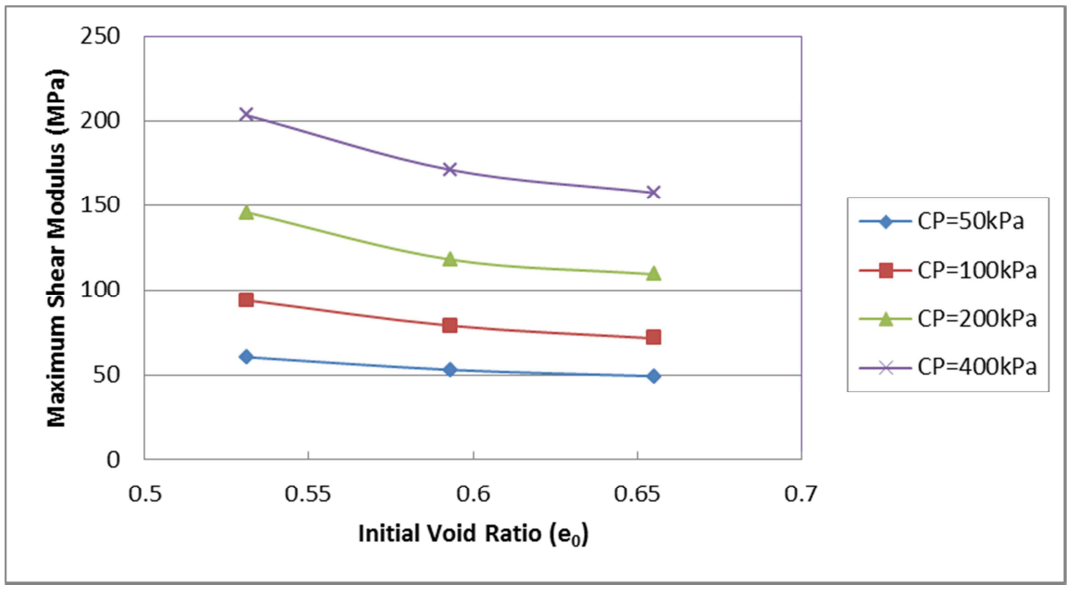



Figure 5.3 Variations of $G_{max}$ with Initial Void Ratio

As observed in Figures 5.4 and 5.5, the $V_p$ and $M_{max}$ decrease as the initial void ratio increases.

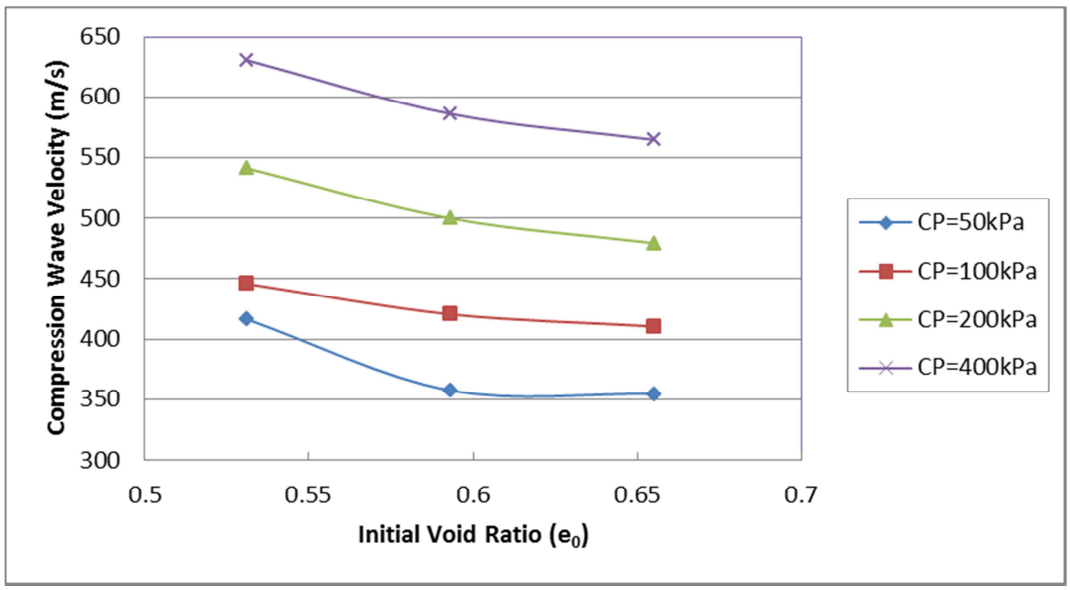



Figure 5.4 Variations of $V_P$ with Initial Void Ratio

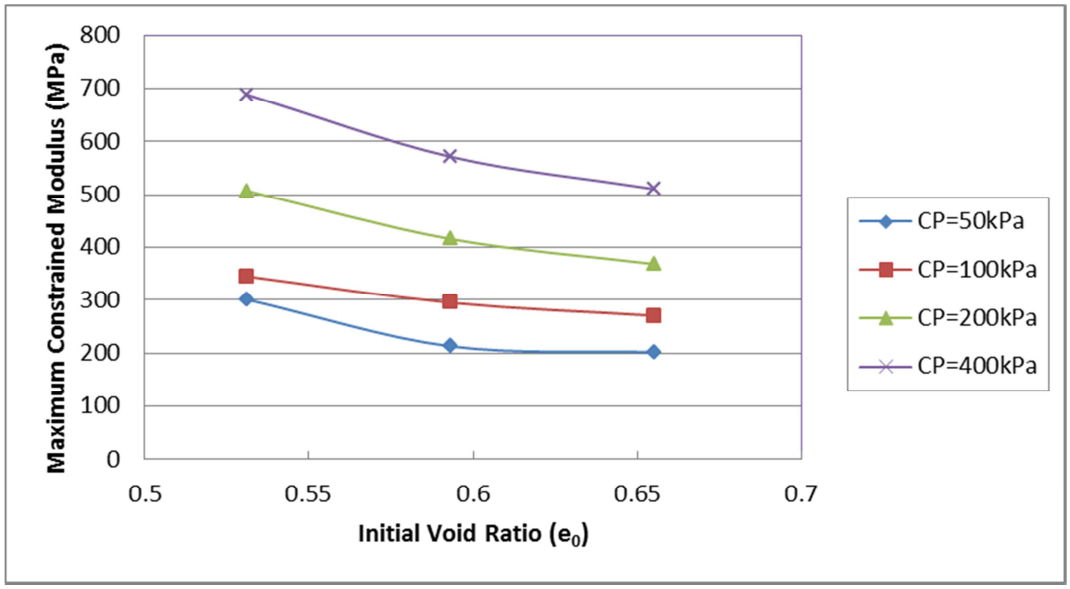



Figure 5.5 Variations of $M_{max}$ with Initial Void Ratio

### 5.2.3 Test Results for Different Relative Densities

The variations of $V_S$, $V_P$ and their corresponding $G_{max}$ and $M_{max}$ with relative density measured with BE elements are presented in Figures 5.6, 5.8, 5.7 and Figure 5.9 respectively. The initial relative density varied from 50 to 90%.

As seen in Figures 5.6 and 5.7, the $V_S$ and $G_{max}$ increase as the initial relative density increases.

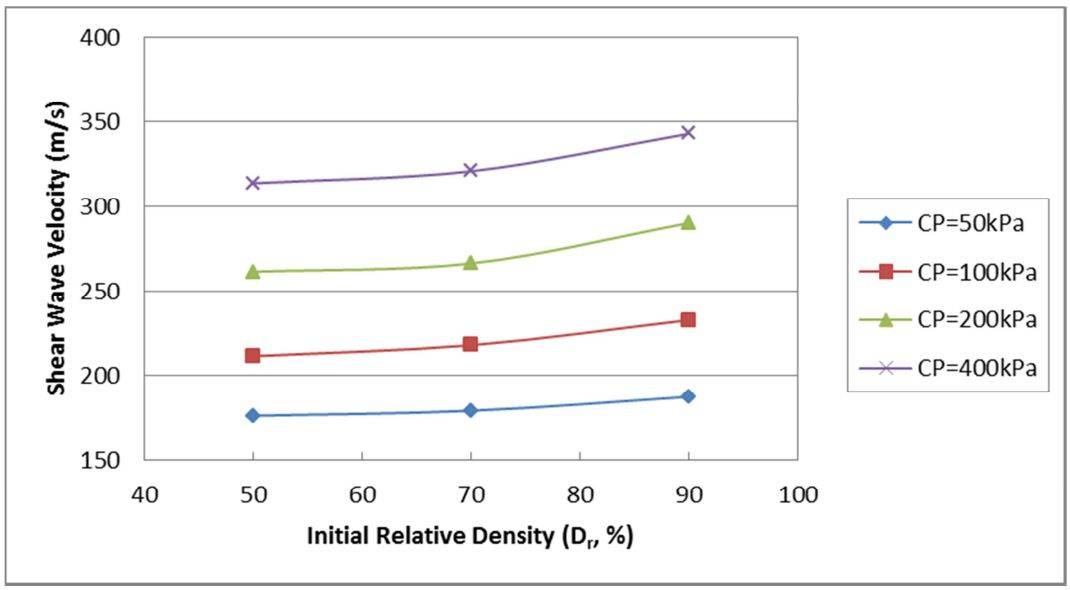



Figure 5.6 Variations of $V_S$ with Initial Relative Density

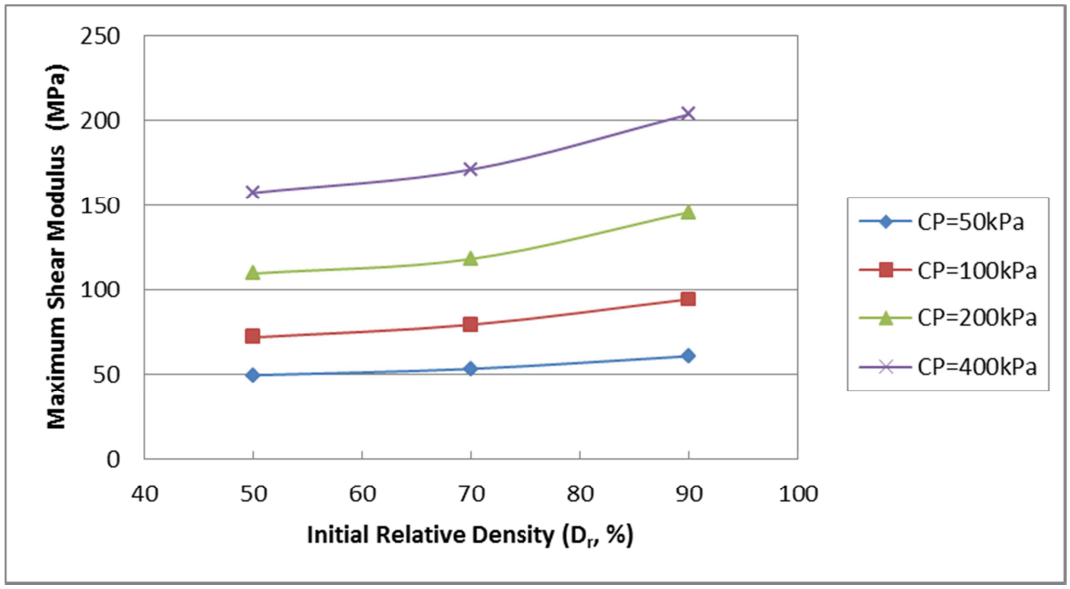



Figure 5.7 Variations of $G_{max}$ with Initial Relative Density

As seen in Figures 5.8 and 5.9, the $V_P$ and $M_{max}$ increase as the initial relative density increases.

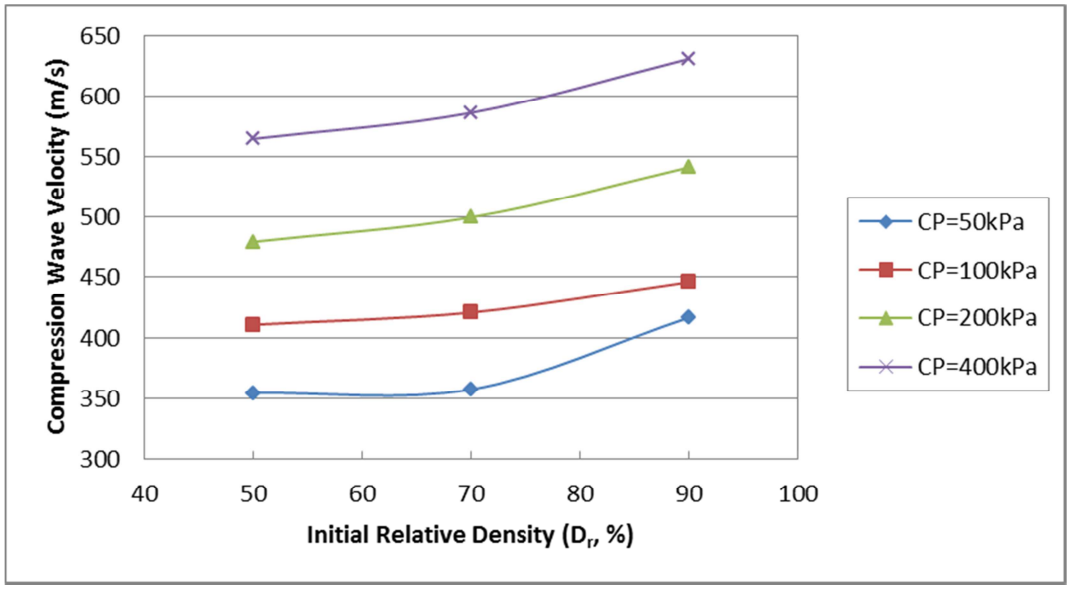



Figure 5.8 Variations of $V_P$ with Initial Relative Density

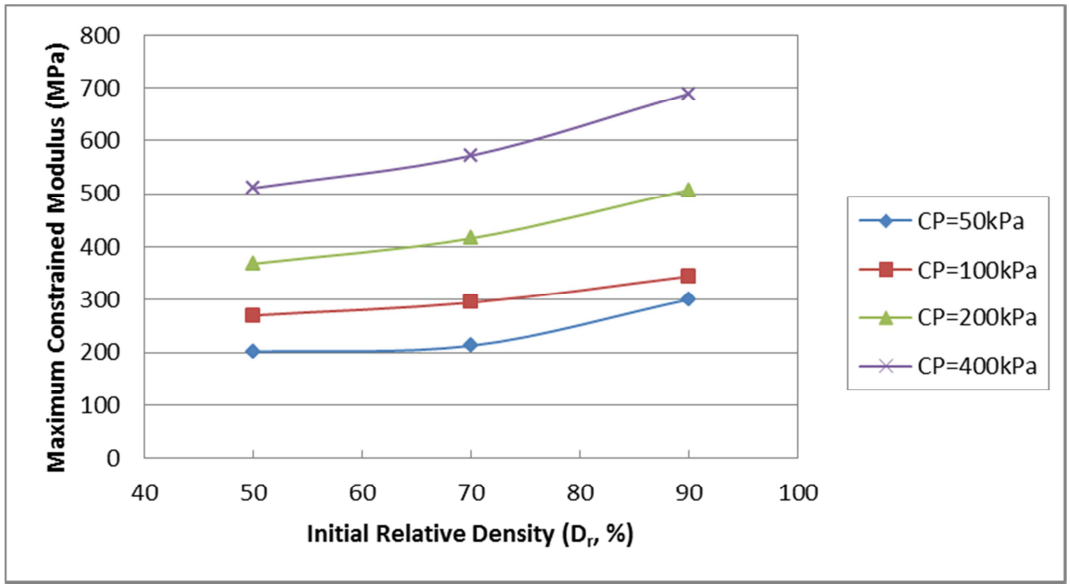



Figure 5.9 Variations of $M_{max}$ with Initial Relative Density

### 5.2.4 Test Results for Different Confining Pressures

The variations of $V_S$ and $V_P$ with isotropic confining pressure measured with BE elements for sand specimen are presented in Figure 5.10 and Figure 5.12 respectively. In addition, Figure 5.11 and Figure 5.13 present variation of their corresponding $G_{max}$ and $M_{max}$ with confining pressure respectively. The applied confining pressure was varied from 50 to 400 kPa.

As observed in Figures 5.10 and 5.11, the $V_S$ and $G_{max}$ increase as the confining pressure increases. Shear wave velocity ($V_S$) varies from 176 to 334 m/s while $G_{max}$ varies from 49.6 to 203.3 MPa (See Table 5.5 for all values).

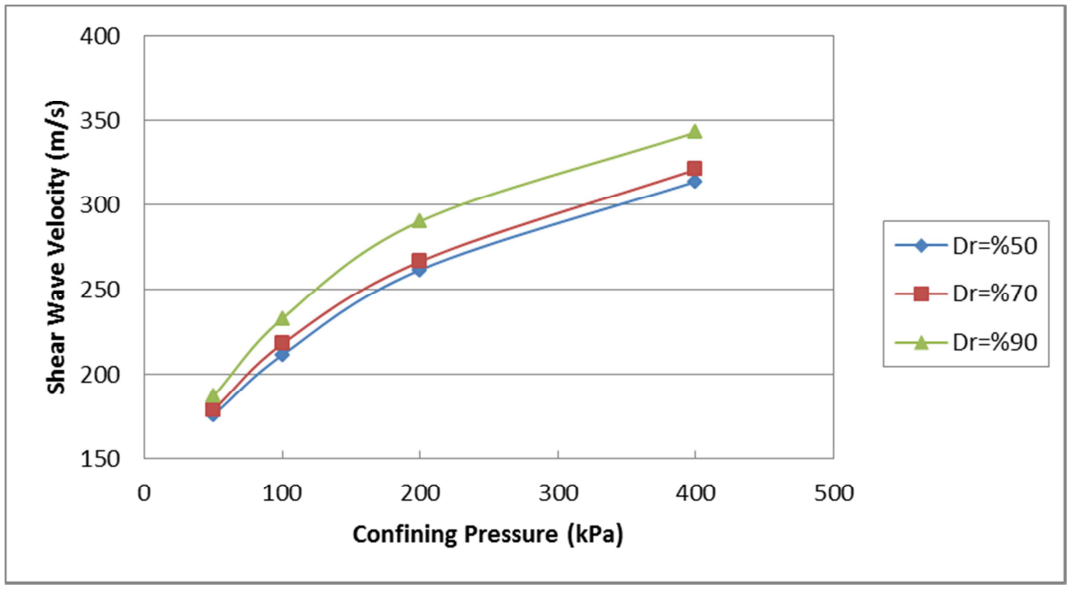



Figure 5.10 Variations of $V_S$ with Confining Pressure

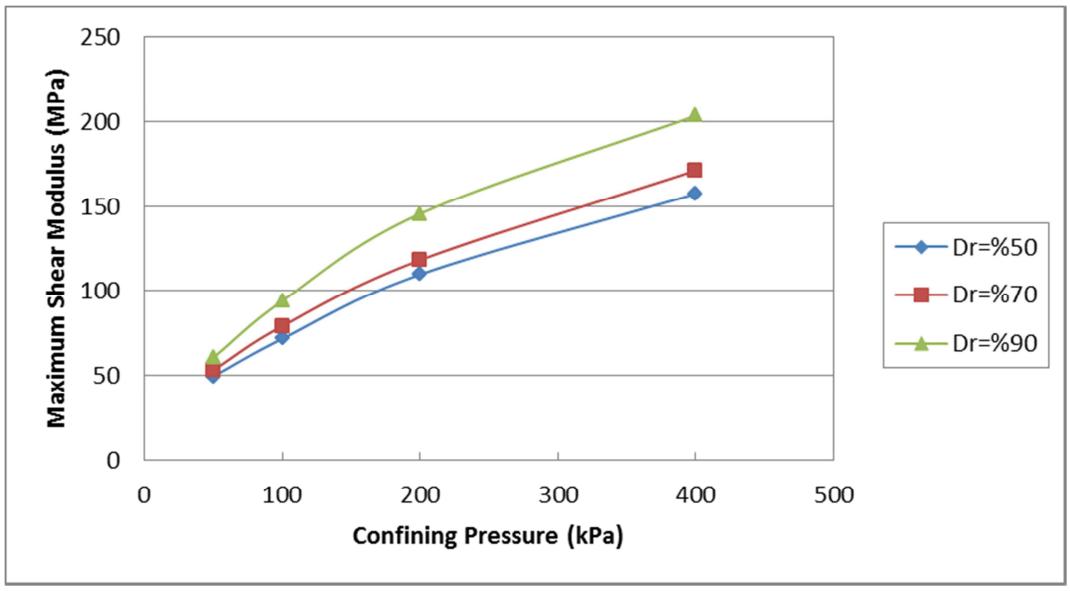



Figure 5.11 Variations of $G_{max}$ with Confining Pressure

Figures 5.12 and 5.13 show the $V_P$ and $M_{max}$ increase as the confining pressure increases. Compression wave velocity ($V_P$) varies from 355 to 631 m/s while $M_{max}$ varies from 201.33 to 688.8 MPa (See Table 5.5 for all values).

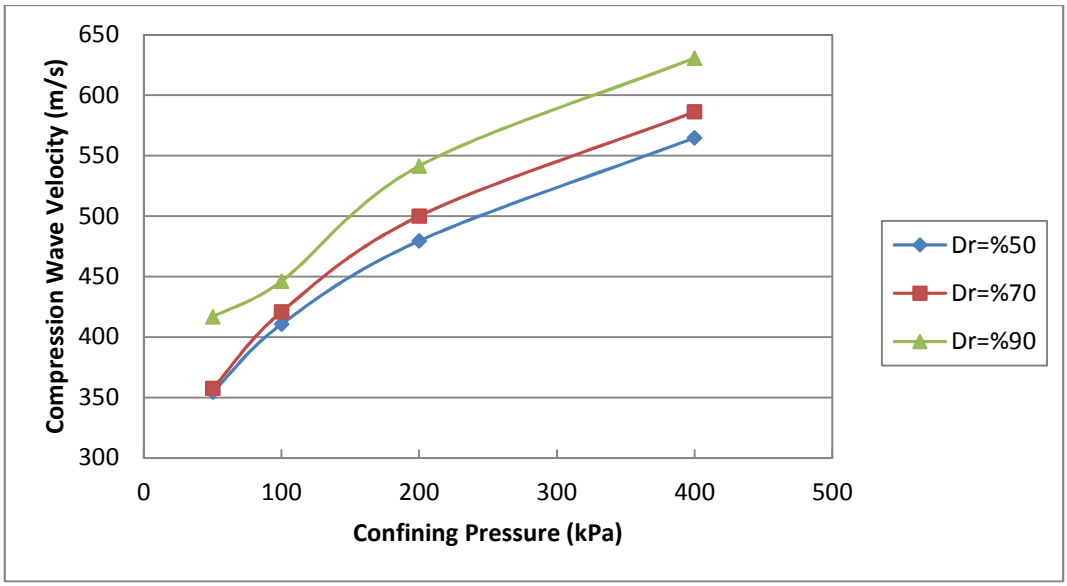



Figure 5.12 Variations of $V_P$ with Confining Pressure

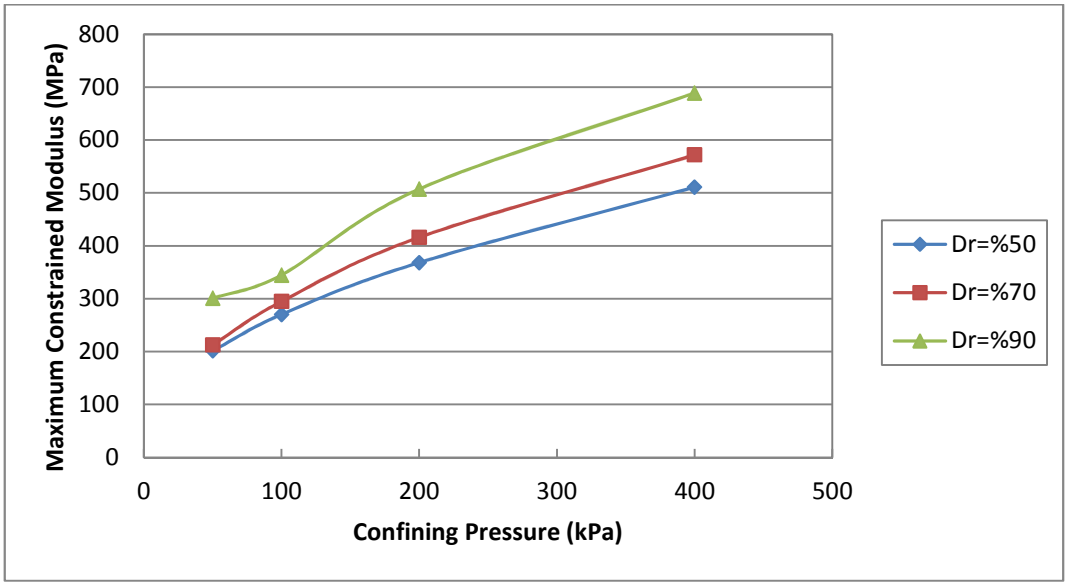



Figure 5.13 Variations of $M_{max}$ with Confining Pressure

Increases in both relative density and confining pressure cause increases in body wave velocities and as expected collected data shows variation of confining pressure have more significant effect on body wave velocity changes.

### 5.2.5 Effect of Relative Density and Isotropic Confining Pressure on Sand Specimen's Poisson's Ratio

Poisson's Ratios were calculated by using equation 2.14. According to past studies Poisson's Ratio decreases as initial relative density increases but as seen in Figure 5.14,

results from this study's tests does not show such behavior. During calculation of Poisson's Ratio by Equation 2.14, it was observed that 1% changes (error) in amount of $V_S$ and $V_P$ in different directions cause chances about 3% in amount of Poisson's Ratio. This issue shows that for finding more accurate Poisson's Ratio by using $V_S$ and $V_P$, more experience and verifying tests are needed. As observed in Figures 5.15, the Poisson's Ratio decreases as the confining pressure increases.

Table 5.5 presents the values of Poisson's Ratio under different density and confining pressure for sand specimens under isotropic stress.

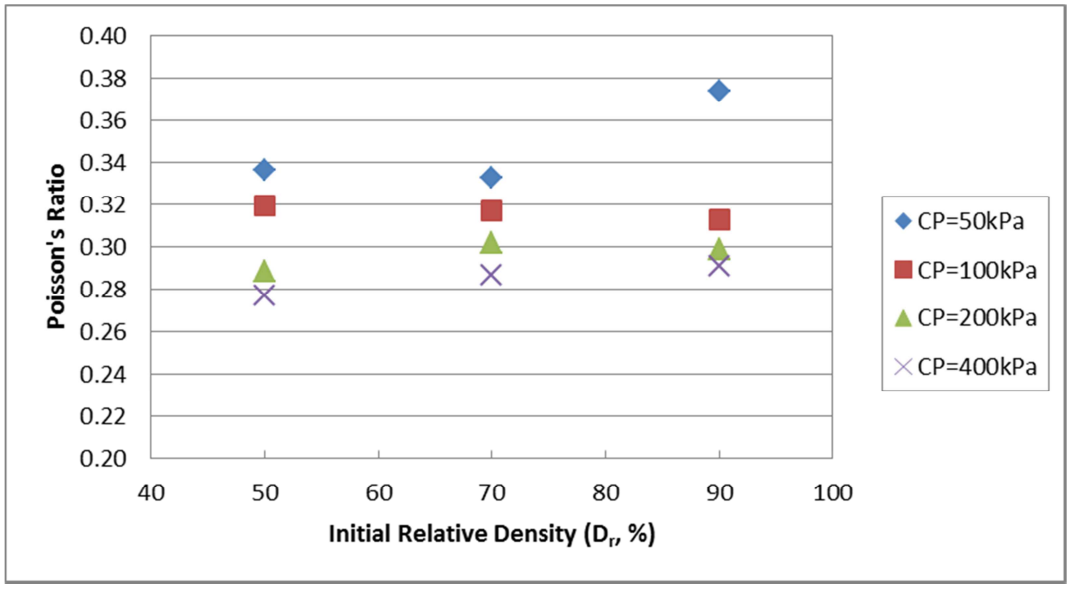



Figure 5.14 Variations of Poisson's Ratio with Initial Relative Density

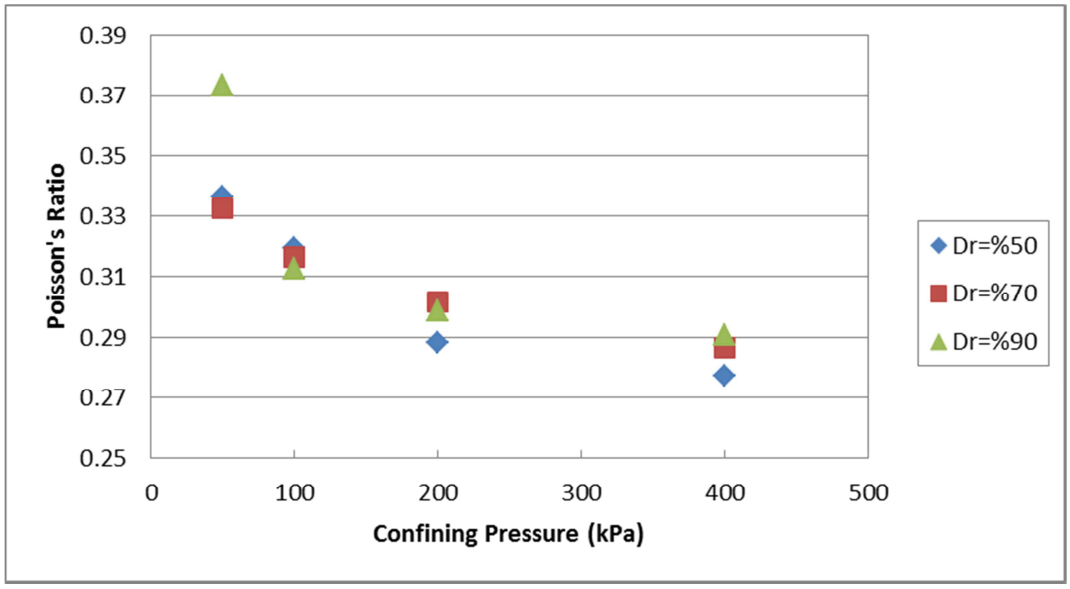



Figure 5.15 Variations of Poisson's Ratio with Confining Stress

Table 5.5 Test Result for Dry Specimens under Isotropic Stress

| Relative Density ($D_r$, %) | Confining Pressure (kPa) | Shear Wave Velocity ($V_S$, m/s) | Compression Wave Velocity ($V_P$, m/s) | Poisson Ratio | Maximum Shear Modulus (MPa) | Maximum Constrained Modulus (MPa) |
|---|---|---|---|---|---|---|
| 50 | 50 | 176 | 355 | 0.337 | 49.6 | 201.3 |
| | 100 | 211 | 411 | 0.320 | 71.6 | 270.0 |
| | 200 | 262 | 480 | 0.288 | 109.5 | 368.2 |
| | 400 | 314 | 565 | 0.277 | 157.5 | 510.8 |
| 70 | 50 | 179 | 358 | 0.333 | 53.3 | 212.6 |
| | 100 | 218 | 421 | 0.317 | 79.0 | 294.6 |
| | 200 | 266 | 500 | 0.302 | 118.1 | 415.9 |
| | 400 | 321 | 586 | 0.286 | 171.2 | 571.7 |
| 90 | 50 | 187 | 417 | 0.374 | 60.7 | 300.5 |
| | 100 | 233 | 446 | 0.313 | 93.9 | 344.6 |
| | 200 | 290 | 541 | 0.299 | 145.7 | 507.4 |
| | 400 | 343 | 631 | 0.291 | 203.3 | 688.8 |

## 5.3 Test Result for Dry Specimens under Anisotropic Stress

### 5.3.1 Test Results for Different Mean Effective Stresses

Figure 5.16 and Figure 5.18 show the variation of $V_S$ and $V_P$ with mean effective stress ($p'$). Variation of $G_{max}$ and $M_{max}$ correspond to these velocities with mean effective stress present at Figure 5.17 and Figure 5.19. Mean effective stress ($p'$) calculated by Equation 5.3. The applied anisotropic confining pressures and their corresponding Mean stress present at Table 5.6.

$$p' = \frac{\sigma_1' + 2*\sigma_3'}{3} \tag{5.3}$$

As observed in Figures 5.16 and 5.17, the $V_S$ and $G_{max}$ increase as the mean effective stress increases. Shear wave velocity ($V_S$) for specimens under anisotropic stress varies from 227 to 413 m/s while $G_{max}$ varies from 83.3 to 287.1 MPa (see Table 5.6 for all values).

As seen in Figures 5.18 and 5.19, the $V_P$ and $M_{max}$ increase as the mean effective stress increases. Compression wave velocity ($V_P$) for specimens under anisotropic stress varies from 532 to 759 m/s while $G_{max}$ varies from 456.2 to 973.9 MPa (see Table 5.6 for all values).

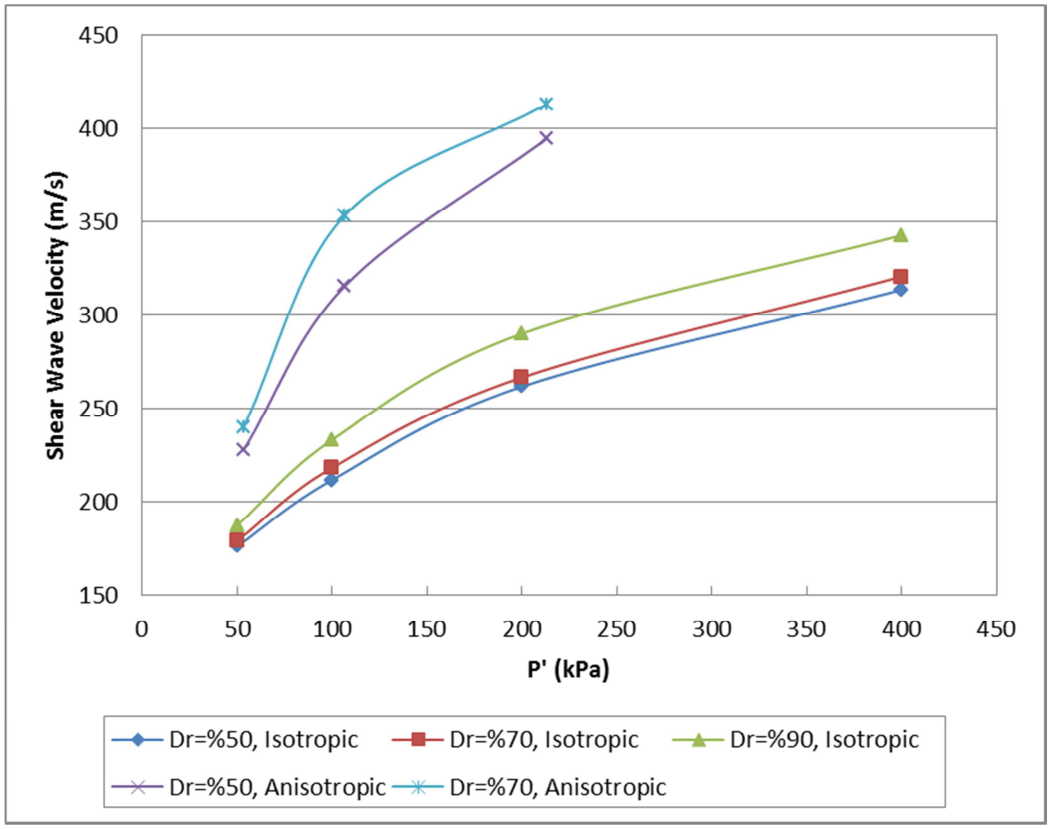



Figure 5.16 Variations of $V_S$ with Mean effective Stress

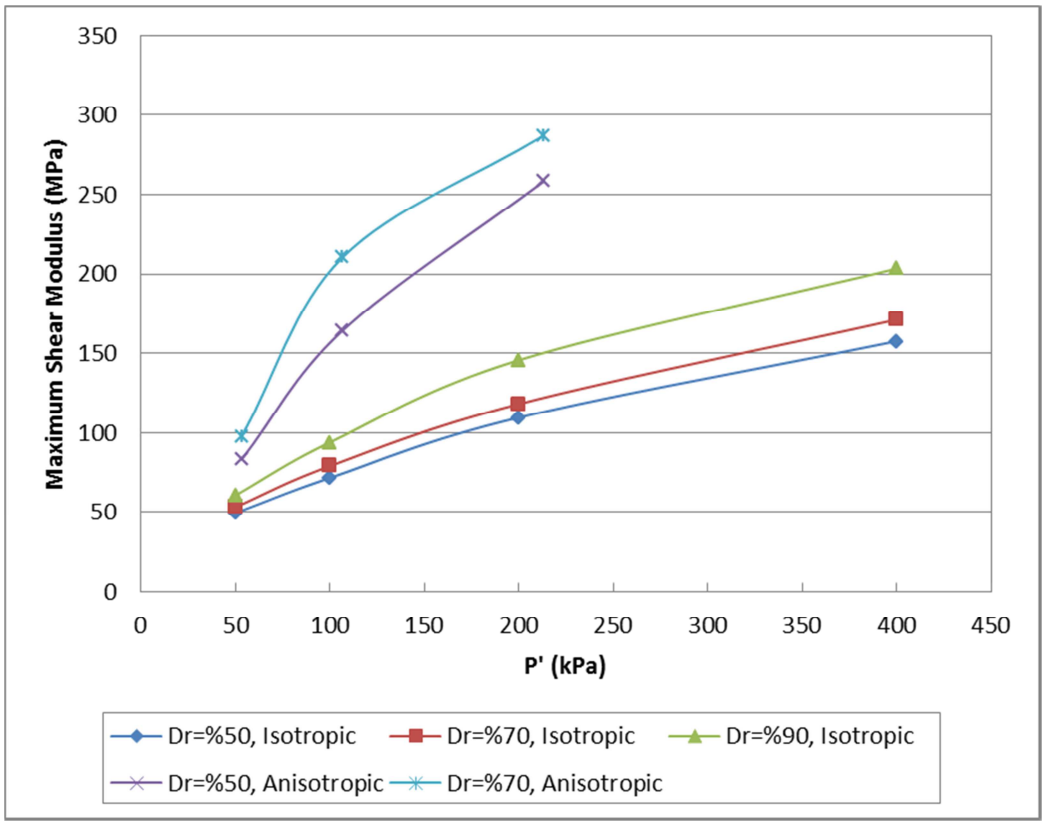



Figure 5.17 Variations of $G_{max}$ with Mean effective Stress

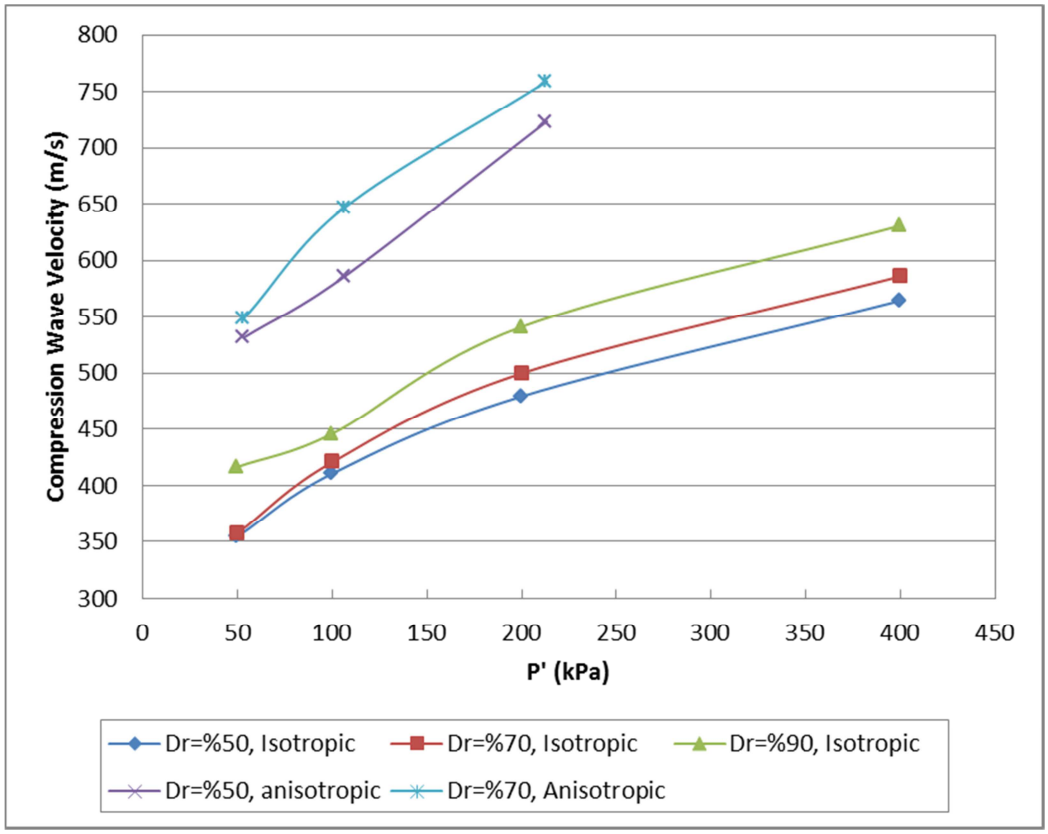



Figure 5.18 Variations of $V_P$ with Mean effective Stress

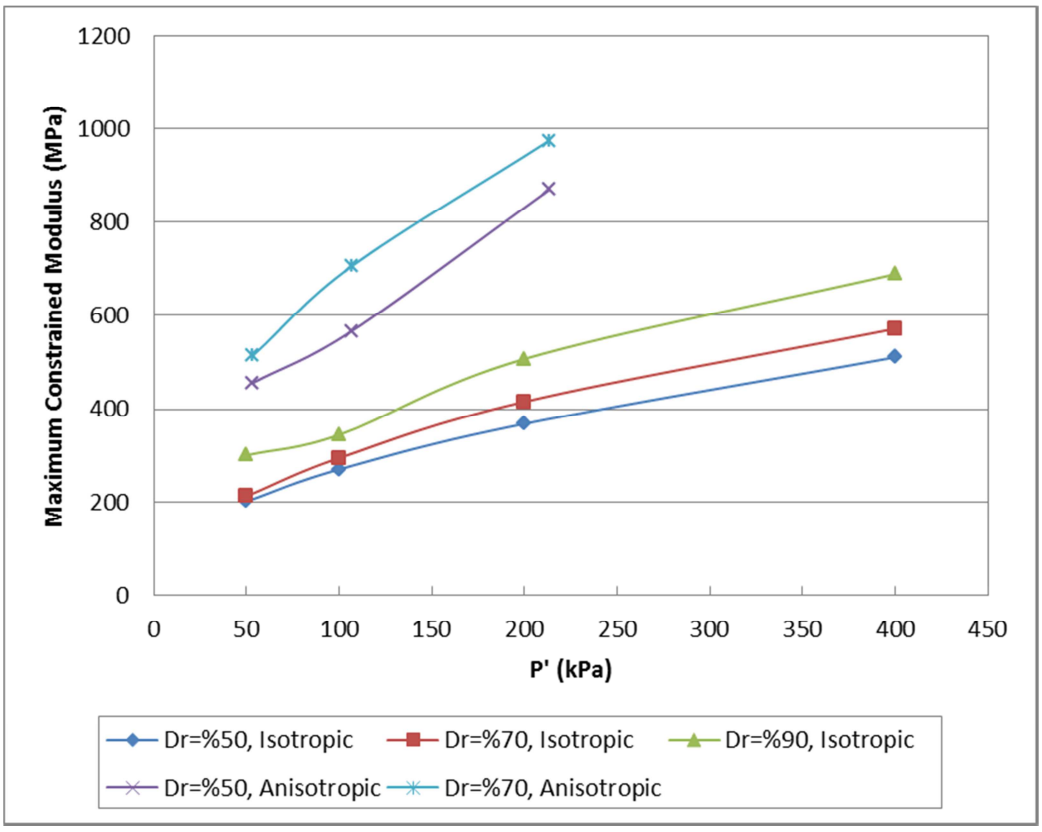



Figure 5.19 Variations of $M_{max}$ with Mean effective Stress

For both under isotropic and anisotropic stress dry sand specimens body wave velocities increases as mean effective stress increases but as observed in Figures  of section 5.3 variation of mean effective stress for specimens under anisotropic stress have more significant effect on body wave velocity changes.

### 5.3.2 Variation of Sand Specimen's Poisson's Ratio with mean Effective Stress

As observed in Figures 5.20, the Poisson's ratio decreases as mean effective stress increases. Table 5.6 presents the values of Poisson's Ratio under different density and confining pressure for sand specimens under anisotropic stress.

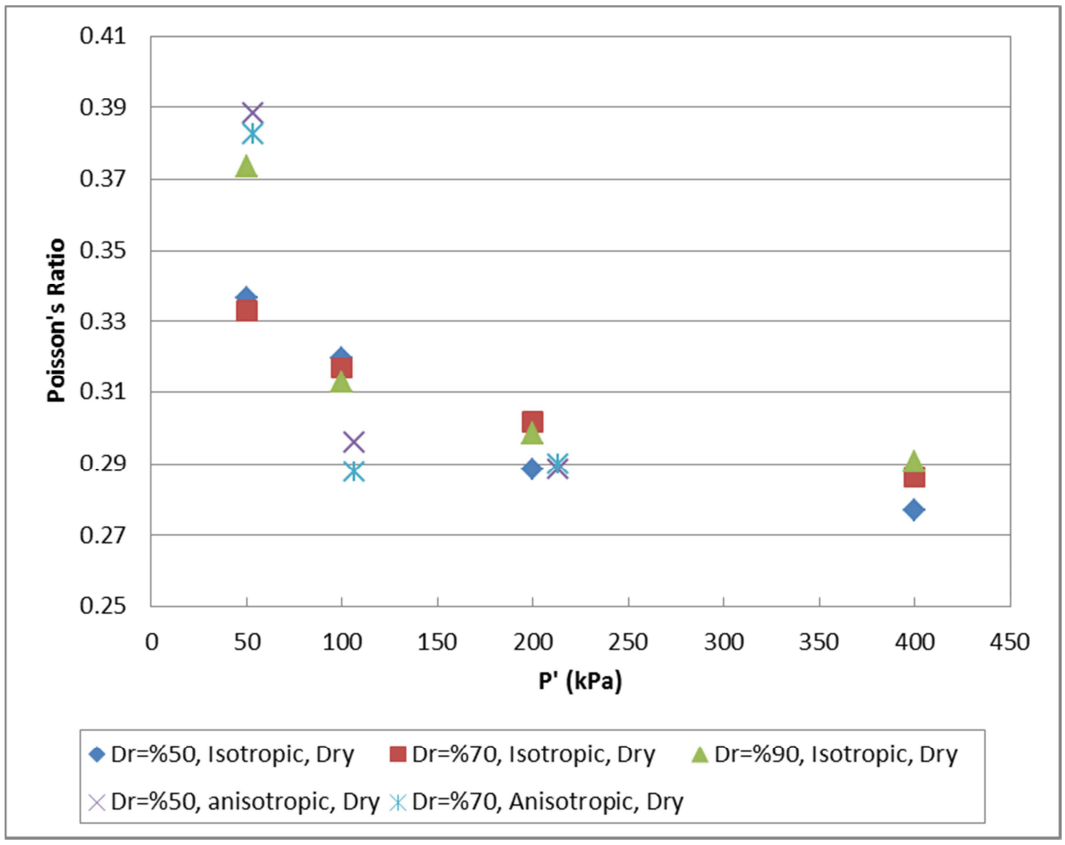



Figure 5.20 Variations of Poisson's Ratio with Mean effective Stress

Table 5.6 Test Result for Dry Specimens under Anisotropic Stress

| Relative Density ($D_r$, %) | Effective Vertical Stress ($\sigma'_1$, kPa) | Effective Horizontal Stress ($\sigma'_3$, kPa) | Mean Effective Stress (p', kPa) | Shear Wave Velocity ($V_S$, m/s) | Compression Wave Velocity ($V_P$, m/s) | Poisson Ratio | Maximum Shear Modulus (MPa) | Maximum Constrained Modulus (MPa) |
|---|---|---|---|---|---|---|---|---|
| 50 | 100 | 30 | 53.3 | 227 | 532 | 0.388 | 83.3 | 456.2 |
| | 200 | 60 | 106.7 | 316 | 586 | 0.296 | 164.2 | 566.6 |
| | 400 | 120 | 213.3 | 395 | 724 | 0.288 | 258.4 | 869.1 |
| 70 | 100 | 30 | 53.3 | 239 | 549 | 0.382 | 97.8 | 514.3 |
| | 200 | 60 | 106.7 | 353 | 647 | 0.288 | 210.3 | 705.5 |
| | 400 | 120 | 213.3 | 413 | 759 | 0.290 | 287.1 | 973.9 |

## 5.4 $V_S$ and $V_P$ Changes during Monotonic Shearing

Test IDs in this section belong to before shearing conditions that are presented at Table 5.2.

### 5.4.1 Drained Monotonic Shearing

Figure 5.21 shows the axial stress-strain behavior of the sand specimens during drained monotonic shearing. $V_S$ and $V_P$ measurements at different strain levels for these specimens are presented at Figure 5.22 and Figure 5.23.

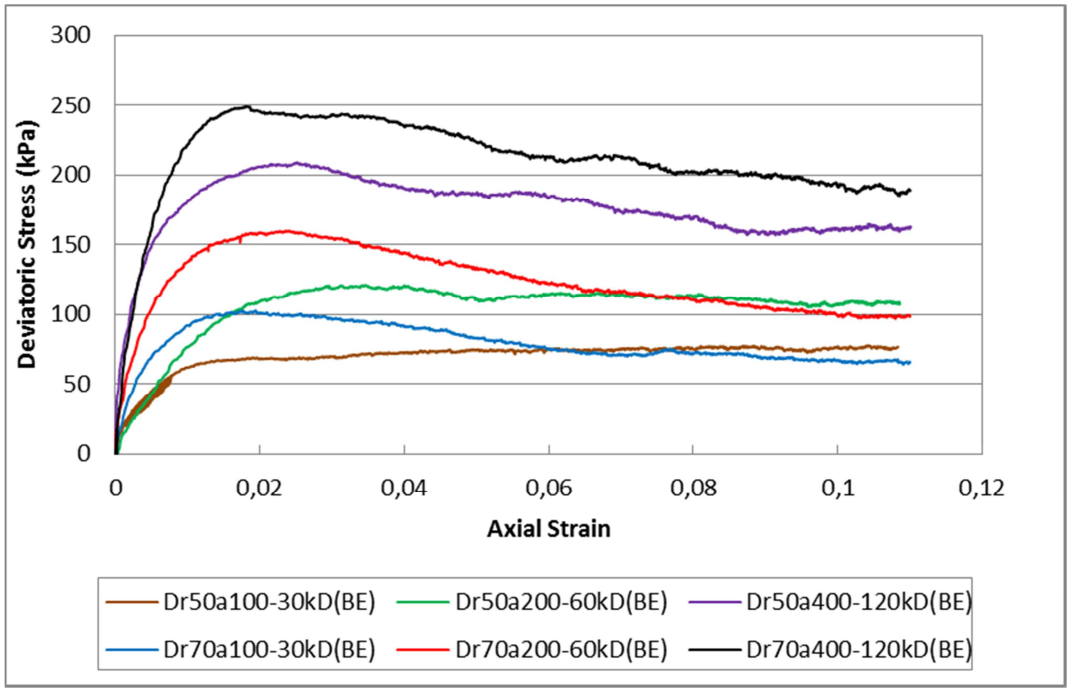



Figure 5.21 Drained Monotonic Shearing Test Stress-Strains Behavior

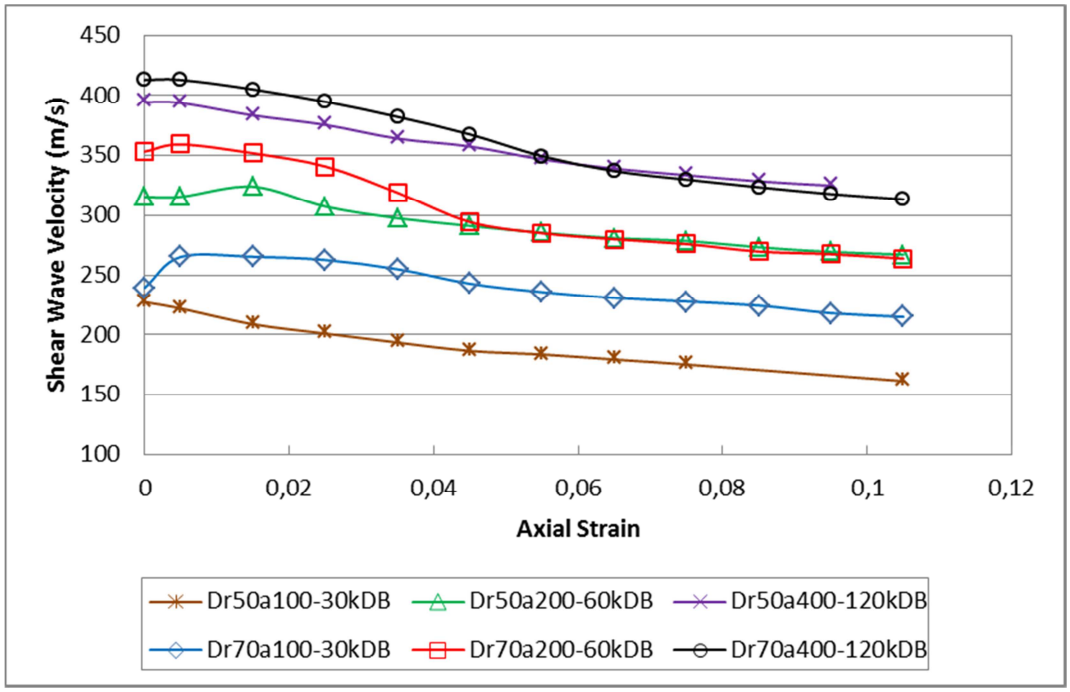



Figure 5.22 Variations of $V_S$ during Drained Monotonic Shearing

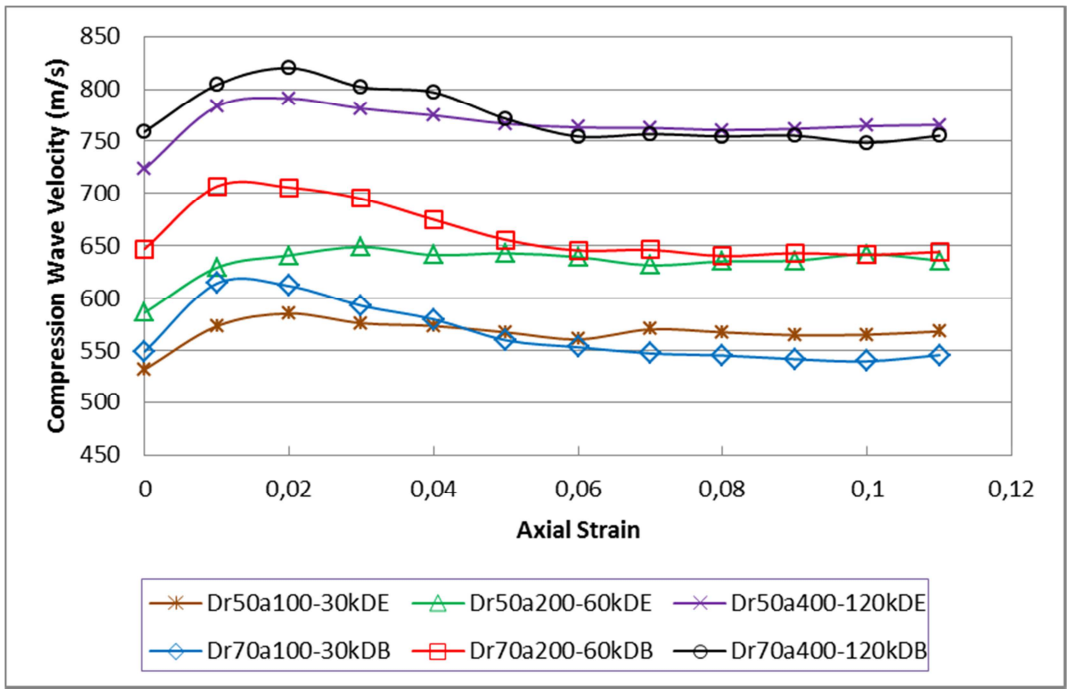



Figure 5.23 Variations of $V_P$ during Drained Monotonic Shearing

Collected test results during drained shearing tests show increase in body wave velocities until certain axial strain level (0.5 to 2 % strain for different specimens) and decrease after this level.

Table 5.7 shows value of measured shear wave velocity at three different strain points during drained tests for comparison.

Table 5.7 $V_S$ and $V_P$ Measurement During Drained Monotonic Shearing

| Test | Axial Strain | Shear Wave Velocity ($V_S$, m/s) | Compression Wave Velocity ($V_P$, m/s) | | Test | Axial Strain | Shear Wave Velocity ($V_S$, m/s) | Compression Wave Velocity ($V_P$, m/s) |
|---|---|---|---|---|---|---|---|---|
| Dr50a100-30kD(BE) | ε =0% | 227 | 532 | | Dr50a100-30kD(BE) | ε =0% | 239 | 549 |
| | $\varepsilon^*$=8.6% | 170 | 566 | | | $\varepsilon^*$=1.9% | 264 | 612 |
| | ε =10% | 164 | 565 | | | ε =10% | 216 | 540 |
| Dr50a200-60kD(BE) | ε =0% | 316 | 586 | | Dr50a200-60kD(BE) | ε =0% | 353 | 647 |
| | $\varepsilon^*$=3.4% | 299 | 646 | | | $\varepsilon^*$=2.4% | 342 | 702 |
| | ε =10% | 268 | 642 | | | ε =10% | 266 | 642 |
| Dr50a400-120kD(BE) | ε =0% | 395 | 724 | | Dr50a400-120kD(BE) | ε =0% | 413 | 759 |
| | $\varepsilon^*$=2.4% | 376 | 787 | | | $\varepsilon^*$=1.8% | 402 | 817 |
| | ε =10% | 325 | 765 | | | ε =10% | 316 | 749 |

$\varepsilon^*$: Axial Strain Corresponds to Maximum Deviatoric Stress.

### 5.4.2 Undrained Monotonic Shearing

Figure 5.24, Figure 5.25 and Figure 5.26 shows the axial stress-strain, pore pressure-strain and axial effective stress-strain behavior of the sand specimens during undrained monotonic shearing, respectively. $V_S$ measurements at different strain levels for these specimens are presented at Figure 5.27.

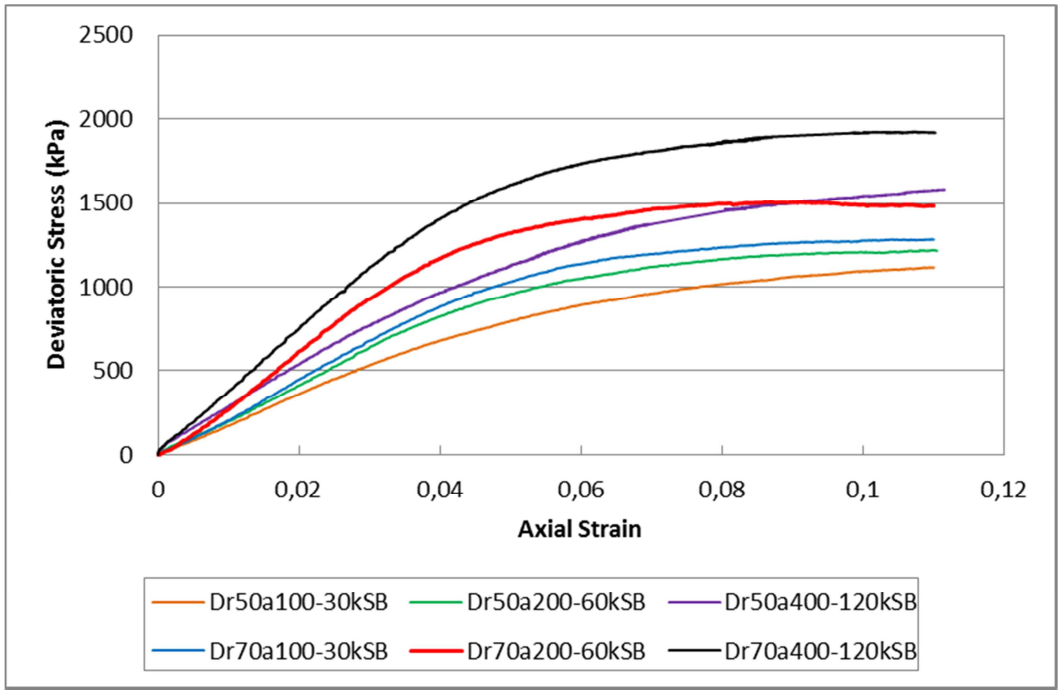



Figure 5.24 Undrained Monotonic Shearing Tests' Total Deviatoric Stress Behavior

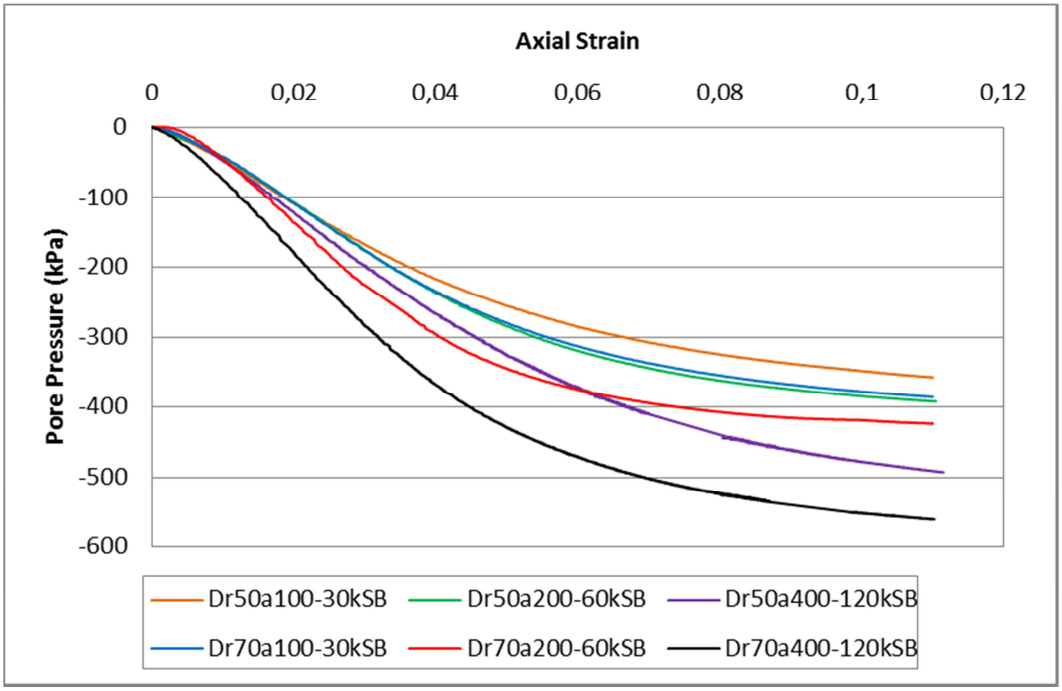



Figure 5.25 Undrained Monotonic Shearing Tests' Pore Pressure Behavior

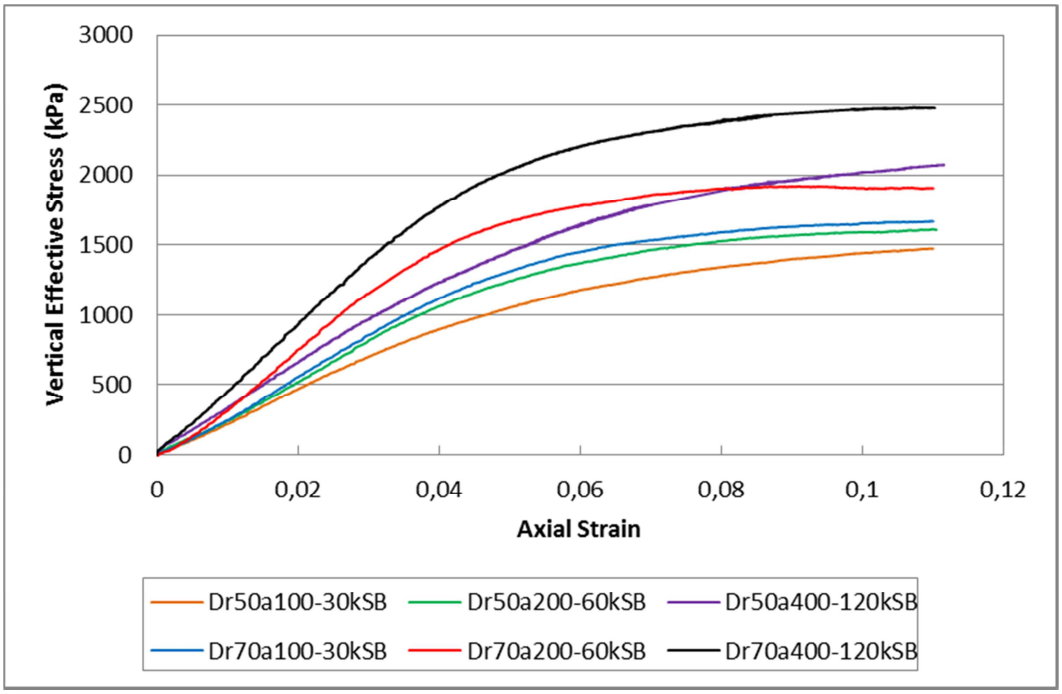



Figure 5.26 Undrained Monotonic Shearing Tests' Effective Deviatoric Stress Behavior

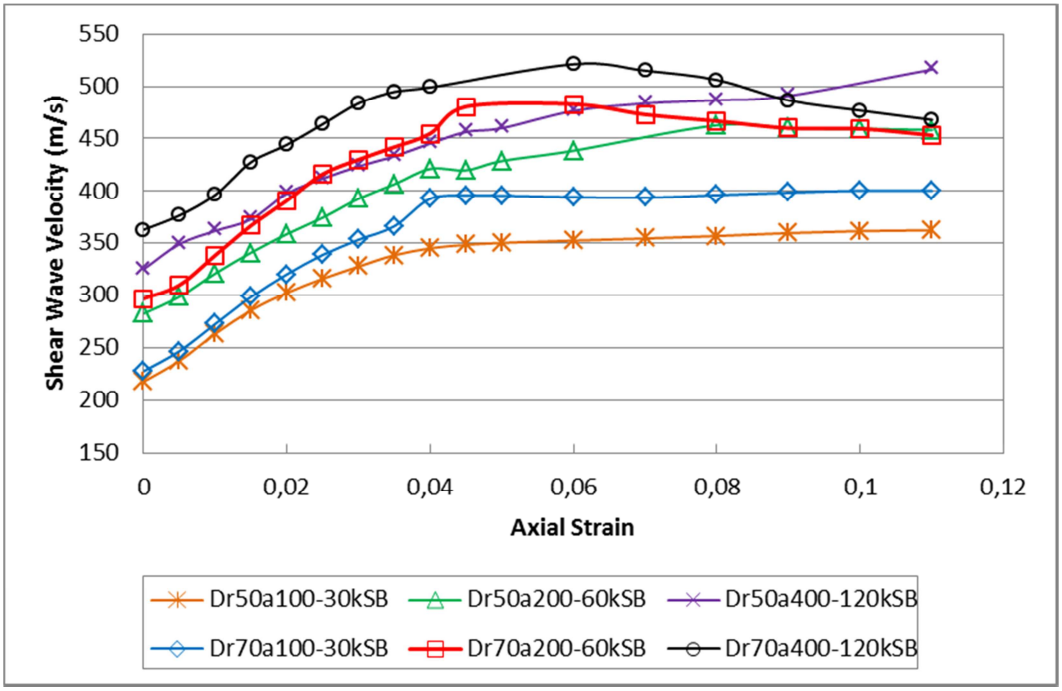



Figure 5.27 Variations of $V_S$ during Undrained Monotonic Shearing

Collected test results during undrained shearing tests show increase in body wave velocities as axial strain increases. This behavior was expected, because continues pore pressure decrement due to dilation tendency of medium dense sand cause increment in effective confining stress.

Table 5.8 shows value of measured shear wave velocity at three different strain points during undrained tests for comparison.

Table 5.8 $V_S$ Measurement During Undrained Monotonic Shearing

| Test | Axial Strain | Shear Wave Velocity ($V_S$, m/s) | Test | Axial Strain | Shear Wave Velocity ($V_S$, m/s) |
|---|---|---|---|---|---|
| Dr50a100-30kSB | ε =0% | 218 | Dr70a100-30kSB | ε =0% | 228 |
| | ε =5% | 350 | | ε =5% | 396 |
| | ε =10% | 362 | | ε =10% | 401 |
| Dr50a200-60kSB | ε =0% | 283 | Dr70a200-60kSB | ε =0% | 297 |
| | ε =5% | 429 | | ε =5% | 498 |
| | ε =10% | 459 | | ε =10% | 459 |
| Dr50a400-120kSB | ε =0% | 325 | Dr70a400-120kSB | ε =0% | 363 |
| | ε =5% | 460 | | ε =5% | 487 |
| | ε =10% | 503 | | ε =10% | 477 |

# CHAPTER 6

## SUMMARY AND CONCLUSION

The main goal of this study was to devise a nondestructive method for measuring the shear and compression wave velocities in dry and saturated sand specimens. The nondestructive method was developed by using piezoelectric transducers. These transducers generate different wave forms when excited by an electric field and thus can be used as wave generators and transmitters. On the other hand the transducers generate low electrical voltage when bent or compressed, thus can act as receivers that sense arriving waves.

The developed test setup includes a computer with PCI data acquisition board (works as signal generator and digital oscilloscope), a power amplifier, piezoelectric transducers that were modified and installed in housing and triaxial test apparatus with specially designed cell and caps. The three-wire configuration used to manufacture bender-extender elements from the transducers. A pair of bender-extender element was installed into top and pedestal caps of triaxial cell in order to measure arrival times of shear and compression waves within triaxial apparatus.

Considerable amount of energy and time was spent for designing and manufacturing bender-extender elements, special triaxial cell and its required component parts. Many issues were encountered during devising a working test setup such as problems related to cell water leakage, elements three-wiring configuration, grounding and waterproofing that were resolved by preliminary tests.

In order to show that main goals of this study were achieved, shear and compression wave velocities measurement tests were run with bender-extender elements on dry and saturated sand specimens under different initial condition (e.g., void ratio and confining pressure).

- The test results show that $V_S$ and $V_P$ decrease as the initial void ratio increases.
- The wave velocitie variation depends mainly on the confining effective stress state and $V_S$ and $V_P$ increase as the confining effective stress (for both isotropic and anisotropic stress conditions) increases.
- Poisson's Ratio decreases as the confining effective stress (for both isotropic and anisotropic stress conditions) increases.
- As expected variation of input frequency does not have a considerable effect on $V_S$ and $V_P$ measurement.
- During drained shearing tests body wave velocities increase until certain axial strain level (0.5 to 2 % strain for different specimens) and decrease after this level.
- During undrained shearing tests body wave velocities increase as axial strain increases. This behavior was expected, because continues pore pressure decrement due to dilation tendency of medium dense sand causes increment in effective confining stress and consequently the confining effective stress increases.

Proper functionality of developed test system is demonstrated by comparison of the test results of this study with other researchers'. Table 6.1 and Figure 6.1 present the index properties and grain size distribution curves of sands that were used in different researches respectively. Figure 6.2 and Figure 6.3 show the test results of this study are in according with the results in the literature.

Regarding the acquired data from shear and compression wave velocity measurement tests, it was determined that bender-extender elements are suited to measure shear and compression waves arrival times. Manufacturing this system also showed the bender-extender test setup can be adapted to a variety of testing devices to independently investigate elastic stiffness without interfering with the original functions of the devices.

Table 6.1 The Index Properties of the Sands in Different Researches

| Sand Used in | This Study | Valle-Molina [37] | Brignoli et al. (Ticino Sand) [5] | Öner [60] | Kumar and Madhusudhan [18] |
|---|---|---|---|---|---|
| Unified Soil Classification | SP | SP | NA | SP | NA |
| Specific Gravity | 2.65 | 2.67 | 2.68 | 2.65 | 2.66 |
| Maximum Void Ratio, $e_{max}$ | 0.81 | 0.74 | NA | 0.88 | 0.99 |
| Minimum Void Ratio, $e_{min}$ | 0.50 | 0.51 | NA | 0.50 | 0.55 |
| Median Grain Size, $D_{50}$ (mm) | 0.76 | 0.31 | 0.71 | 0.28 | 0.70 |
| Effective Grain Size, $D_{10}$ (mm) | 0.35 | 0.16 | NA | 0.18 | 0.47 |
| Uniformity Coefficient, $C_u$ | 2.57 | 2.32 | NA | 1.85 | 2.01 |
| Coefficient of Curvature, $C_c$ | 0.92 | 1.12 | NA | 0.87 | 1.10 |

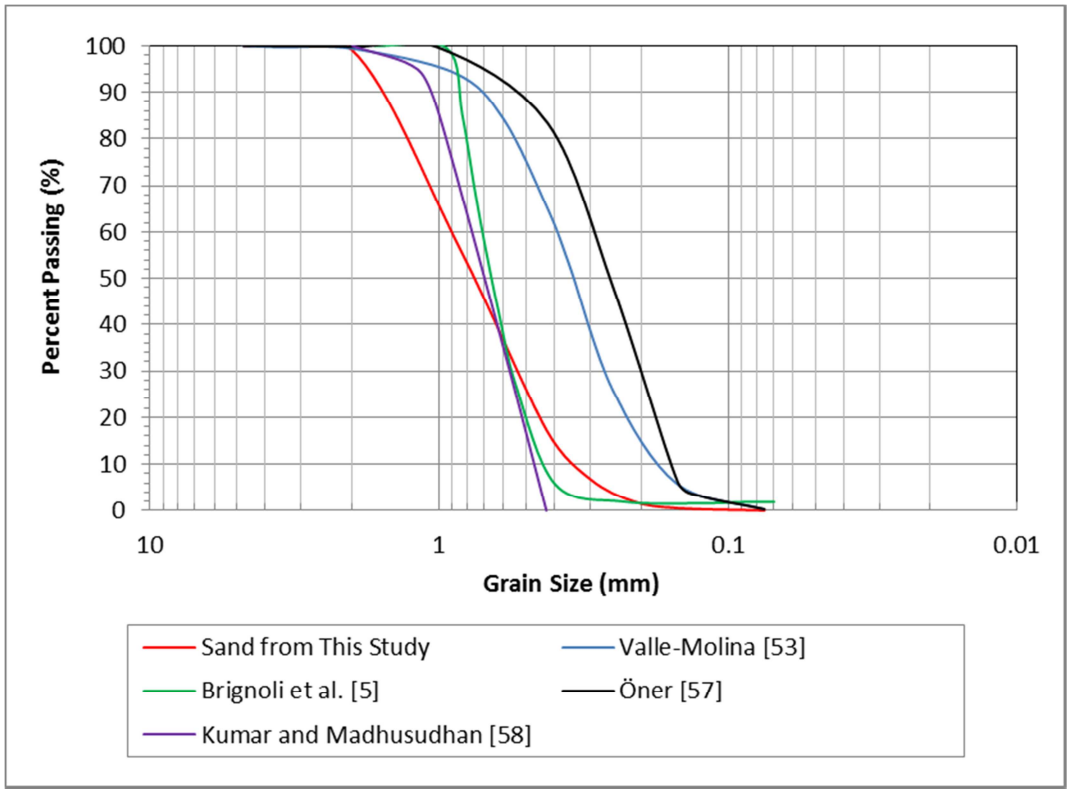



Figure 6.1 Grain Size Distribution Curves in Different Researches

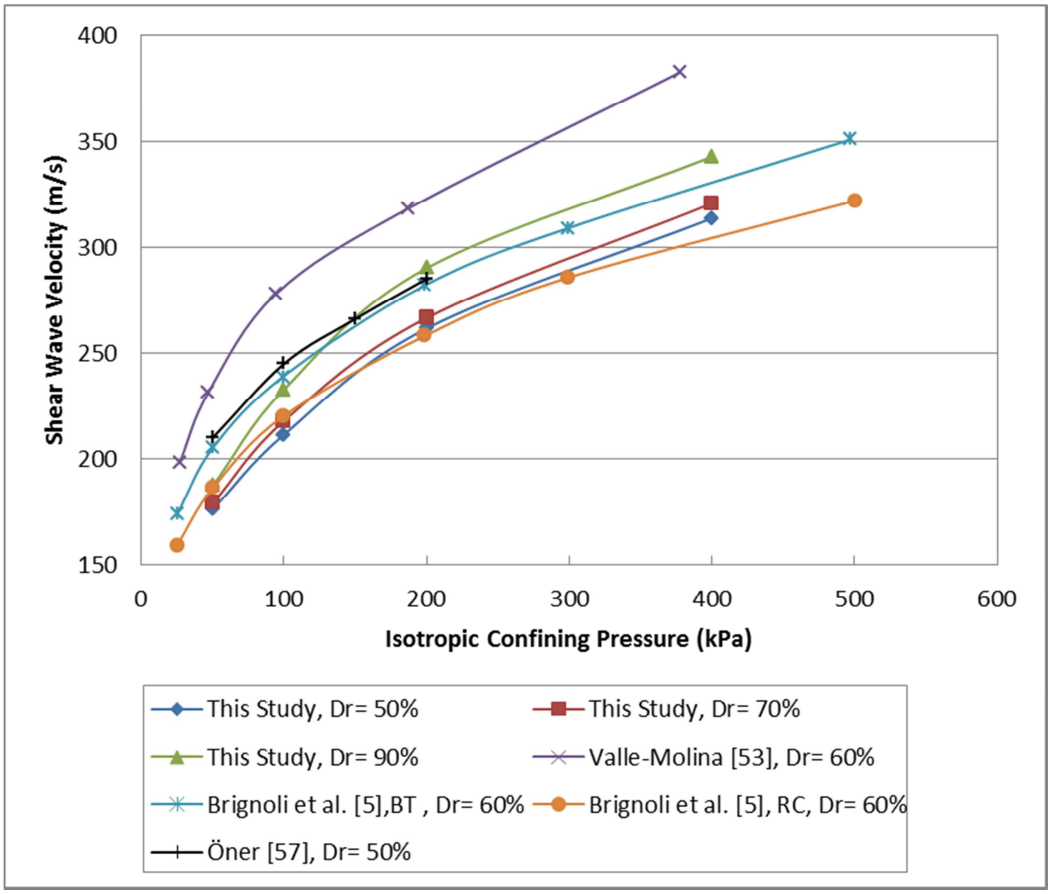



Figure 6.2 Variations of $V_S$ with Isotropic Confining Pressure in Different Researches

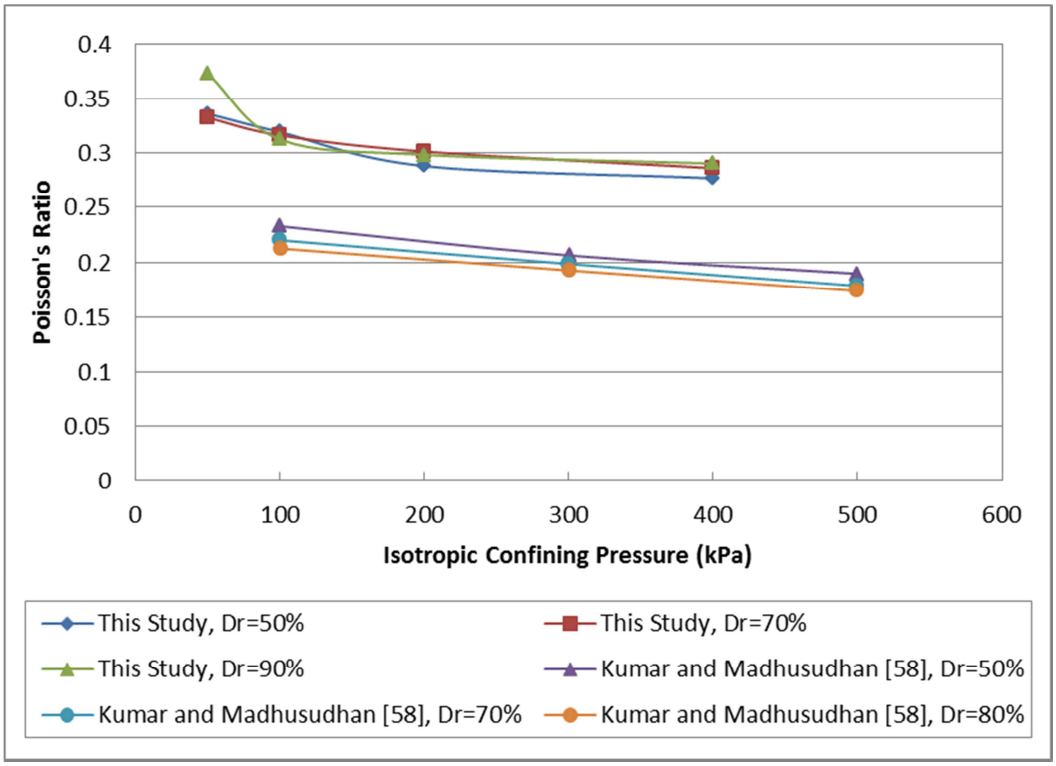



Figure 6.3 Variations of Poisson's Ratio with Isotropic Confining Pressure

# REFERENCES


[1] Okura, D. V. and Ansal, A. (2007). “Stiffness degradation of natural fine grained soils during cyclic loading”. Soil Dynamics and Earthquake Engineering 27: 843–854.

[2] Burland, J. B. (1989). “Ninth laurits bjerrum memorial lecture: ’small is beautiful´- the stiffness of soils at small strains”. Canadian Geotechnical Journal 26: 499–516.

[3] Atkinson, J. H. (2000). “Non-linear soil stiffness in routine design”. Gétechnique 50(5): 487–508.

[4] Bodare, A and Massarsch, K. R. (1984). “Determination of shear-wave velocity by different cross-hole methods”. Generic.

[5] Brignoli, E. G. M., Gotti, M. and Stokoe, K. H. (1996). “Measurement of shear waves in laboratory specimens by means of piezoelectric transducers”. Geotechnical Testing Journal 19(4): 384–397.

[6] Richart, F. E., Hall, J. R. and Woods, R. D. (1970). Vibration of soils and foundations. Prentice Hall. Englewood Cliff, New Jersey.

[7] Hamilton, E. L., (1963), “Sediment Sound Velocity Measured In Situ from TRIESTE,” Journal of Geophysics Res. 68: 5991-5994.

[8] Lawrence, F. V. (1963). “Propagation of ultrasonic waves through sand”. MIT Research Report, March.

[9] Shirley, D. J, Anderson, A. L., and Hampton, L. D. ,(1973). “In situ measurements of Sediment sound Speed under Coring”, ARL-TR-73-1, Applied Research Lab, The University of Texas at Austin, 88.

[10] Shirley, D. J. and Anderson, A. L. (1974). “Compression Wave Profilometer for Deep Water Measurements”, ARL-TR-74-51, Applied Research Lab, The 383 University of Texas at Austin, 82.

[11] Shirley, D. J., and Anderson, A. L. (1975). “Acoustical and Engineering Properties of Sediments”, ARL-TR-75-58, Applied Research Lab, The University of Texas at Austin, 73.

[12] Shirley, D. J. and Hampton, L. D. (1978). “Shear-wave measurements in laboratory sediments”. The Journal of the Acoustical Society of America, 63(2): 607-613.

[13] Schultheiss, P. J. (1981). “Simultaneous measurement of p and s wave velocities during conventional laboratory soil testing procedures”. Marine Geotechnology 4(4): 343–367.

[14] Dyvik, R. and Madshus, C. (1985). “Laboratory measurements of gmax using bender elements”. Advances in the engineering (161): 117–137.

[15] Dyvik, R. and Olsen, T. S. (1987), “Gmax Measurements in Oedometer and DSS using Bender Elements,” Proceedings of the 12th International Conference on Soil Mechanics and Foundation Engineering, Rio de Janeiro, 39-42.

[16] Fam, M. A. and Santamarina, J. C. (1997), “A Study of Consolidation Using Mechanical and Electromagnetic Waves”, Geotechnique 47(2): 203-219.

[17] Jovicic, V., Coop, M. R. and Simi´c, M. (1996). “Objective criteria for determining g(max) from bender element tests”. Géotechnique 2(46):357–362.

[18] Kumar, J. and Madhusudhan, B. N. (2010). “Effect of Relative Density and Confining Pressure on Poisson Ratio from Bender and Extender Elements Tests”. Géotechnique 60(7): 561–567.

[19] Arulnathan, R., Boulanger, R. W., Kutter, B. L. and Sluis, W. K. (2000). “New tool for shear wave velocity measurements in model tests”. Geotechnical Testing Journal 23(4): 444–453.

[20] Brocanelli, D. and Rinaldi, V. (1998). “Measurement of low-strain material damping and wave velocity with bender elements in the frequency domain”. Canadian Geotechnical Journal 6(35): 1032–1040.

[21] Cuccovillo, T. and Coop, M. R. (1997). “The measurement of local axial strains in triaxial tests using lvdts”. Géotechnique 47(1): 167–171.

[22] Da-Re, G., Santagata, M. C. and Germaine, J. T. (2001). “Lvdt based system for the measurement of the prefailure bahaviour of geomaterials”. Geotechnical Testing Journal 24(3): 288–298.

[23] Redwood, M. (1960). Mechanical waveguides. Pergamon Press

[24] Stokoe, K. H., Hwang, S. K., Roesset, J. M.and Sun, C. W. (1994). “Laboratory measurement of small-strain material damping of soil using free-free resonant column”. In: Earthquake Resistant Construction and Design: Proceedings of the Second International Conference on Earthquake Resistant Construction and Design, 195–202.

[25] AnhDan, L., Koseki, J. and Sato, T. (2002). “Comparison of young’s moduli of dense sand and gravel measured by dynamic and static methods”. Geotechnical Testing Journal.

[26] Audisio, A., Bonani, S. and Foti, S. (1999). Advances in spectral analysis for sasw test. In: Pre-failure Deformation of Geomaterials. Jamiolkowski, Lancellotta & Lo Presti (eds), 395–402.

[27] Hope, V. S., Clayton, C. R. I. and Butcher, A. P. (1999). “In situ determination of g(hh) at bothkennar using a novel seismic method”. Quarterly Journal of Engineering Geology 32: 97–105.

[28] Nazarian, S. and Stokoe K. H. (1984). “In situ shear wave velocities from spectral analysis of surface waves". 8th World Conference on Earthquake Engineering, 31–38.

[29] Arroyo, M., Muir-Wood, D. and Greening, P. D. (2003a). “Source near-field effects and pulse tests in soil samples”. Géotechnique 53(3): 337–345.

[30] Thomann, T. G. and Hryciw, R. D. (1990). “Laboratory measurement of small strain shear modulus under ko conditions”. Geotechnical Testing Journal 13(2): 97–105.

[31] Viggiani, G. and Atkinson, J. H. (1995). “Interpretation of bender element tests”. Géotechnique, 45(1): 149–154.

[32] Connolly, T. M. and Kuwano, R. (1999). “The measurement of gmax in a resonant column, bender element, torsional shear apparatus”. Generic.

[33] Lings, M. L. and Greening, P. D. (2001). “A novel bender/extender element for soil testing”. Géotechnique, 51(8): 713–717.

[34] Dano, C., Hocine Hareb and Pierre Y. Hicher (2003). “Characterization of loire river sand in the small strain domain using new bender-extender elements”. 16th ASCE Engineering Mechanics Conference.

[35] Leong, E.C., Cahyadi, J. and Rahardjo, H. (2009). “Measuring shear and compression wave velocities of soil using bender–extender elements”, Can. Geotech. J. 46: 792–812.

[36] Bolt, B,A., (1976). Nuclear Explosions and Earthquakes, W.H. Freeman and Company.

[37] Celestino Valle-Molina (2006). Measurements of Vp and Vs in Dry, Unsaturated and Saturated Sand Specimens with Piezoelectric Transducers. PhD Thesis/dissertation. The University of Texas at Austin, Faculty of the Graduate School.

[38] Kolsky, H., (1963). Stress Waves in Solids, Dover Publications, 213.

[39] Kuwano, R., Connolly, T. M. and Kuwano, R. (1999). “Shear stiffness anisotropy measured by multi-directional bender element transducers”. Pre-failure Deformation Characteristics of Geomaterials, 205–212.

[40] Dano, C. and Pierre-Yves Hicher (2002). “Evolution of elsatic shear modulus in granular materials along isotropic and deviatoric stress paths”. 15th ASCE Engineering Mechanics Conference.

[41] Kawaguchi, T., Mitachi, T. and Shibuya, S. (2001). “Evaluation of shear wave travel time in laboratory bender element test”. 15th international conference on soil mechanics and geotechnical engineering 1: 155–158.

[42] Pennington, D. S., Nash, D. F. T. and Lings, M. L. (2001). “Horizontally mounted bender elements for measuring anisotropic shear moduli in triaxial clay specimens”. Geotechnical Testing Journal 24(2): 133–144.

[43] Fam, M. and Santamarina, J. C. (1995). “Study of geoprocesses with complementary mechanical and electromagnetic wave measurements in an oedometer”. Geotechnical Testing Journal 18(3: 307–314.

[44] Kumar, J. and Madhusudhan, B. N. (2010). “A note on the measurement of travel times using bender and extender elements”. Soil Dynamics and Earthquake Engineering 30: 630–634.

[45] Rio, J. F. M. E. (2006). Advances in laboratory geophysics using bender elements. PhD Thesis/dissertation. UCL, Department of Civil & Environmental Engineering.

[46] Santamarina, J. C. (2001). Soils and waves. John Wiley and Sons. Chichester.

[47] Lee, J. S. and Santamarina, J. C. (2005). "Bender elements: Performance and signal interpretation". Journal of Geotechnical and Geoenvironmental Engineering 131(9): 1063–1070.

[48] Leong, E. C., Yeo, S. H. and Rahardjo, H. (2005). "Measuring shear wave velocity using bender elements". Geotechnical Testing Journal 28(5): 488–498.

[49] Sanchez-Salinero, I., Roesset, J. M. and II Stokoe, K. H. (1986). "Analytical studies of body wave propagation and Attenuation". Report GR 86-15, Civil Engineering Department, University of Texas at Austin.

[50] Arulnathan, R, Boulanger, R. W. and Riemer, M. F. (1998). "Analysis of bender elements tests". Geotechnical Testing Journal, ASTM 21(2): 120–131.

[51] Jovicic, V. and Coop, M. R. (1997). "Stiffness of coarse-grained soils at small strains". Géotechnique 47(3): 545–561.

[52] Pennington, D. S. (1999). The Anisotropic Small Strain Stiffness of Cambridge Gault Clay. Thesis/dissertation.

[53] Eldin, A. K. G. (1951). Some Fundamental Factors Controlling the Shear Properties of Sand. PhD Thesis, University of London.

[54] Atkinson, J. H. and Bransby, P. L. (1978). The Mechanics of Soils, An Introduction to Critical State Soil Mechanics. McGRAW-HILL, Berkshire.

[55] Bishop, A. W. and Henkel, D. J. (1962). The Measurement of Soil Properties in the Triaxial Test. Edward Arnold, London.

[56] Piezo System, Inc., www.piezo.com. 21/02/2012.

[57] Deniz, R. O. (2008). Bender elements and bendıng disks for measurement of shear and compressıonal wave velocities in large sand specimens. MSc Thesis/dissertation. Northeastern University, Department of Civil and Environmental Engineering.

[58] National Instruments, www.ni.com. 30/04/2013.

[59] Geocomp Corporation, www.geocomp.com. 10/12/2008.

[60] Öner, L. (2013). Determinatıon of Maximum Shear Modulus of Dry Sands Using Piezoelectric Bender Elements. MSc Thesis/dissertation. Yıldız Technical University, Department of Civil Engineering.

# CURRICULUM VITAE

## PERSONAL INFORMATION

**Name Surname** : Babak ROUZEGARI

**Date of birth and place** : 14.05.1986 – MARAGHEH

**Foreign Languages** : English

**E-mail** : babakrouzegari@gmail.com

## EDUCATION

| **Degree** | **Department** | **University** | **Date of Graduation** |
|---|---|---|---|
| Undergraduate | Civil Engineering | Maragheh Islamic Azad University | 2010 |
| High School | Mathematics | Nuredanesh High School | 2005 |